CMU-DOE/ER/40315-195

DOE/ER/40315--195

DE92 040008

Annual Progress Report

Experimental Medium Energy Physics

Carnegie Mellon University

Pittsburgh, Pennsylvania 15213

June 1991 - May 1992

DOE Contract: DE-FG02-87ER40315

DISCLAIMER

This report was prepared as an account of work sponsored by an agency of the United States Government. Neither the United States Government nor any agency thereof, nor any of their employees, makes any warranty, express or implied, or assumes any legal liability or responsibility for the accuracy, completeness, or usefulness of any information, apparatus, product, or process disclosed, or represents that its use would not infringe privately owned rights. Reference herein to any specific commercial product, process, or service by trade name, trademark, manufacturer, or otherwise does not necessarily constitute or imply its endorsement, recommendation, or favoring by the United States Government or any agency thereof. The views and opinions of authors expressed herein do not necessarily state or reflect those of the United States Government or any agency thereof.

Carnegie Mellon

MASTER

DISTRIBUTION OF THIS DOCUMENT IS UNLIMITED

CONTENTS

I. Introduction

Research by the CMU Medium Energy Physics group has been largely focused on data-taking and analysis of the H dibaryon experiment. The H dibaryon is a unique 6-quark particle, predicted to be stable against strong decays. Years of development led to the first run of our search experiment, E813, at Brookhaven National Laboratory (BNL) in the spring and summer of 1991. Now in the spring of 1992 the first "production" run is just getting underway. The group maintained activity in a number of other experiments, however, some in the early stages of design, some in the construction phase, and some in the late stages of analysis. This report will summarize activities on all our ongoing projects during the past year.

It has been an exciting and productive year for our H particle experiment. In last spring's run the new 2 GeV/c beam line, detectors, and other instrumentation were all tested, most of them for the first time. Enough high quality data were obtained to prove that all elements of the apparatus were working as designed. Analysis of the data at CMU showed that each step in the chain of events leading to H-particle formation was well under control and understood. The next data taking period, which is now underway, should provide us with the statistics we need to obtain our first physics results from this experiment. Since the CMU group is leading this experiment, a significant portion of our time has been spent coordinating the many facets which come together in running an experiment of this size. Chapter III is a discussion of all aspects of this effort, from the theoretical motivation for the search, to a summary of the performance of the CMU-built apparatus.

We remain involved in a series of experiments at BNL which measure the rates of several weak decay modes of light hypernuclei. The most recent of these experiments, proposed and organized by CMU, completed data taking in early 1990. The data from this experiment, E788, is being analyzed as the Ph.D. thesis topic of graduate student Michael Athanas. This experiment is described and the status of the analysis is outlined in Chapter IV.

Strangelets are nucleus-like objects with an unusually large amount of strange matter in them. A feasibility run was conducted this spring to search for such exotic objects using the BNL 2 GeV/c beam line at BNL and some of the instrumentation used for the H particle search. Silicon and gold ions bombarded a massive target, and the beam line was shown to have good sensitivity for detecting these hypothetical particles by exploiting their anomalously low value of Z/A and low speed. CMU provided a substantial amount of manpower and expertise in the running of this preliminary search, which we hope will be approved to run again next year. Chapter V describes this experiment in some detail.

Hypernuclei containing not one but two strange particles have been sought for many years without finding definitive evidence that such nuclei even exist. Detection and characterization of double-lambda hypernuclei would provide important insights into the baryon-baryon weak

interaction. A new experiment was proposed and approved at BNL to perform the first non-emulsion search for double-lambda hypernuclei, with Professor Franklin as co-spokesman. This experiment is discussed in Chapter VI.

The elementary electro- and photo- production of hyperons will be investigated in an approved experiment at the Continuous Electron Beam Accelerator Facility (CEBAF). This new laboratory is presently the highest priority new facility in medium energy physics. Chapter VII describes the physics motivation for this work. We are presently deeply involved in a design and development project for the superconducting toroidal-magnet CLAS spectrometer facility. CLAS will be used in our experiment, and many other experimental efforts as well. Carnegie Mellon is designing and fabricating the innermost tracking drift chamber for the spectrometer, in collaboration with the University of Pittsburgh and the University of Massachusetts at Amherst. This is a large construction project which will occupy several years. In the past year we have made substantial progress on the design and prototyping of the device, as discussed in Chapter VIII. Recently Professor Schumacher was awarded a grant from CEBAF to build a full-scale prototype of this so-called "Region 1" drift chamber.

The strange-quark content of the nucleon is a quantity which has received much attention in the physics community. CMU is helping to develop a proposal for measuring the flavor singlet structure function of the nucleon, called G^0, which is related to the strange quark content. The measurement would be of the parity violating electron scattering helicity asymmetry off the nucleon. If approved, this experiment would run at CEBAF using a dedicated apparatus built in Hall C. Our contribution would be to develop the fast electronics needed for this novel type of device. Chapter IX describes the experiment and the work we have done to prepare for this measurement.

Chapter X briefly discusses soon to be published results from an experiment which has been completed for some time. Some of our work on relativistic heavy ion collisions at the CERN SPS, which was the basis for the recent Ph.D. thesis of CMU graduate student Guy Diebold, is presented. Finally, we list all our professional activities, publications, reports, and talks in Chapters XI and XII.

II. Group Personnel

The members of the Carnegie Mellon experimental medium energy physics group during the past year were:

Physics Staff

- Peter D. Barnes, Professor of Physics (On leave starting August, 1991)
- Gregg B. Franklin, Principal Investigator, Associate Professor of Physics
- Reinhard A. Schumacher, Assistant Professor of Physics
- Brian P. Quinn, Assistant Professor of Physics
- Valdis Zeps, Research Associate
- Francis Martin Rozon, Research Associate
- Richard Magahiz, Special Faculty Research Associate
- Chris Maher, Senior Research Associate (20 %, until December, 1991)
- Michael Athanas, Graduate Student
- Irianto R. Sukaton, Graduate Student
- Frank Merrill, Graduate Student
- Toru Iijima, Graduate Student, visiting from Kyoto University

Support Staff

- Kimberley Minihan, Technical Assistant
- Gary R. Wilkin, Laboratory Technician

Peter Barnes has been on a leave of absence from the University for most of the past year, and is serving as the director of the Los Alamos Meson Physics Facility. Gregg Franklin has assumed the position of Principal Investigator for the group. Marty Rozon left the group in September for a new position at the University of Alberta at Edmonton.

Toru Iijima has been with us at CMU for most of the year, visiting from Kyoto University, Japan. He is working on the analysis of the H-particle experiment which currently forms the heart of the group's activity.

III. Search for the H Dibaryon at the AGS

III.A. Introduction

The existence of multi-quark hadron states beyond $q\bar{q}$ and qqq has been discussed for many years. Investigations of the role of the spin-spin interactions among the quarks has led to quantitative estimates of the baryon and meson masses and other properties. The six-quark state with the flavor content of two lambda hyperons has been of particular interest. This state was originally discussed by Jaffe[1] in 1977 and labeled the "H particle". More recently it has become the object of extensive discussion in the literature both in terms of calculated properties and experimental searches. We have developed two experiments to search for this particle. Experiment E813 is designed to search for the H particle in the mass region between 15 MeV unbound (relative to $\Lambda\Lambda$) and approximately 100 MeV bound. Experiment E836 is designed to have complementary sensitivity to the first experiment, searching the region of higher binding. A third experiment which has just been approved this year, an experiment to detect $\Lambda\Lambda$ Hypernuclei (E886), also has potential impact in the field of H-dibaryons and is discussed in Chapter VI.

In an investigation of low mass six-quark states, Jaffe found that the system **uuddss** can have especially low mass in a state with total spin zero, charge zero, isospin zero, and positive parity. The six quarks in the system have the same spatial wave functions (s-wave), and in this respect the system is rather unlike a deuteron. Among wave functions of six quark systems, the H particle belongs to the **490** representation in the SU(6) color-spin group and is a singlet in the SU(3) flavor group.

The essential ingredient in the binding of the H particle is the color-magnetic interaction of the six quarks due to gluon exchange. The H is the spin zero state whose eigenvalue has the largest downward shift under this interaction. Jaffe calculated the six quark mass spectrum[1] in the bag model and obtained an H particle mass of 2150 MeV and thus a binding energy of about 80 MeV.

Since the original bag model calculations of the H particle mass by Jaffe, the properties of this state have been analyzed in a variety of calculations such as quark potential models and lattice gauge calculations. Fig. III.A.1 shows a comparison of known baryon masses with the mass of the H as predicted in different types of models. At the left are various mass pairs with the $\Lambda\Lambda$ being the lowest S = –2, B = 2 system but substantially more massive than several of the S = –1 and S = 0 systems.

The mass calculations at the right in Fig. III.A.1 vary significantly in technique and in their results. MIT bag model and cloudy bag model estimates generally tend to give a positive binding, B_H, although effects like center-of-mass corrections and pressure from the pion cloud require special attention. Topological soliton (Skyrmion) models continue to give rather low masses. Oka *et al*[2] have shown that a nonrelativistic quark potential model calculation gives an H unbound by 70 MeV. A more recent quark cluster calculation[3], however, finds the H to be 15 MeV bound.

Lattice Gauge Theory (LGT) calculations are of particular interest. A calculation by MacKenzie and Thacker[4] in 1985 generated an H which was unbound, or perhaps slightly bound. More recently, a LGT calculation by Iwasaki *et al*[5] on a larger lattice predicts a very light H. While the explanation for the discrepancy between the two calculations appears to be that the lattice used in the original calculation was too small, the new results give an H mass below the deuteron mass, which may be too light to be physical. If the H is lighter than the deuteron, the universe could decay to strange matter. A search for the β-decay of nuclei through a ΔS=2 channel to the H by Ejiri *et al*[6] gave an upper limit for this process which, when combined with an H-particle production rate calculation, gives a lower limit on the H mass within a few MeV of the deuteron mass.

Indirect evidence of limits on the H mass comes from double-Λ hypernuclei.[7,8] In the 1960's, two reports were published of the observation of the formation and subsequent weak mesonic decay of a nucleus with two bound Λ's. Presumably, if the H existed and was bound by more than 10 MeV, the two Λ's would have formed an H before the weak decay occurred. This was not observed. Unfortunately, the events have not been confirmed in later experiments. If correctly interpreted, the data may place a lower limit on the H mass around 2220 MeV. There have been arguments that the production rate of the H from a double-Λ hypernucleus may be severely depressed if the H is very light, but these arguments are controversial.

A more recent hybrid emulsion search for double-Λ hypernuclei at KEK has identified a third double-Λ hypernuclear candidate. The analysis of the event by the collaboration that performed the experiment concludes that it is either a ${}^{10}_{\Lambda\Lambda}$Be or a ${}^{13}_{\Lambda\Lambda}$B hypernucleus.[9] An analysis by Dover *et al*[10] argues for the ${}^{13}_{\Lambda\Lambda}$B interpretation which gives a strongly attractive ΛΛ interaction consistent with both theoretical expectations and the analysis of the two earlier double-Λ hypernuclear events. The emulsion contains a track identified as a π^- emitted from the first decay vertex and the experimenters conclude that this excludes the existence of an H dibaryon lighter than 2203.7±0.7 MeV/c. This corresponds to a limit of B_H<27 MeV. If the interpretation of this event is correct, the allowed range of H particle mass falls within the range of greatest sensitivity of the present experiment.

There is an assortment of H-searches in the literature. The most direct attempt to find evidence for the H was an experiment performed at the AGS by Carroll et.al.[11] using the reaction $p+p\rightarrow K^++K^++X$. An upper limit of σ<40nb was reported, but it has been argued that production of the H through this channel could have a cross section of less than 1 nb. More recently, a hybrid emulsion experiment has been performed at KEK to search for H dibaryon production in complex nuclei using the (K^-,K^+) reaction[12]. The significance of their null result cannot be judged until more reliable estimates of the H production cross sections in complex nuclei are available. The hypernuclear weak decay studies at the AGS have the ability to look for the signature of a very

tightly bound H particle through the reaction ${}^{4}_{\Lambda}He \rightarrow H+p+p$, but the sensitivity is unknown since no rate calculation has been performed for this channel.

In summary, although it is quite important to make an experimental verification of the existence of the H particle, no measurement performed to date has had the required sensitivity to either find the H or to disprove its existence. This experiment will provide a highly sensitivity search in the region of the $\Lambda\Lambda$ mass and below. If the H dibaryon is not found, we will set meaningful upper limits on its production cross section.

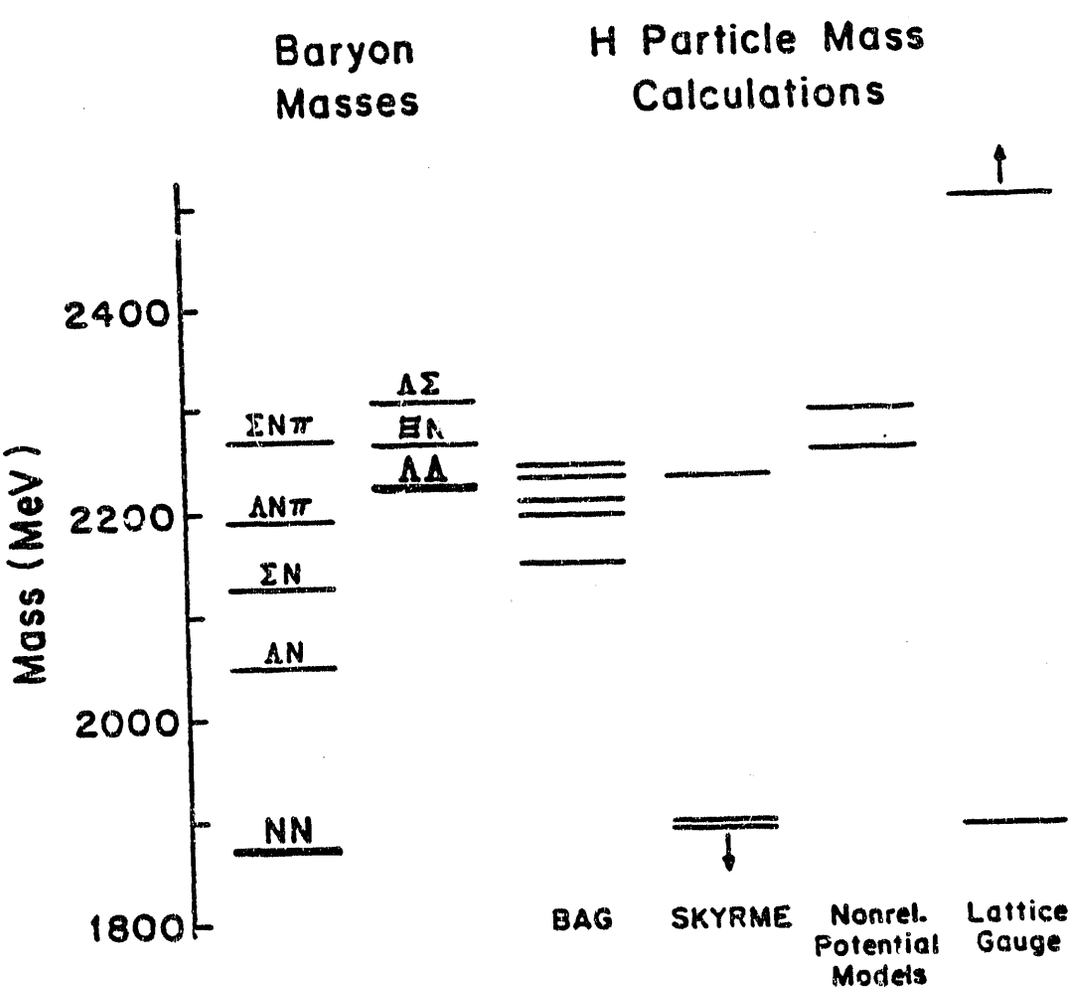

Fig. III.A.1 H Particle mass calculations relative to the baryon masses.

III.B. Experimental technique

In experiment 813, formation of (Ξ^-,d) atoms leading to the reaction $\Xi^- + d \rightarrow H + n$ is used as a sensitive search for the H. The experiment, shown in Fig III.B.1 and Fig III.B.2, involves creating the Ξ^- hyperons in a liquid hydrogen target with the reaction $K^-+p \rightarrow K^++\Xi^-$. The Ξ^- hyperon is then stopped in a liquid deuterium target (by passing through tungsten degraders between the liquid hydrogen and liquid deuterium cells) and detection of the monoenergetic neutrons from the reaction $(\Xi^-,d)_{atom} \rightarrow H+n$ gives a clear, unambiguous signature for the formation of the H. Background levels are greatly reduced by Si detectors, inside the cryogenic target, which tag those events in which a Ξ^- leaves the tungsten degrader at low speed, as indicated by large pulse in one of the detectors.

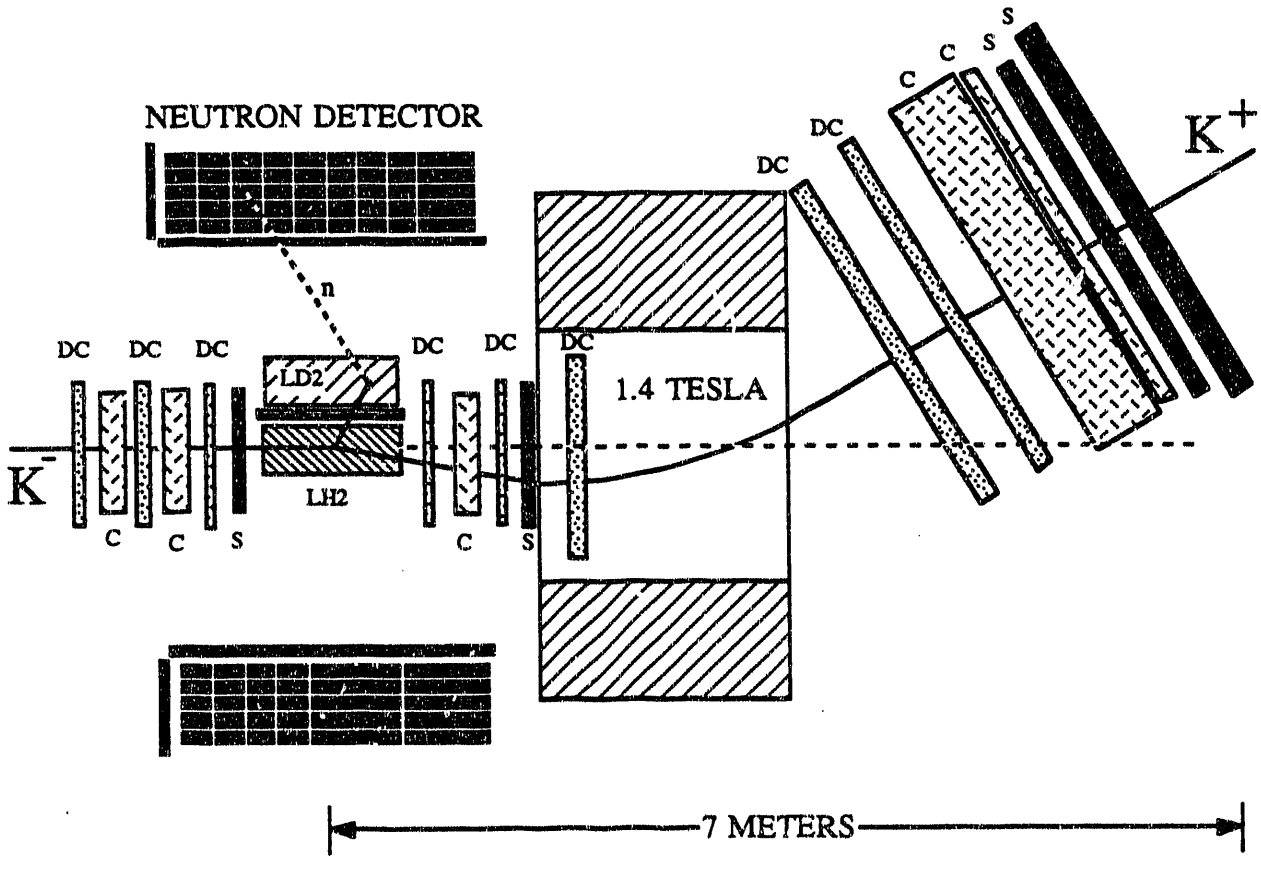

Fig. III.B.1. Schematic layout of the $(\Xi^-,d)_{atom}$ experiment. The detection of neutrons from the reaction $(\Xi^-,d)_{atom} \rightarrow H + n$ will be the signature of H particle production.

The number of detected neutrons resulting from H particle formation then depends on the Ξ^- counting rate, neutron detector solid angle and efficiency and the probability, R, that the $(\Xi^-,d)_{atom}$ will form an H. The calculation of R as a function of B_H by Aerts and Dover[13] have shown that R is near 1.0 if the H mass is near the mass of two Λ's and R decreases to 0.1 as B_H increases to 100 MeV. The experiment will be sensitive to branching ratios as low as ten percent.

To form the H from the $(\Xi^-,d)_{atom}$ and transfer sufficient energy to the neutron to allow its detection, the H must be less than 15 MeV unbound. Thus this experiment is expected to be sensitive in the mass range 100 MeV $>B_H>-15$ MeV.

The original proposal for this experiment discussed the possibility of replacement of the two-component target, used in the $(\Xi^-,d)_{atom}$ H search, with a single ^{3}He target to be used in the reaction $K^-+{}^3He\rightarrow K^++H+n$. Dover[14] has shown that the detection of the outgoing K^+'s is sufficient to prove the formation of the H in the ^{3}He reaction. Its signature is a peak in the K^+ momentum spectrum with FWHM of 30 MeV/c. The centroid of the peak indicates the mass, as shown in Fig. III.B.3. The similarity between the two reaction mechanisms is illustrated in Fig. III.B.4. In May of 1986 a second proposal entitled "Search for a Strangeness –2 Dibaryon Using a ^{3}He Target" requested 700 hours of running for that alternative measurement. That proposal was approved as AGS experiment E836. With the ^{3}He target, greater sensitivity to a more tightly bound H is achieved. Although this second measurement has the advantage of covering a wider mass region, it is technically more difficult due to the need to reject pion contamination to better than $1:10^4$. It also has poor sensitivity in the region of small binding energy because of the large K^+ background resulting from quasi-free Ξ^- production. This region, which may be considered to be the most promising mass region for an H search, is also the region in which the $(\Xi^-,d)_{atom}$ measurement has the highest sensitivity. For this reason, the two measurements are considered complementary.

Fig. III.B.2 shows the detectors used during the 1991 running of E813. The incident K^- beam is momentum analyzed and there are three independent methods of rejecting the π^- contamination. An eighteen meter flight path from the first mass slit to the target area gives a 2.0 ns time of flight (TOF) separation between π and K mesons. Two aerogel Čerenkov detectors each provide additional PID. The presence of three independent tests gives excellent redundancy in particle identification.

The outgoing K^+ mesons are momentum analyzed and again there are again three independent methods of pion rejection. The TOF path is extended past the momentum analyzing chambers of the spectrometer with an array of scintillators approximately seven meters downstream from the target. This gives a 1.1ns TOF separation which is used in conjunction with the two

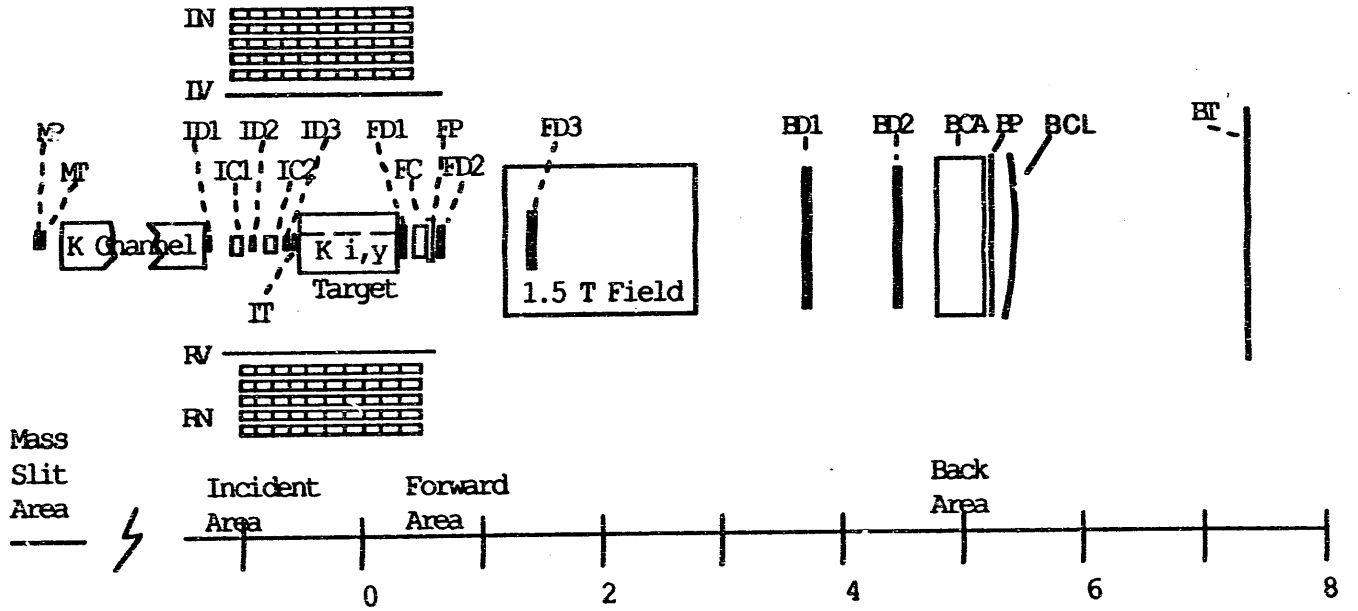

ID1, ID2, ID3, FD1, FD2	x u v Drift Chambers	BCL	Lucite Cherenkovs
FD3, BD2	u y y x Drift Chambers	IN, RN	Neutron Det. Arrays
BD1	u y v Drift Chambers	IV, RV	Neutron Det. Vetoes
MP, FP, BP	Position Hodoscopes	Ki,y	Silicon Pad Detectors (E813 only)
MT, IT, BT	Timing Hodoscopes		
IC1, IC2, FC, BCA	Aerogel Cherenkovs	Target	LH2/LD2 (E813)
			LHe3 (E836)

Fig. III.B.2. Experiments E813 and E836 setup.

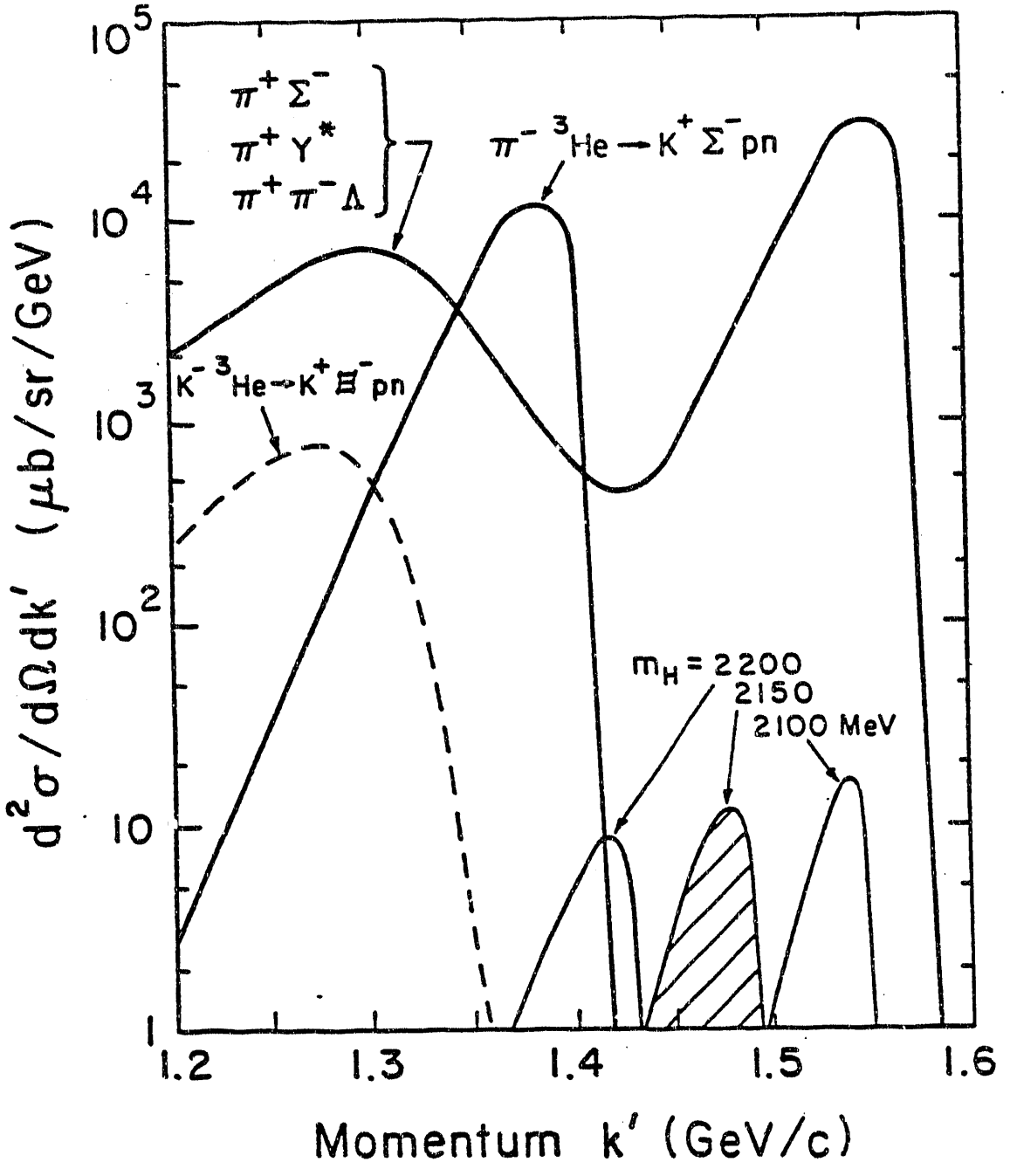

Fig. III.B.3 Predicted K^+ spectrum[14] for ^3He target experiment for three masses of H particle shown with background reactions.

aerogel Čerenkov detectors. Again, any two of the three PID methods should be sufficient for π rejection.

In the K^+ spectrometer, protons can be identified both by TOF and by a critical angle lucite Čerenkov detector. There is a substantial rate of protons from K^- scattering, which would cause an unacceptably large trigger rate if protons are not suppressed. In future running, the proton trigger rate will be reduced by a second-level TOF trigger (with flight-path corrections), and by selecting events of interest by requiring hits in the Si detectors. This should eliminate the inefficiency in the K^+ trigger introduced by the lucite Čerenkov.

An array of neutron detectors surround the target, having a one meter TOF path for measuring the neutron energy. A peak in the neutron TOF spectrum will be the signature of H formation, and the kinetic energy of the emitted neutron will indicate the mass of the H.

Chapter III.A & III.B References

1) R. L. Jaffe, Phys. Rev. Lett. **38**, 195 (1977).
2) M. Oka *et al*, Nucl.Phys. A464 (1987) 700.
3) U. Straub *et al*, Nucl.Phys. A508 (1990) 385c.
4) P. B. Mackenzie and H. B. Thacker, Phys. Rev. Lett. **55**, 2539 (1985).
5) Y. Iwasaki, T. Yoshie, and Y. Tsuboi, Phys. Rev. Lett. **60**, 1371 (1988).
6) H. Ejiri *et al*,, Phys. Lett. B **228**, 24 (1989).
7) M. Danysz *et al*, Nucl. Phys. **49**, 121 (1963).
8) D.J. Prowse, Phys. Rev. Lett. **17**, 782 (1966).
9) S. Aoki *et al*, Prog. Th. Phys. **85**, 1287 (1991)
10) C.B.Dover *et al*, Phys. Rev. C44, 1905 (1991).
11) A.S. Carroll *et al*, Phys. Rev. Lett. **41**, 777 (1978).
12) S. Aoki *et al*, Phys. Rev. Lett. **65**, 1729 (1990).
13) A.T.M. Aerts and C.B. Dover, Phys. Rev. **D29**, 433 (1983).
14) A.T.M. Aerts and C.B. Dover, Phys. Rev. Lett. **49**, 1752 (1982).

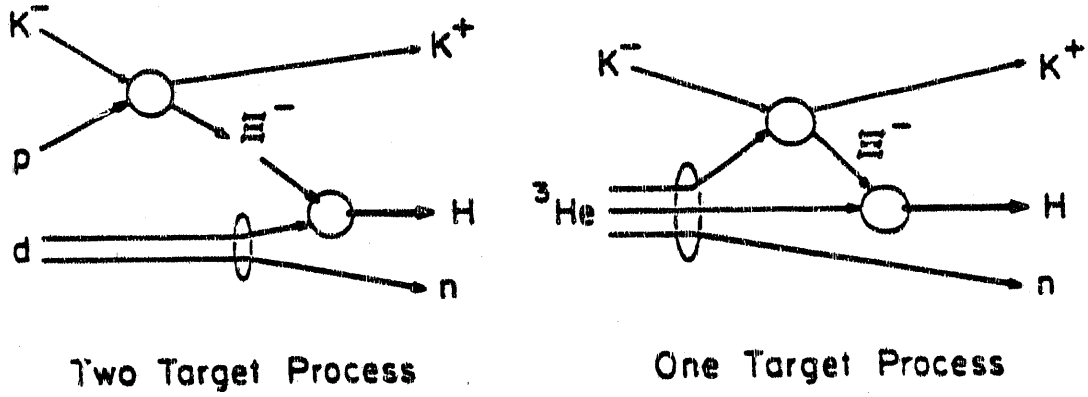

Fig. III.B.4. Comparison of the $(\Xi^-,d)_{atom}$ and the ^3He target production mechanism.

III.C. Results of 1991 Run

All major construction projects needed to undertake the E813 H Dibaryon search were completed by the start of the AGS's 1991 Slow Extracted Beam (SEB) period (April-June). Startup problems encountered during the early portion of the SEB period, both in the beam line elements and the detectors, were solved such that production running could begin after a period of beam-line tuning and conditioning lasting several weeks.

One problem encountered on the beam line concerned the two new electrostatic separators built according to a design not previously used at Brookhaven. The two new beam line separators needed more time to condition than was expected and did not achieve their specified operating voltages. The compromise solution implemented for the 1991 SEB period was to operate the beam line to deliver K^-'s at a momentum of 1.7 GeV with a π/K ratio of 4/1 (the original design called for 1.8 GeV with a π/K ratio of 1/1). Problems with the remote control collimation and slit control were also encountered.

During the final stages of preparation some problems were noted in the performance of the 5 inch Photo Multiplier Tubes (PMT's) in the fringe field of the 48D48 spectrometer magnet. This would affect the efficiencies of the detector elements using these PMT's. Major modifications on the affected detectors were needed to allow the experiment to proceed. The detectors employing 5 inch PMT's are all the Aerogel Čerenkov detectors IC1, IC2, FC, and BCA. Significant shielding improvements were made to the Forward Čerenkov (FC) and both Incident Čerenkovs (IC1 & IC2). The Back Čerenkov Aerogel detector (BCA), underwent a minor modification in the placement of its 5 inch PMT's within their individual magnetic shields. This enhanced BCA's performance to a level acceptable for the E813 experiment.

Contamination of the primary trigger due to kaon scattering proved to be a major problem. Events of the type $p(K^-, p)X$ were inadvertently included as events of type $p(K^-,K^+)\Xi^-$ due to mis-identifying the proton as a K^+. This problem had been foreseen, but the actual trigger rate was even greater than anticipated. Prior to the 1991 run, two ideas had been brought up to counter this problem. These solutions were based on the fact that protons and K^+s emerging from the 48D48 spectrometer hitting BT at identical vertical positions have different velocities and must differ either in their trajectories or flight times.

The first solution involved building critical angle Čerenkov detector, the Back Čerenkov Lucite detector (BCL), which was placed immediately behind BCA. The lucite radiator elements were curved so they would always be roughly perpendicular to the particles striking them. The Čerenkov light from kaons was emitted at a large enough angle that some of it was internally reflected and guided to the PMT's. The light from the slower protons escaped from the lucite and did not reach the PMT's.

The other solution for rejecting proton events involved implementing a second level trigger into the Data Acquisition (DAQ) program. The DAQ would be provided with a look-up table which tabulates hits on Forward Drift Chamber 3 (FD3) and Back Time-of-flight wall (BT) giving the maximum expected time of flight for a K^+ emerging from the 48D48. When implemented, the DAQ would abort an event if hits on FD3 and BT do not correspond to the observed time of flight for the particles of interest: the K^+s. This is called a second level trigger because partial event readout would be needed to determine in software whether the event is good (to be fully read out), or bad (to be aborted). Fast encoding FERA and FERET electronics were used to read out the BT and Incident Timing (IT) elements and a custom-built board was made to provide the FD3 hit pattern.

Both solutions were pursued vigorously early in 1991. BCL, known as 'Lucy', was completed, installed, and calibrated late in May. By early June, Lucy's trigger bit was in the data stream. After a check-out period, to make sure that the bit did not introduce unintended bias in the data, Lucy was included in the trigger definition. A pre-scaled fraction of events which did not require Lucy was also included as a precaution. Unfortunately, Lucy proved to be only 60% efficient for kaons, and although it reduced the (K^-,p) trigger rate by more than a factor of six, the dead time was only reduced to 40%.

The implementation of the second level trigger turned out to be more complicated than expected. Problems were encountered interfacing the main DAQ processor with the slave processor that would actually do the fast readout and second-level trigger decision. After this was solved, calibration studies had to be made to create the look-up tables. The required careful calibration of the flight time counters took some time, so reliable cuts were not ready during this running period. The entire system was successfully tested however, and it is expected to be implemented for the 1992 running period.

At the end of the SEB period on June 30, 1991, E813 had accumulated 703 hours of production running out of the 1000 hours requested. We estimate 250 of the charged hours were used for tune-up and calibration and 450 hours could be considered production running. The proton flux on the production target was quite low during most of these 450 hours. We received approximately 6×10^{10} K^-'s during the production running and more than 60% of these were during the last 8 days of the run during the period that the proton flux exceeded 5×10^{12} protons/pulse. This represents only 6% of our goal of 10^{12} total K^-'s on the E813 target.

The beam line performed very well; the measured flux scales to 8×10^5 K^- per 10^{13} protons. We expect the K^- flux to be significantly greater in the future runs. Since the 1991 run, the AGS separator group has greatly improved the separator performance; this will allow us to run at 1.8 GeV/c in 1992 and should produce a cleaner K^- beam. This higher momentum, along with

repairs and modifications to the 2 GeV/c beam line, should also increase our K^- flux. We expect to reach our goal of 10^6 K^- 's per pulse at 1.8 GeV/c if we receive ~ 6×10^{12} protons per pulse. Assuming a flux of 10^6 K^-'s per pulse and 3.5 seconds/pulse during the 1992 running we would get 10^9 K^- / hour.

Approximately 10% of the 1991 data was reduced by November of 1991, the bulk of the data was reduced in February of 1992. The results are very encouraging. Time-of-flight cuts correlated to hit positions in FD3 have been developed and used in this first data-reduction pass. In future runs, a similar procedure will be used on-line as a secondary trigger.

The experimental apparatus as been proven successful in identification of the $K^-+p\rightarrow K^++\Xi^-$ reaction. This is done by determining the momentum and path length of the particles passing through the 48D48 spectrometer using the drift chamber information. This is then combined with the time-of-flight measured by detectors IT and BT to determine the particle's mass. Figure III.C.1 shows a 2-dimensional plot of measured particle momentum vs. measured mass. The $K^-+p\rightarrow K^++\Xi^-$ events can be clearly seen. A 1-dimensional histogram of measured particle mass is shown in Fig. III.C.2. The kaon events can be cleanly separated from the pions and protons. Once these K^+ events are selected, the measured K^+ momentum can be combined with the K^- momentum measured by the beam-line detectors to produce the missing mass plot shown in Fig. III.C.3. The peak corresponds to production of Ξ^- hyperons.

The Ξ^- hyperons which pass through the tungsten energy degraders are tagged by diffused junction silicon detectors. Considerable effort went into the development of these specialized de ectors which operate at 20° K. Figure III.C.4 shows a time vs. pulse height distribution. Although we were initially concerned that the halo of the K^- beam interacting with the tungsten would create an intolerable background in the silicon detectors, we can now see that nearly all the large pulse height silicon hits are in-time with the in-beam trigger and accidental coincidences are not a significant problem. In future runs, a silicon-hit will be required in the on-line trigger to reduce the demands on the data-acquisition system.

It is interesting to consider the fraction of (K^-,K^+) events which have hits in the silicon detectors as a function of the outgoing K^+ angle. For small outgoing K^+ angles, the Ξ^- is produced with a kinetic energy around 100 MeV and should not penetrate the tungsten energy degrader. Although their decay products may reach the silicon detectors, the pulses from these tend to be smaller than pulses from the heavily ionizing Ξ^- Figure III.C.5 shows that the fraction of events with hits in the silicon detectors dramatically increases as the outgoing K^+ angle increases. For large K^+ angles, the Ξ^- has a relatively large probability of penetrating the tungsten and reaching the silicon detectors. However, these Ξ^-'s tend to have kinetic energies well above 30 MeV as they reach the silicon detectors. They will give a smaller signal and have a

low probability of stopping in the liquid deuterium. Monte Carlo simulations indicate that events with K^+ angles between 7° and 9° which have silicon tags with pulse heights greater than 1.0 MeV. The events with K^+ mesons in this region are denoted "interesting K^+ events". The simulations indicate that ~4% of the interesting K^+ events should have a corresponding silicon tag greater than 1.0 MeV. This is in good agreement with the value of 3.4 % which was extracted from the actual data.

The fraction of silicon-tagged events which result in a $(\Xi^-,d)_{atom}$ is predicted to be 25%. Our ability to stop Ξ^-'s in liquid deuterium along with the neutron detector efficiencies will be cross checked using a trigger which selects $\pi^- + p \rightarrow K^+ + \Sigma^-$ events. For K^+ production angles near 9°, the corresponding Σ^-'s have a range and trajectory matching the Ξ^-'s from the $K^- + p \rightarrow K^+ + \Xi^-$ reaction and thus have a similar stopping probability. We will attempt to identify pseudo-monoenergetic neutrons from the reaction $(\Sigma^-,d)_{atom} \rightarrow n + \Lambda + n$. In a model which treats the initial neutron is treated as a spectator we expect to observe energetic neutrons with a narrow spread in energy peaked near 42 MeV. We should have sufficient statistics to search for this calibration signal when the 1992 running is completed.

The coincident neutron spectra for events with K^+'s production angles between 7° and 9° and coincident silicon tags greater than 1.0 MeV is shown in Figs. III.C.6.1 and III.C.6.2. These spectra, based on 0.06×10^{12} K^-'s on target, do not have the statistics to extract a signature of H-particle production. While it is statistically possible that one or two of the events in these figures are from the reaction $(\Xi^-,d)_{atom} \rightarrow H+n$, it is not possible to distinguish them from the background. The goal of E813 to achieve a sensitivity to H production from the reaction $(\Xi^-,d)_{atom} \rightarrow H+n$ for branching ratios as low as $R = 10\%$. We estimate that this will require a total of 10^{12} K^- mesons on target as illustrated in the following discussion.

Monte Carlo simulations show that reactions in which the K^+ is produced at a scattering angle between 7° to 9° produce Ξ^-'s which have a 1% probability of forming a $(\Xi^-,d)_{atom}$ and undergoing a strong interaction before decaying. The 1991 analysis shows that we are extracting 6.8×10^4 these "interesting K^+ events" per 10^{12} K^-. This number is affected by the low efficiency of the lucite Čerenkov used to reject protons (60%), low data acquisition live time (60%), and the fraction of K^+'s which survive to the time-of-flight wall BT (43%). Assuming a reconstruction efficiency of 80% leads to a result consistent with the expected cross section of 30μb/sr. This results in an overall efficiency of 12%. In future runs, the use of the silicon detectors in the trigger combined with an on-line time-of-flight cut should allow us to take the lucite Čerenkov out of the trigger and still increase the live-time from 60% to better than 85%. Increasing the incident beam momentum from 1.7 GeV/c to 1.8 GeV/c will increase the K^+ survival factor to 46%. We have made significant improvements in the target area drift chambers and are adding an additional plane

to BD1. Assuming that this results in a 10% increase in reconstruction efficiency, we should gain a factor of (1 / 0.60)·(0.85 / 0.60)·(0.46 / 0.43)·(1.1) = 2.8. Thus we expect:

$$1.9 \times 10^5 \text{ interesting } K^+\text{'s per } 10^{12}\, K^-$$

Approximately 1% of these events form $(\Xi^-,d)_{atoms}$ and undergo a strong interaction. The neutron detector array efficiency times solid angle is ~9%. This gives:

$$170 \cdot R \quad \text{detected neutrons per } 10^{12}\, K^-$$

where R is the branching ratio for $(\Xi^-,d)_{atom} \rightarrow H+n$

The signal to noise can be calculated by considering the subset of interesting K^+ events in which the silicon detectors tag a low energy Ξ^- exiting the tungsten energy degrader. Approximately 4% of the interesting K^+ events should give tagged Ξ^- signals. This gives:

$$N_{tag} = 7.6 \times 10^3 \text{ tags per } 10^{12}\, K^-$$

The simulations show that 25% of these tagged events should have Ξ^-s which stop and interact before decaying. The number of neutrons from H production, N_H is related to the number of tagged Ξ's, N_{tag} and the neutron efficiency and solid angle:

$$\begin{aligned} N_H &= R \cdot 0.25 \cdot 0.09 \cdot N_{tag} \\ &= R \cdot 0.02\, N_{tag} \end{aligned}$$

The existing data can be used to extract the background signal per 0.5 ns bin in the neutrons detectors. A preliminary analysis gives:

$$\begin{aligned} N_B &= 0.005\, N_{tag} \\ &= \sim 38 \end{aligned}$$

The signal to noise is thus $R \cdot 0.02 / 0.005 = 4 \cdot R$.

If the H mass is near the mass of two Λ's and the Nijmegen model D for the hyperon-nucleon interaction is assumed , we expect:

branching ratio	$R = \sim 80\%$
detected neutrons from H production	$N_H = 130$

background under peak	N_B = 38
significance	21 standard deviations

If the branching ratio is only 10%, we would get:

branching ratio	R = ~ 10%
detected neutrons from H production	N_H = 17
background under peak	N_B = 38
significance	2.7 standard deviations

The branching ratio calculation by Aerts and Dover indicate that this would result in a sensitivity to an H mass as low as ~80 MeV below the $\Lambda\Lambda$ mass. This provides a large overlap with the region of sensitivity of our complementary experiment, E836. The present experiment will be highly sensitive in the region around the $\Lambda\Lambda$ mass when increased statistics are obtained.

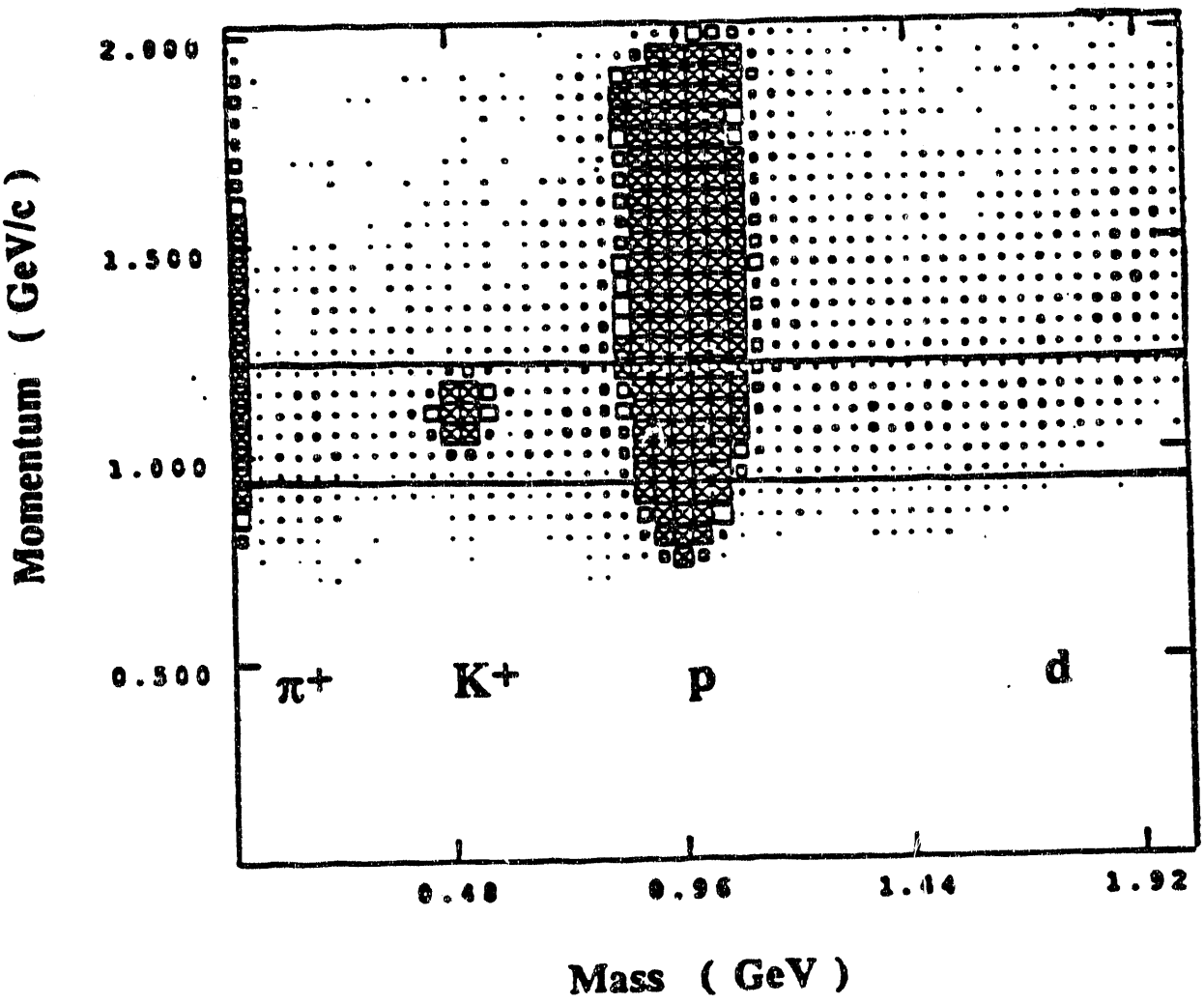

Fig. III.C.1 Two-dimensional plot of the momentum vs. the calculated mass of particles passing through the 48D48 magnet.

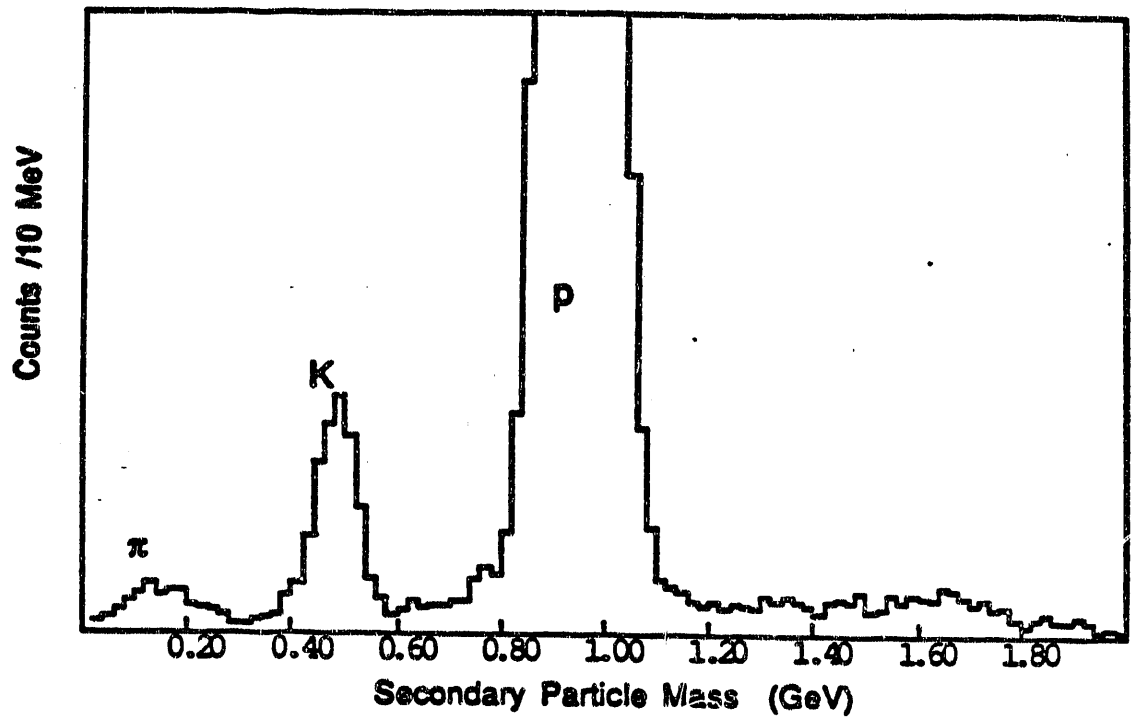

Fig. III.C.2 Mass spectrum of particles passing through 48D48 spectrometer from 1991 E813 run. Mass is calculated from the IT to BT time-of-flight combined with momentum and path length determined by drift chambers.

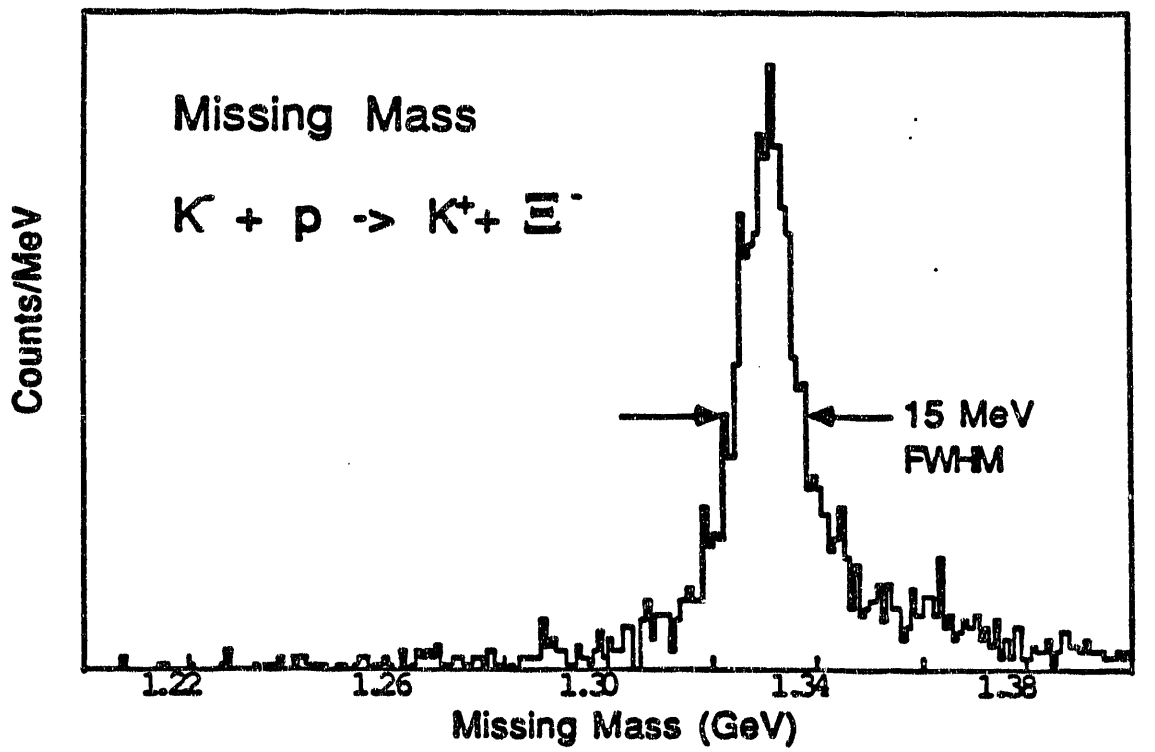

Fig. III.C.3 Missing mass determined by incident K^- and secondary K^+ momentum and trajectories from 1991 E813 run. Peak corresponds to production of Ξ^- hyperons from the reaction $K^-+p \rightarrow K^+ + \Xi^-$.

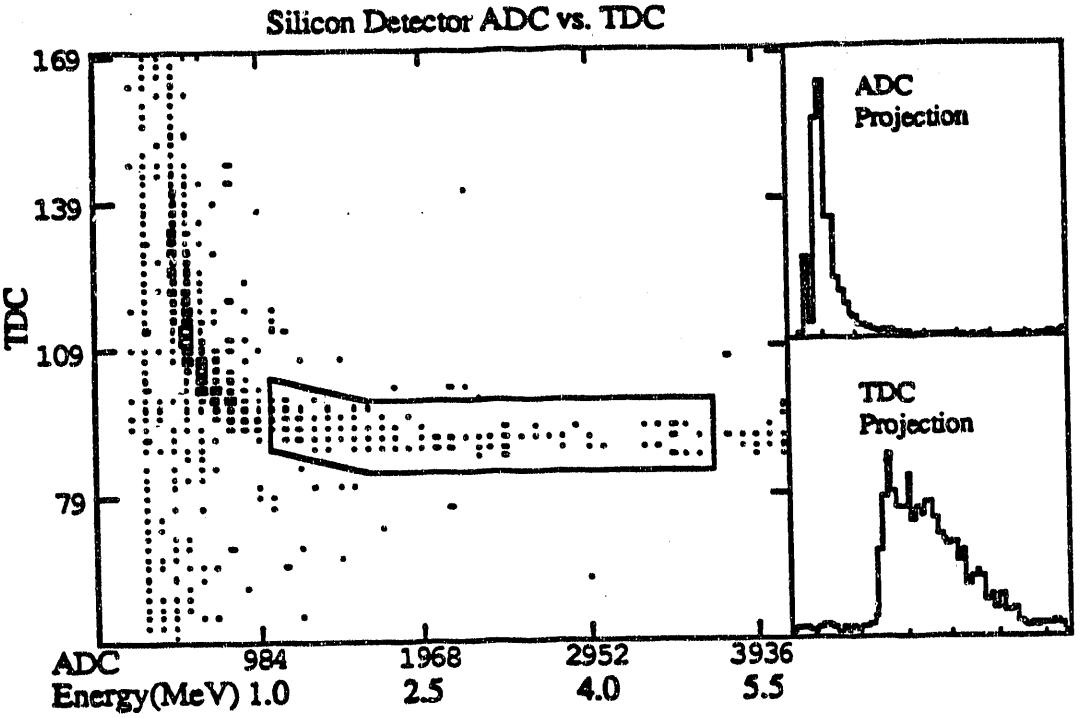

Fig. III.C.4 Sample of ADC vs. TDC distribution for hits in the silicon detector array, summed over all 160 detectors, taken during the 1991 run. The y-axis shows the time relative to the (K^-, K^+) trigger with an arbitrary offset. The plot illustrates the low accidental background for large pulse heights. The ADC scale is also converted to a rough energy loss scale. The blocked region indicates the region where we expect to find Ξ^- hyperons which have a large probability of stopping in the liquid deuterium.

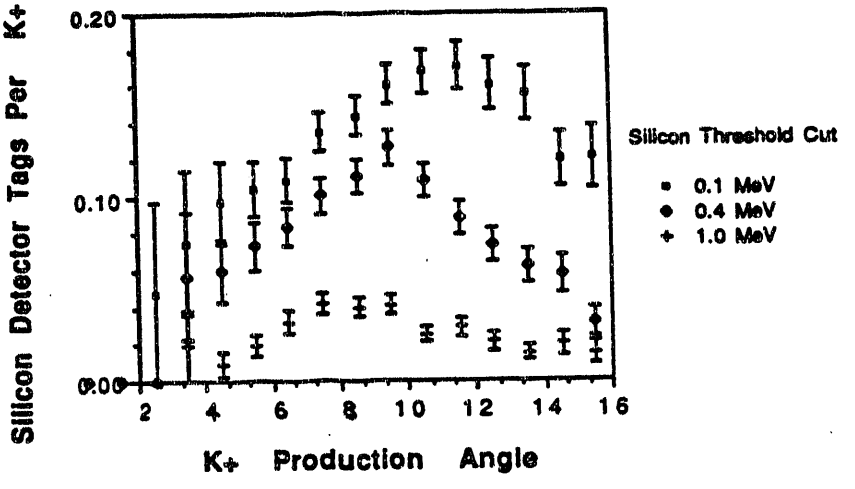

Fig. III.C.5 Fraction of $K^- + p \rightarrow K^+ + \Xi^-$ events which result in a silicon detector hit. This fraction is shown as a function of K^+ angle for three different silicon pulse height thresholds. Small K^+ angles correspond to events in which the Ξ^-'s will decay or stop in the tungsten. Large K^+ angles correspond to events with energetic Ξ^-'s which give small signals in the silicon detector. Intermediate K^+ angles correspond to low energy (~20 to 30 MeV) Ξ^-'s which give large signals in the silicon detector and have a high stopping probability.

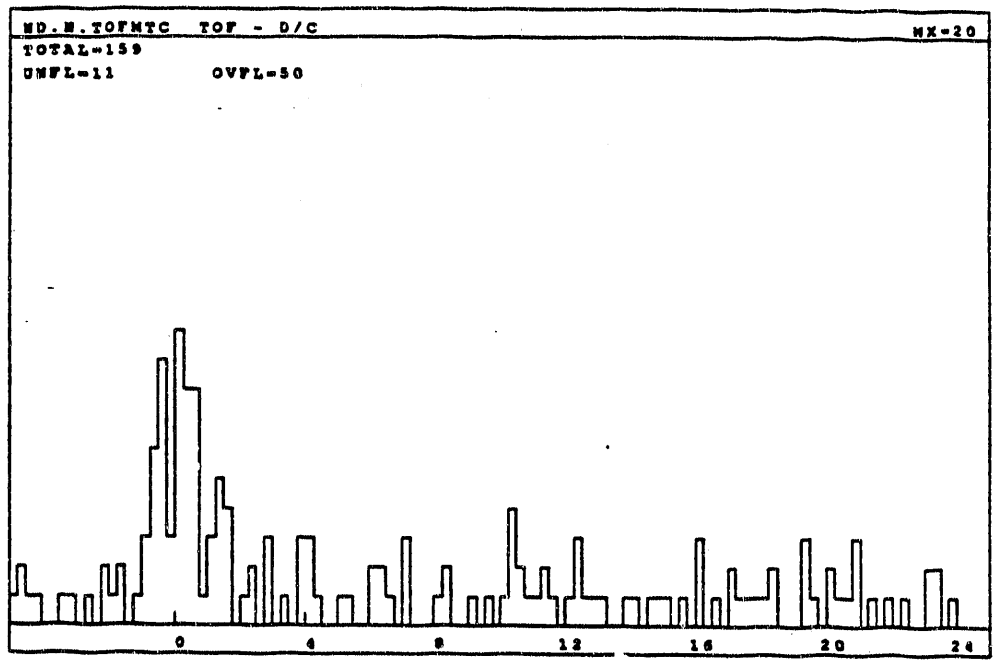

Fig. III.C.6.1 Neutron time-of-flight spectrum for events which have been tagged as candidates for stopping Ξ^-'s. The expected travel time for a $\beta = 1$ particle has been subtracted off so photons will be aligned at zero.

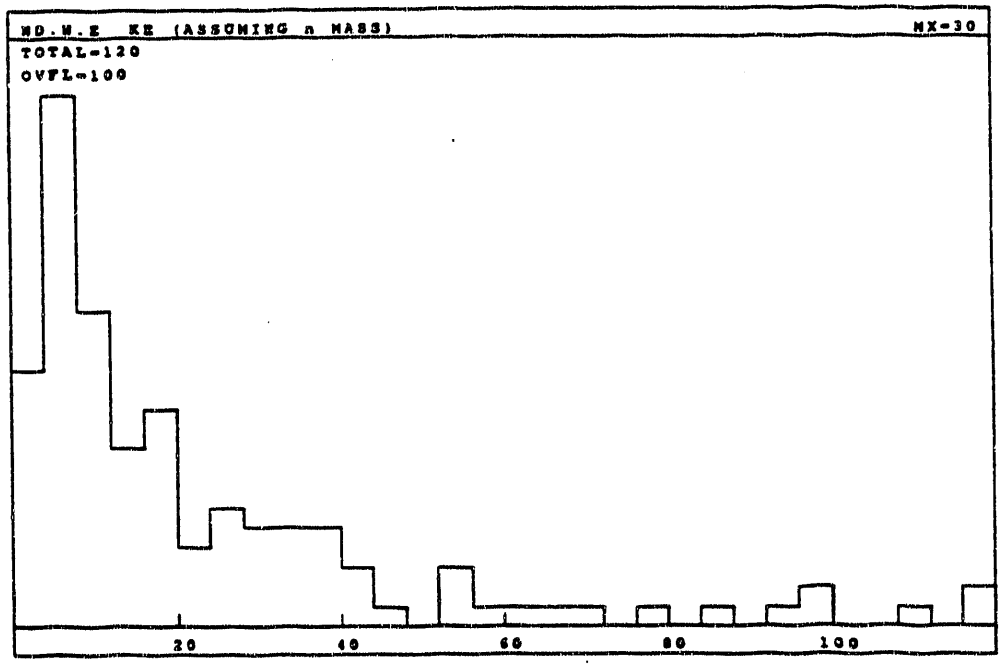

Fig. III.C.6.2 Neutron kinetic energy spectrum (as determined by time of flight with flight path determined by position of the hit) for the same events included in figure III.C.6.1.

III.D. Equipment Performance Update

The Carnegie Mellon Medium Energy Physics group has developed and built a substantial number of the hardware and software items used in the H particle searches. Reports on these projects have appeared in our annual progress reports over the past several years. Most of these projects have been completed and the results are presently in use during the running of the experiments at BNL. In this section we discuss only briefly the status and operational experience with a number of the items developed by our group. The reader is referred to our progress reports of 1989-1990 and 1990-1991 for extensive discussions of these projects.

III.D.1. Cryogenic Targets for the H Searches

The $(\Xi^-,d)_{atom}$ version of the H search, E813, uses a highly specialized target design, since the number of stopped Ξ^-'s and the experiment's signal-to-noise ratio are critically sensitive to the target geometry. Extensive work went into the design, optimization, and construction of this hydrogen/deuterium cryogenic target.

The design studies required accurate simulation of the Ξ^- stopping power, straggling, and multiple scattering effects. A specialized Monte Carlo code was written to study alternative target designs after the GEANT3 package was found to be too slow and inaccurate. The results have been reported in CMU internal report CMU/ME - 006/88 and in our 1987-88 progress report.

These studies produced the present target design. A 82 cm liquid hydrogen (LH2) target lies below a liquid deuterium (LD2) vessel which has twenty Ξ^- stopping regions or "cells", each 2 cm long. Each stopping cell is preceded by a 1 cm long energy degrading cell which consists of a beveled tungsten slab followed by a diffused-junction silicon-pad detector. Using the Monte Carlo code, the geometry was optimized to maximize the fraction of those Ξ^-'s created in the LH2 target which come to a stop in the LD2 target. A silicon detector array, which tags the Ξ^- hyperons as they exit the tungsten energy degrader and enter the liquid deuterium vessel, has three primary functions: 1) redundant instrumentation to the in-beam detectors to help generate a clean tag of $K^-+p\rightarrow K^++\Xi^-$ 2) identification of events in which the Ξ^- travels through the liquid hydrogen and tungsten energy degrader without decaying, and 3) identification of the Ξ^-'s which enter the liquid deuterium vessel with a kinetic energy low enough to have an appreciable probability of stopping and forming a $(\Xi^-,d)_{atom}$. Additional discussion of the silicon-pad detectors can be found in section III.D.2.

The conceptual design of the cryogenic target was done at Carnegie Mellon and the detailed engineering drawings were developed R. Meier and L. Addessi of the AGS cryogenics group working closely with Carnegie Mellon. The main components of the vessels were manufactured by Hall Industries (Pittsburgh, PA) under contract to CMU and completed in the summer of 1990. The system worked nearly flawlessly throughout the 1991 running period, and it is again in operation during the 1992 running period.

III.D.2 Silicon Detectors for Tagging Ξ^- Particles

A critical component of experiment E813 is the set of silicon detectors mounted in the cryogenic vessel which tags those events in which a very low energy Ξ^- particle enters the liquid deuterium vessel. The diffused-junction silicon detector project was completed in time for last year's running and was reported in last year's annual report. At that time, we reported 154 out of 160 operational detector elements, with reliable detection of Ξ^- signals in the energy region of interest. These results are discussed in section III.C. This status has not changed; we did not attempt to improve the number of working detectors due to the large turn-around time required for target disassembly and reassembly.

Since last years report we have calibrated, by pulser, the pulse height for each of the detector/preamp channels. This is the simplest approach we have for determining the variation in the gains for the detector/preamp system, however, it assumes that the detector thickness and the effective detector capacitance are related simply. This is not obvious, since the significant capacitance of the leads must be taken into account. We are presently trying to use a scheme that takes advantage of $K^- + p$ elastic scattering at back angles. The back-scattered kaons should produce a signal roughly three times minimum ionizing pulse height. At present, we find that determining sufficiently precisely which detector was most likely to have a back scattered kaon signal based only on the proton information is still somewhat problematic, thus it is hard to discern the kaon peak from noise. We anticipate that with further efforts to reduce this uncertainty, as well as efforts to reduce the amount of noise seen in the ADC's, a clear signal can be seen, giving us a reliable way to calibrate precisely the detector/preamp gain.

III.D.3 FD3 Drift Chamber and Gas Mixing System

Drift chambers for experiments on the 2 GeV/c beam line were constructed and are maintained by three groups. The FD3 drift chamber, which sits inside the spectrometer magnet, was constructed at CMU. Brookhaven provided the chambers upstream of the spectrometer, and the University of Freiburg provided the downstream chambers. Figs. III.B.1 and III.B.2 illustrate the position of these detectors.

FD3 has a cell structure with four layers of sense wires which measure, in the coordinate system of the experiment, u, y, y' (same as the y coordinate but offset vertically by one-half cell in the y direction), and v. Since particles traversing the 48D48 magnet are bent vertically, the y measurements are of primary importance, while the u and v position information is useful mainly in track reconstruction. The overall dimensions of the detector are 24" by 38", while the active area is 18" by 32". The chamber has a spatial resolution, while operating in a 1.4 Tesla magnetic field, of about σ=200μm.

During the 1991 run, FD3 performed well mechanically and electrically. Dark currents remained under 10 nA, and efficiencies were well over 90% per plane. Distortions in some of the drift-time spectra from this detector were traced to a faulty TDC, which was replaced, however, before the bulk of the "good" 1991 data were collected. Also, a second FD3 chamber was completed in the early fall of 1991, so that we now have a complete spare detector in the event of a serious problem with the first one.

A special function of FD3 is that of a fast position measuring device for scattered particles. This is needed in connection with the second level trigger which is used to separate scattered kaons from scattered protons. It is far enough from the long LH2 target to give an approximate scattering angle, which can be correlated with the time of flight of the particle to the rear time-of-flight wall (See section III.D.8); this correlation is used to make an on-line rejection of proton events. The fast position information from FD3 is obtained using a CMU-built circuit board which OR's signals from the LeCroy 1879 TDC's in such a way as to present a 16-bit wide pattern of hits to an input register in our FERA/FERET readout crate. This circuit and the associated software were developed during the 1991 run and are ready for full implementation in 1992.

The gas mixture we are using in FD3 is 76% argon, 20% isobutane, and 4% methylal, a mixture which has been shown to have good chamber aging characteristics. A gas filtering and mixing system was built two years ago which allows precise control of the gas mixture, so that long-lasting high pressure gas bottles can be used rather than low-pressure bottles of premixed gas. In 1991, the gas mixing system was used to supply gas to FD3 as well as the large Freiburg drift chambers placed downstream of the spectrometer magnet. In 1992, all the drift chambers in the experiment (including the upstream BNL chambers) operate with gas from this mixing system.

III.D.4. Neutron Counters

The signature of H dibaryon production in experiment E813 is the detection of mono-energetic neutrons emitted in the $\Xi^- d \rightarrow H\, n$ reaction. If a peak is found in the neutron energy spectrum, the energy of these neutrons will reveal the mass of the H particle. A large array of neutron counters with good energy resolution is, therefore, an important component of this experiment. These detectors were designed at CMU. The detector-elements were built jointly by CMU and University of Manitoba.

The neutron detectors are grouped into two arrays of 50 logs each. The logs are 2" × 6" × 72" blocks of BC-408 scintillator with tapered light guides and XP-2262H PMT's at each end. The PMT bases and housings are our own design, one which makes them particularily easy to install and change. Each array consists of 5 layers of 10 logs, a thin charged-particle veto layer and a rigid support frame which protects the logs. The frames are designed to allow the arrays to be easily lowered from their normal operating positions (in which the logs stand on end) to a horizontal position in which the counters can be calibrated with cosmic rays and serviced, if necessary. Each log has a quartz optical fiber connected at the center to allow testing and calibration by sending a sub-nanosecond U.V. laser flash to each log, causing scintillation. The support frame and laser calibration system were designed and built at CMU.

Energy of the detected neutrons is determined by time of flight, which can be measured to 300ps FWHM for 10 MeV (electron equivalent) energy deposited. Position within a log can be determined to several centimeters from the difference in arrival time of the light at each end.

Analysis of the data from the 1991 running period of the H-particle search (E813) has shown the accidental coincidence rate in the neutron counters to be only a few percent, integrated over the entire time of flight range of interest. The rate of n-counter coincidences was higher for good tagged Ξ^- events, indicating that the background rate is dominated by particles originating from the decays or interactions of the Ξ^-, as expected. With average hardware thresholds of approximately 2 MeVee (MeV electron equivalent), the background rate for the entire array of 100 detector logs was found to be 0.004 hits per ns of flight time per event. Refer to Figs. III.C.6.1 and III.C.6.2. They were based on a somewhat restrictive definition of neutron candidates. It required not only that the vetoes did not fire, but also that other logs within the stack did not fire. This latter requirement was included to eliminate photon-induced showers. Further study is continuing to find less restrictive definitions which will continue to reject most photon-induced events but will not reject events in which a neutron causes ejection of a high energy proton, firing additional counters. Along with the increased sensitivity resulting from implementing an improved algorithm, the background rate may be expected to increase somewhat, but by less than a factor of two. Because the signal of H particle production may be expected to be a peak only 0.5 ns wide (dominated by the resolution and finite thickness of the counters) the background neutron signal

may be expected to be no more than 0.004 per tagged event . A tagged event is one which has a Ξ^- is produced in the proper angular range and shows a large pulse in a nearby silicon detector. Only tagged events will contribute to the final background under any H-production signal.

After the 1991 run of E813, the two neutron counter stacks were lowered to allow calibration with cosmic rays. This included determination of appropriate time offsets for all PMT's to compensate for any differences in cable delays. The use of vertical cosmic rays to align the timing of logs relative to each other was simplified by the arrangement of the neutron counters in staggered layers so that adjacent logs in one layer were vertically in line with a common log in another layer. The cosmic ray calibration data was also used to determine the gains of all PMT's and to deduce voltages which should equalize the gains of the PMT's for all logs. These voltages were set before the beginning of the 1992 running period and the gain-equalization was refined with additional cosmic-ray calibration. The gains were set to a higher value, to allow greater efficiency for detecting neutrons during the 1992 running. If the accidental coincidence rate is found to be too large, a software threshold will be imposed on the geometric mean of the ADC's.

Very little maintenance has been required on the neutron counters in the two and a half years since the stacks were assembled. All 100 logs are operational for the 1992 running of E813.

III.D.5. Forward Position Hodoscope

Early in 1990, it was decided that a scintillation detector should be added to the H-particle experiment between the target and the 48D48 magnet. This device, the Forward Position Hodoscope (FP), consists of 16 horizontal strips of 4mm thick scintillator material. Each strip is 1.5 cm high by 21 cm wide and the total device has an active area of 21.0 × 24.0 cm. The light from the scintillator is directed by L-shaped light pipes to 1.9 cm Hamamatsu H3167 PMT's.

FP was positioned between the Forward Cerenkov counter (FC) and the second Forward Drift Chamber (FD2), which is immediately in front of the 48D48 magnet gap. Both the beam and scattered particles pass through FP. Because of its proximity to the magnet, heavy iron shielding was required around the PMT's. Due to this weight, the detector was designed to retract from the 48D48 field clamp aperture by sliding the detector along mounting rails to allow access to FD2.

The FP hodoscope has several functions: 1) Its upper, in-beam elements are used as beam vetoes. 2) Its lower, out-of-beam elements define the acceptance of the spectrometer. 3) It reduces ambiguities due to multiple hits in the Forward Drift Chambers FD1 and FD2.

Construction of FP was completed in the first months of 1991. Despite one PMT that failed during the 1991 run, FP performed all it's tasks. The broken PMT served an in-beam element and continued to function as a beam veto, operating with only one PMT throughout the rest of the running period. FP's performance has so far been analyzed using hit distributions only. The broken PMT has been replaced and FP is ready for 1992 SEB period.

III.D.6 Electronics

A significant fraction of the electronics for the H-particle search were provided by CMU; this includes nearly 700 channels of both discriminators and NIM-to-ECL converters, 500 channels of scaler multiplexers, patch panels for all the Fastbus ADC inputs, and a third of all Fastbus modules used for data acquisition. Of particular note are the NIM-to-ECL converters, scaler multiplexers, and patch panels, which were designed and built at CMU. All this hardware was available and operational during last year's run, and no significant changes to this hardware was needed for use in the 1992 run. Some minor modifications were made to accommodate the strangelet search experiment (E886) run this spring (see Chapter V). Here, the range in flight times of interest far exceeds the 100 ns range of the Fastbus TDC's. We found that we could internally modify the TDC's to change the time range to ~400 ns without degrading the performance (linearity, stability, etc.), thus allowing these TDC's to be used in the strangelet experiment without fundamental changes in the data acquisition hardware. The trigger electronics for the strangelet experiment were, for the most part, added parasitically so as to minimally disrupt the normal H-particle search electronics set-up. This could be done because of the sufficiently modular design of the electronics lay-out.

One major problem in the hardware was uncovered during the 1991 run. It appeared that the KineticSystems (KS) TDC's, while stable for single inputs, suffered severe time shifts when multiple hits were registered in a given module. Not all channels were affected, and some channels exhibited larger time shifts than others. This effect was not seen earlier because it was much more pronounced in the modules purchased just prior to the 1991 run. At CMU, we determined the cause to be a design flaw in the routing of certain signals on the motherboard of the TDC. We brought this to the attention of KS engineers and offered a solution; all of the TDC modules we had on hand have now been corrected. We also discovered a cross-talk problem in the TDC paddle card inputs. Again, KS engineers were quick to redesign the paddle cards and these new cards will be available for the 1992 run. These problems did not severely affect the results of the 1991 run, but would have been a problem with the anticipated increased beam intensity for the 1992 run.

III.D.7 Spectrometer Modeling

In the summer of 1991, a Runge Khutta track fitting routine was used to examine data obtained for E813. This method of tracking was found to be prohibitively slow, and alternative methods of track fitting were explored. A method using first order transport theory was found to be promising. A program using this method was developed and tested using Monte Carlo data as well as data from the 1991 run of E813.

The track fitting routine, called PEANUT, approximates tracks in a small region of phase space with a linear extrapolation from a central track. This allows tracking through the 48D48 spectrometer magnet with one matrix multiplication. The errors introduced due to this linear approximation is directly related to the size of the region of phase space for which the matrix is assumed valid. With the acceptance of the spectrometer broken into many regions, the errors introduced can be made arbitrarily small. These errors were studied, and the number of regions was chosen to keep the errors smaller than the errors in the measured magnetic field map. The field map of the 48D48 magnet was fitted with harmonic polynomials (see Annual Progress Report 1991); the measurements and the results of the fit agree to within 0.3%. By breaking the spectrometer acceptance into 480 regions, the errors due to the linear approximation were found to be within this limit.

The matrices used to track the particles through the field consist of partial derivatives of the outgoing track parameters as functions of the incoming track parameters. These partial derivatives were calculated using reference tracks created using the Runge Khutta tracking routine in each of the 480 regions of the spectrometer acceptance . The partial derivatives were computed only once, organized into matrix form, and stored on disk.

To fit tracks to data, a Ξ^2 minimization of the track positions at FD1, FD2, BD1, and BD2 was used while simultaneously requiring that the fitted track be reproduced using matrix tracking. Since the matrix tracking approximation is linear, the Ξ^2 minimization procedure results in a simple solution for the fitted track positions at the detectors. The fit positions are found by multiplying a matrix which depends only on the transport matrix elements by a vector which is a function of measured hit positions. Since the transport matrix elements are constant for a region of phase space, the matrix used in the Ξ^2 minimization can be calculated once and stored along with the transport matrices. The vector used in the Ξ^2 minimization can be calculated for each event.

Tests of PEANUT were performed with Monte Carlo data to understand the errors due to the linear approximation of matrix tracking. The Runge Khutta routine was used to create tracks through the spectrometer and PEANUT was then used to fit these tracks. The momentum found by PEANUT is ususally within 0.3% of the actual momentum. The tracks with large momentum errors correspond to tracks which originate in a region of phase space far from any reference tracks. There are various possible means of decreasing these maximum errors. One solution is to increase

the density of reference tracks and the number of transport matrices stored on disk. A second solution is to create functional forms for the transport matrix elements and allow PEANUT to interpolated to regions far from any reference tracks. It is not clear that these rare bad spots pose a problem, but plans have been made to study these effects and make changes if needed.

Other improvements of PEANUT have been planned for the present year. So far PEANUT does not use information from FD3. This information is useful tracking information and should be included in a track fitting routine. This improvement is presently being developed and should be implemented by early summer. A second improvement of PEANUT is to include track length fitting. Track length information is useful in combination with time of flight and momentum for particle identification. The program can be easily improved to make an accurate estimation of the particle track length using linear interpolation from a reference track in the same manner that momentum is presently estimated.

PEANUT has been developed as part of the Interactive Data Analyzer (IDA) environment. It is presently being used to analyze the data from the 1991 run of E813 and will provide quick track reconstruction and momentum fitting used for monitoring during the 1992 run of E813.

III.D.8. On-Line Time-Of-Flight Trigger

During the 1991 run of E813, unwanted elastic scattering events of the type $p(K^-,p)K^-$ were unavoidably included with events of the type $p(K^-,K^+)\Xi^-$. These background proton events were roughly one order of magnitude more numerous than K^+ events at the trigger level. A solution to this proton contamination problem was the introduction of a second level trigger into the data acquisition system (DAQ).

A proton and a kaon of identical momentum will have different times of flight between the target and the back time-of-flight wall (BT). Over the seven meter flight path the protons are separated from the kaons by about 5ns. A particle originating in the target and passing through FD3 and BT will have a well defined momentum, given the positions at FD3 and BT. A "front end" computer, an ACC Firecracker, is used to select kaons via a table of maximum kaon time of flight for each FD3 and BT combination. The ACC is presented with information about detector position and time of flight through fast FERA and FERET electronics. During data acquisition the ACC compares each event against the appropriate entry in the TOF cut table. If the time of flight is less than the table entry the event is written to tape, otherwise the event readout is aborted and the DAQ is reset for the next event.

Problems interfacing the ACC with the other DAQ computers hampered the full implementation of the second level trigger in the 1991 run of E813. These problems have been resolved and a streamlined method for creating the time of flight cut table from data has been developed. This method accumulates events with the second level trigger turned off, and uses the time-of-flight spectrum of these events to create the time of flight cut table. The second level trigger will be used to reduce the proton contamination by rejecting in excess of 70% of the events with elastically scattered protons.

A procedure for monitoring these cuts has been developed to ensure that kaon events are not improperly aborted due to time drifts in the electronics. The second level trigger software will allow a small fraction of the proton events to pass. The fastest protons, which pass the second level trigger, will appear as a sharp peak on a time of flight spectrum. By examining these spectra the validity of the time of flight cut table will be verified, and any drifting electronics will become apparent.

III.D.9. Data Acquisition System/Programs

The data acquisition (DAQ) system used for experiment E813 was largely based upon one developed by our University of Birmingham collaborators for use in the NA36 collaboration. The system is centered on a pair of VME-based microprocessors (FIC 8230/16) from CES. One of these performs the event readout while the other handles event building and output to Exabyte tape cartridges. Transfer of a fraction of the data to microVAXes for on-line monitoring is effected through a dual-port memory which resides on both VME and Q-bus.

The CMU group has begun to acquire additional hardware which is compatible with this system. This equipment will be available in case of failures of critical components during running. It will also be used to upgrade and expand the acquisition system, allowing faster event readout. Over the past year we have purchased a FIC 8232/24 microprocessor, a 4 MB dual-ported memory system (for linking Q-bus and VME bus), a VME-based CAMAC crate controller, a VME spy module, and a VME enclosure. This is a sufficiently complete set of equipment that it will allow a working system to be set up at CMU. This will provide a platform to allow development of improvements in the data acquisition system. It will also be useful for high-speed readout of a variety of 'table-top' equipment tests in the lab at CMU.

The purchase of dual-ported memory cards has already proven to be extremely useful. During the early running of experiment E886 (see Chapter V) the data acquisition system failed for reasons which were not immediately obvious. The problem manifested itself as a variety of malfunctions of several components of the VME system, including the FIC's, themselves, which exhibited a number of pathological symptoms, including system crashes, during data acquisition. All the problems were found to be resolved when the new dual-ported memory VME board was installed. E886 ran with the replacement board while the old one was removed to be studied for diagnosis of its subtle fault.

Development and debugging on the data acquisition system has continued with the goal of making it faster, easier to operate, and more reliable. Several significant improvements have been made. This includes diagnosis and correction of a subtle conflict of computer interrupts, which had been causing corruption of a fraction of the data written to tape. Development and operation of this system will continue as a joint effort of University of Birmingham and CMU.

III.D.10. On-line / Off-line Analysis Software

The IDA package was chosen to form the basis of the on-line/off-line code for analysis of the H particle experiments. IDA, or Interactive Data Analyzer, is a group of subroutine packages which CMU helped to develop, and originally written for th. NA36 experiment at CERN. The structure of IDA has been discussed in previous progress reports. The packages were designed to be easily adaptable to the needs of other experiments. Some improvements were made in the IDA structure to make it easier to add and delete experiment-specific code called "analyzers". A generalized, table driven, FASTBUS data unpacking routine was also developed.

IDA was set up to run on multiple microVAXes. Data buffers can be read from tapes created by the data acquisition, from disk files, or directly from the VME-based data acquisition system over an Ethernet link for parallel online analysis. Physicists from several institutions within the collaboration have developed packages for converting drift chamber information into coordinates, determining particle tracks and time-of-flights, computing kinematics, etc. Three microVAXes running IDA were used on-line to monitor the experiment, in 1991. In 1992 there may be as many as five.

During the period between the 1991 and 1992 SEB periods at the AGS, most of the collaboration's efforts have been directed toward data reduction. All of the analyzing software underwent changes. A key issue during these modifications was the minimization of analysis time. See Section III.D.7 for an example of this work. A good feature of our system is that IDA is used, without modification, in both our on-line and off-line work, making all software development applicable in both areas.

IV. Hypernuclear Weak Decay Studies at the AGS

IV.A. Introduction

A Λ hyperon[†] replaces a neutron in a nucleus to form a Λ hypernucleus. Since the bound Λ has an additional quantum number which distinguishes it from the rest of the nucleons in the hypernuclear system, it is not Pauli excluded from filled nucleon orbitals and can penetrate deep inside the nucleus. The study of hypernuclei can advance our understanding of details of nuclear structure and provide insight into hyperon-nucleon interactions which are inaccessible in unbound systems.

Hypernuclei can be formed from the strangeness exchange reaction ${}^{A}X(K^{\pm},\pi^{\pm})^{A}_{\Lambda}X$. A K^- beam of momentum 750MeV/c was incident on ^{4}He and ^{5}He targets for Brookhaven National Laboratory Experiment 788 at the Alternating Gradient Synchrotron facility.[1] An overview of the most recent run of this experiment is provided in this chapter.

A free Λ predominantly decays via the two mesonic decays, $\Lambda \rightarrow p\pi^-$ (B.R. 64.1%) and $\Lambda \rightarrow n\pi^o$ (B.R. 35.7%) with a final state nucleon momentum of about 100MeV/c (the branching ratio for Λ decay to leptons is less that 0.2% and will be neglected). When the Λ is embedded in nuclei these mesonic decay modes, characterized by the decay widths Γ_{π^-} and Γ_{π^o}, are suppressed, especially in heavier nuclear cores, because of the relatively large nuclear Fermi momentum of $k_f \approx 270$MeV/c. In other words, the decay nucleon from the $\Lambda \rightarrow N\pi$ reaction, where N can be n or p, within a hypernucleus is Pauli blocked from occupying a filled orbital and may not have enough kinetic energy to overcome the binding energy to escape the nuclear core. Also, when the Λ is embedded in a nucleus the Λ-hypernucleus can decay via the nucleon-stimulated nonmesonic decay channels $\Lambda p \rightarrow np$ and $\Lambda n \rightarrow nn$, characterized by the decay widths Γ_p and Γ_n respectively. The large momentum of the decay nucleon in stimulated decay of $\approx$ 405MeV makes this reaction easily identifiable.

There have been numerous theoretical models[2-5] developed to calculate the decay rates. The measured ratio of neutron to proton stimulated decays Γ_n/Γ_p for light hypernuclei is key to understanding the isospin structure of the interaction and differs greatly from model to model. Unfortunately, even after a decade of experimental research, too little data exists on the ratios Γ_n/Γ_p, mostly because of inadequate Γ_n measurements.[6] The present experimental values[7,8] for this ratio for ${}^{5}_{\Lambda}$He and ${}^{4}_{\Lambda}$He are 0.93 ± 0.55 and 0.40 ± 0.15, respectively.

For one pion exchange calculations the ${}^3S_1 \rightarrow {}^3D_1$ parity conserving transition domi-

[†]A Λ (lambda) hyperon has a mass 1115.6MeV, lifetime 263ps, and quark content *uds*.

nates. Since the $^3D_1$ state must have zero isospin, a two neutron final state is excluded and thus one would expect a neutron stimulated fraction $\Gamma_n/\Gamma_p << 1$. This may be contrary to Grace's measurement[7,9] of $\Gamma_n/\Gamma_p = 1.33^{1.12}_{-0.81}$. Dubach[3] obtains an enhanced $^3S_1 \rightarrow ^3P_1$ transition when he includes the exchange of K, K^*, and other heavy mesons. This increases the rate of the neutron stimulated channel, but even with this enhancement his calculations are still below the measured rates. It is also possible that initial P-wave ΛN states, not present in the nuclear matter calculations, contribute to the neutron stimulated rates.

It has been pointed out[6,10] that further measurements of light hypernuclear systems will provide insight into the form of the effective Hamiltonian governing weak interactions in the presence of hadronic fields. One goal is a fundamental understanding of the empirical $\Delta I = \frac{1}{2}$ rule in weak interactions which has been observed in $\Delta S = 1$ mesonic decays. As of yet, there is no evidence for the existence of such a rule for $\Delta S = 1$ baryon-baryon interactions such as $\Lambda N \rightarrow nN$.

IV.B. Previous Involvement in Hypernuclear Physics

The Carnegie Mellon Medium Energy Physics research group began its investigations into hypernuclear decay in 1982 with Brookhaven experiment E-759. The focus was $^{12}_{\Lambda}$C decay, the Ph.D. thesis research topic for Richard Grace.[9]

Inspired by a need for experimental data on light nuclei, experiment E-788 was proposed and approved in October of 1983 for 150 hours of $^5_{\Lambda}$He measurements and 400 hours of $^4_{\Lambda}$He measurements. The $^5_{\Lambda}$He measurement served as Ph.D. thesis topic for John Szymanski.[11] Due to early tear-down of E-788 required to prepare for another experiment (E-773) scheduled for the same beamline in May 1985, E-788 was abruptly postponed after running for only 100 hours.

IV.C. The 1990 Run of E-788

The E-788 measurements were completed in early 1990 when a second run at the AGS was undertaken. The beamline at which the first phase of E-788 ran, LESB-I, had been dedicated to a long-term project examining rare kaon decays (E-787). In order to permit the continuation of the hypernuclear research program, the AGS moved the entire Moby Dick spectrometer to another beamline, LESB-II. This transition took place in a four year period between the first and second phase of E-788.

The second running period utilized a significantly expanded system of out-of-beam detectors which were operationally different from the range spectrometer used in E-759 and the first phase of E-788.

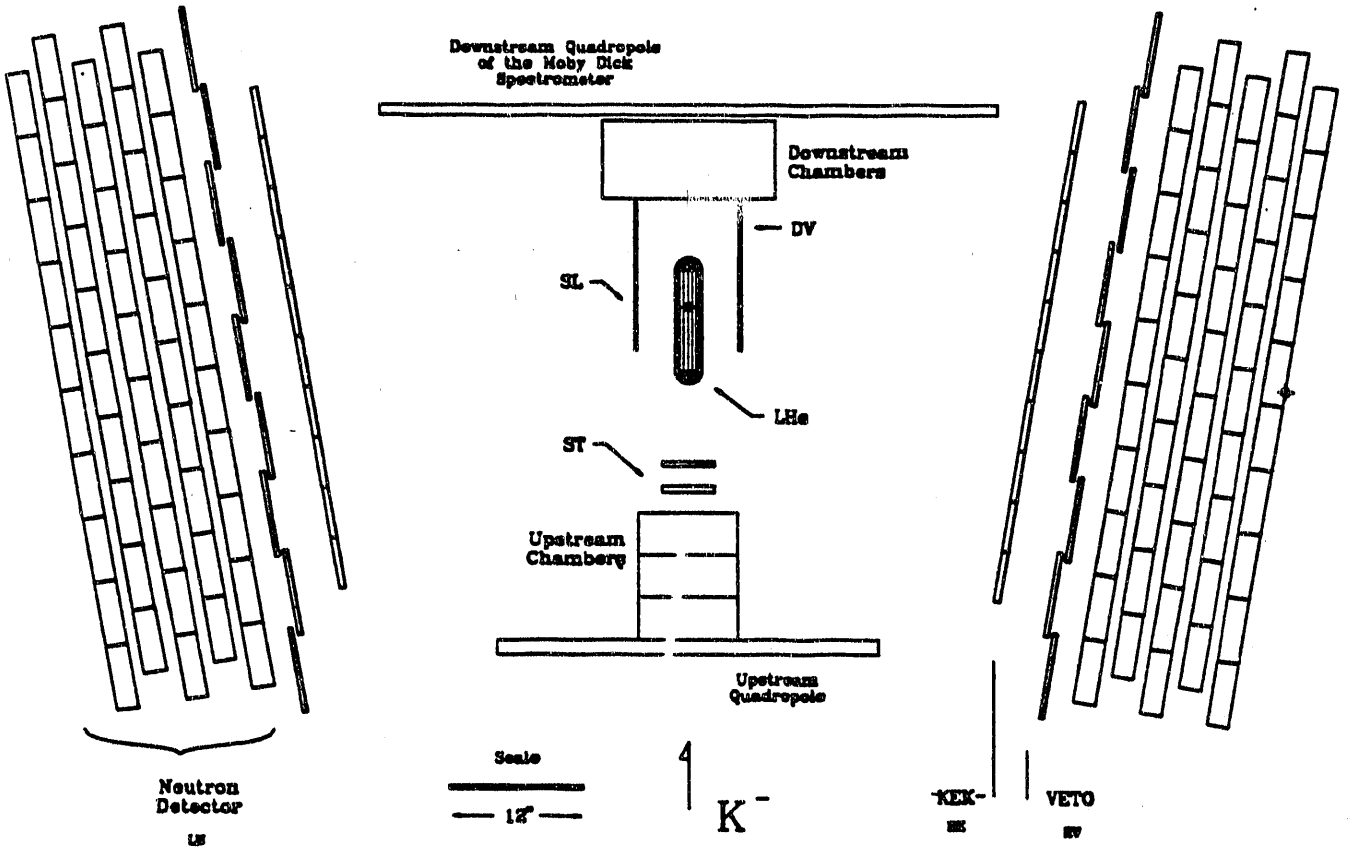

Fig. IV.C.1 Plan view of the target area of the E-788 experiment illustrating the ${}^{4}_{\Lambda}$He detector configuration. Only active areas of scintillation counters are shown. Also not shown are the upstream and downstream spectrometers used for momentum analysis of the (K^-, π^-) beam particles.

The goals of the second phase of E-788 were to make credible measurements of the partial and total rates for mesonic and non-mesonic decay, i.e., Γ_{π^0}, Γ_{π^-}, Γ_p, Γ_n, and Γ_{total}, with emphasis upon the Γ_n measurement. The detector design was optimized to detect neutrons and distinguish π^- from protons without the use of a magnetic field. Two large arrays of plastic scintillator located at either side of the target served both as neutron detectors and as a range spectrometer. The detector layout for the ${}^{4}_{\Lambda}$He is illustrated in Fig. IV.C.1. The arrays were designed for compatibility for AGS experiments E-813 and E-836. Each array has 50 elements (5 layers deep and 10 elements wide) and each element has dimensions of $2'' \times 6'' \times 72''$ and photomultiplier tubes attached at each end. Because neutron energy is identified by time of flight, the best timing resolution is desirable. To efficiently utilize the large volume of these scintillator arrays for neutron detection, a 9-element scintillator layer consisting of $3/8'' \times 8'' \times 72''$ overlapping elements constitute a charged particle veto. The timing and energy resolution of this veto layer is only fair and thus not sufficient for making a charged particle time-of-flight measurements. A moderate

resolution 10 element array consisting of elements with dimensions 1.5cm × 11cm × 150cm was used on each side. The detectors were salvaged from a Japanese experiment and are referred to as the KEK layer (LK and RK for the left and right array).

Arrays of five plastic scintillators on either side of the target, SL and SR, were used to measure the stop-time for the hypernuclear lifetime measurement and also provide a start-time for charged particle time-of-flight measurements. Each array consists of 5 Pilot U type scintillators with dimension $\frac{1}{4}$"×4.5cm × 20cm. The start-time for the hypernuclear decay was directly measured by the high quality in-beam scintillators ST which have a timing resolution of $\sigma = 80$ps.

The major background of in-time neutrons is due to π^- interactions with non-target material resulting in an emitted neutron. For the ${}^{5}_{\Lambda}$He experiment this does not pose much of a problem since the solid ^{6}Li target was enclosed within a system of veto scintillators. The solution was not as obvious for the cryogenic ${}^{4}_{\Lambda}$He target. Two steps were taken to reduce the π^- background:

- A low density PVC foam material was used instead of aluminum to provide structural support for the target vessel in crucial areas which coincided with acceptance of the out-of-beam detectors.

- An internal cylindrical scintillator system was placed inside the cryogenic vessel used to tag charged particles emitted from the target. The scintillator used was $\frac{1}{4}$" thick and coupled to the exterior by a light guide gasket. This gasket was then coupled to 6 photomultiplier tubes via light guides.

In conjunction with the internal scintillators, a system of target-external scintillators was added to redundantly provide full charged particle coverage.

IV.D. Data Analysis of E-788

The task of software development for this project has been predominately carried out by graduate student Michael Athanas. A portion of the analysis code has been adapted from analysis software libraries developed at CMU and the University of Birmingham for CERN experiment NA36. The in-beam tracking code was developed by the BNL Medium Energy Group.

During the past year, the most headway was made in the analysis of the ${}^{4}_{\Lambda}$He data set. Recent progress include:

- complete time calibration of all necessary detectors

- total energy calibration for all detectors
- a high efficiency of particle identification for pions, protons, and neutrons
- monte carlo analysis of detector acceptance
- a direct measurement of the ${}^{4}_{\Lambda}$He decay time
- the partial decay rates Γ_π, Γ_p have been determined
- the primary data reduction of the ${}^{5}_{\Lambda}$He data set

The hypernuclear excitation energy is defined as the calculated mass of the hypernuclear state minus the known mass of the system. It is determined from the three kinematical variables measured from the (K^-, π^-) in beam tracking: (1) the kaon momentum p_K, the pion momentum p_π, and the scattering angle between the two tracks θ_s. The excitation energy is a property of the formation of the hypernucleus. It is independent of the kinematics for the subsequent decay of the hypernuclear system. The typical procedure for extracting the hypernuclear decay products relies upon isolated exclusively from the out of beam detector arrays. The excitation energy spectrum is then calculated for this event sample.

The design goal of the out of beam detector arrays include the ability to discriminate between pions, protons, neutrons, and gammas. One of our greatest challenges involve the separation of pion and protons. The charged particle identification process takes advantage of energy loss, direct velocity measurement, and range. We have achieved an estimated 97% efficiency rate for correct particle identification.

Fig. IV.D.1 illustrates the excitation energy for (K^-, π^-) events which were identified as protons in the out of beam detector array. The cuts which went into this analysis include: (1) elimination of events which had poor tracking characteristics in the in-beam spectrometers, (2) the elimination of the background process $K^- \longrightarrow \pi^\circ + \pi^-$, and (3) requiring at least one identified proton, zero pions, and up to 2 neutrons in the out of beam detector array. As seen in this figure, there is very little contamination in the hypernuclear proton decay sample.

The excitation energy for identified pions is shown in Fig. IV.D.2. The only difference in the selection criteria compared to the proton sample is that we require a single pion in the out of beam detector array. The outstanding difference between the pion and proton spectrum is the extended tail on the high end of the ground state peak. This tail is consistent with the mesonic decay of quasi-free lambda's. That is, a Λ hyperon is produced in the (K^-, π^-) reaction but is not bound to the residual nucleus. Since it is not bound, the

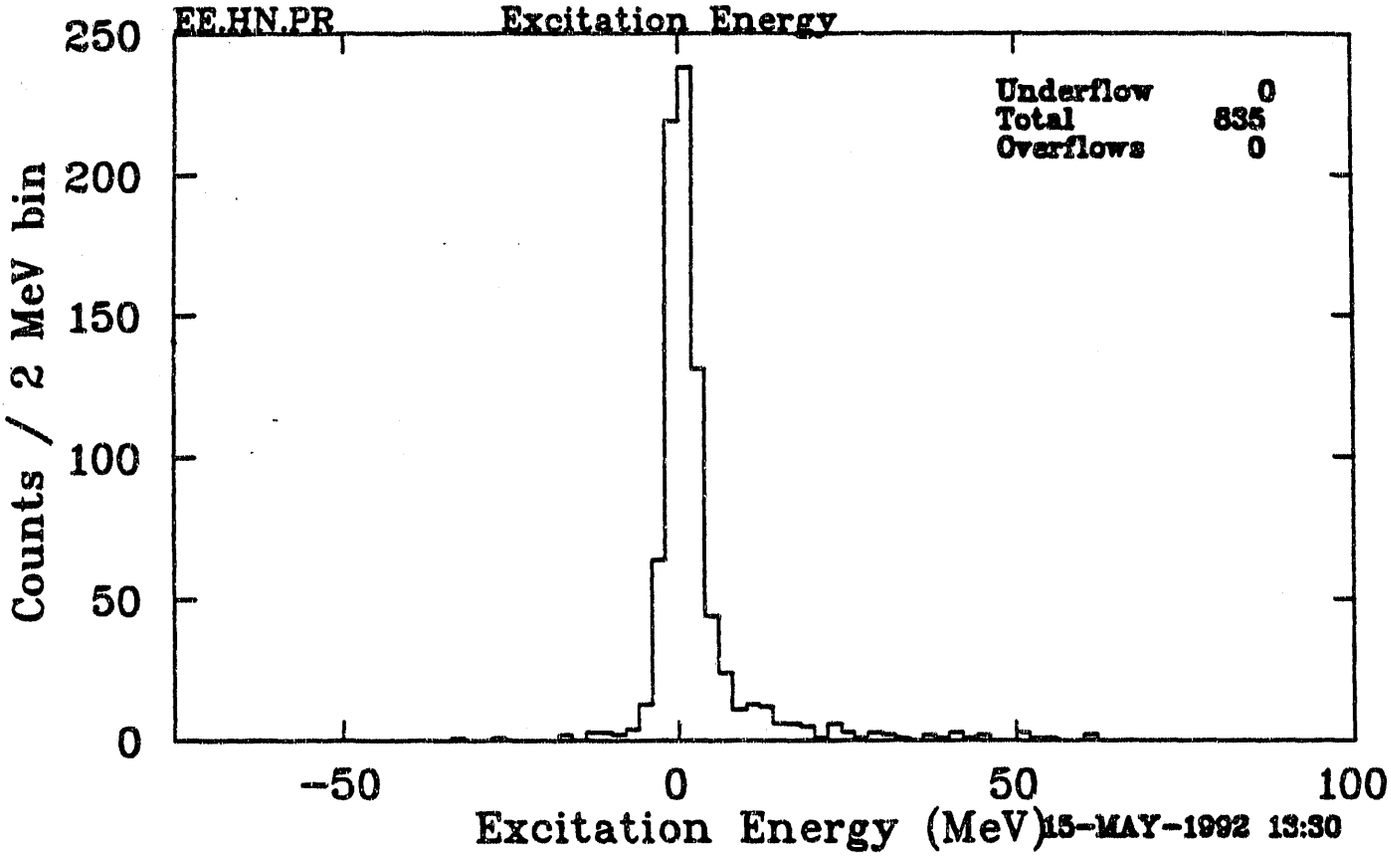

Fig. IV.D.1 The excitation energy spectrum for identified protons. The minimum cuts included in the generation of this histogram include (1) requiring a (K^-, π^-) formation reaction, (2) removal of the background reaction $K^- \rightarrow \pi^- + \pi^\circ$, and (3) requirement of a proton in the out of beam detector array. A gaussian fit is made to this distribution and is used a measurement of the spectrometer resolution.

nucleon stimulated decay channel is unavailable. Thus, proton emission is excluded from quasi-free Λ production.

We anticipate completing the ${}^{4}_{\Lambda}$He analysis by early summer. This analysis is serving as the dissertation topic of graduate student Michael Athanas. The ${}^{5}_{\Lambda}$He analysis is planned for early fall.

References for Chapter IV

1) Peter D. Barnes and Gregg B. Franklin. AGS Research Proposal Status Report E-788. 1987.

2) M. M. Block and R. H. Dalitz. Structure of the weak interaction $\Lambda + N \rightarrow N + N$. *Phys. Rev. Lett.*, 11, 1963.

3) John F. Dubach. Non-mesonic decay modes of hypernuclei. *Nucl. Phys.*, A450, 71, 1986.

4) B. H. J. McKellar and B.F. Gibson. Nonmesonic decay of heavy Λ hypernuclei. *Phys. Rev.*, C30, 322, 1984.

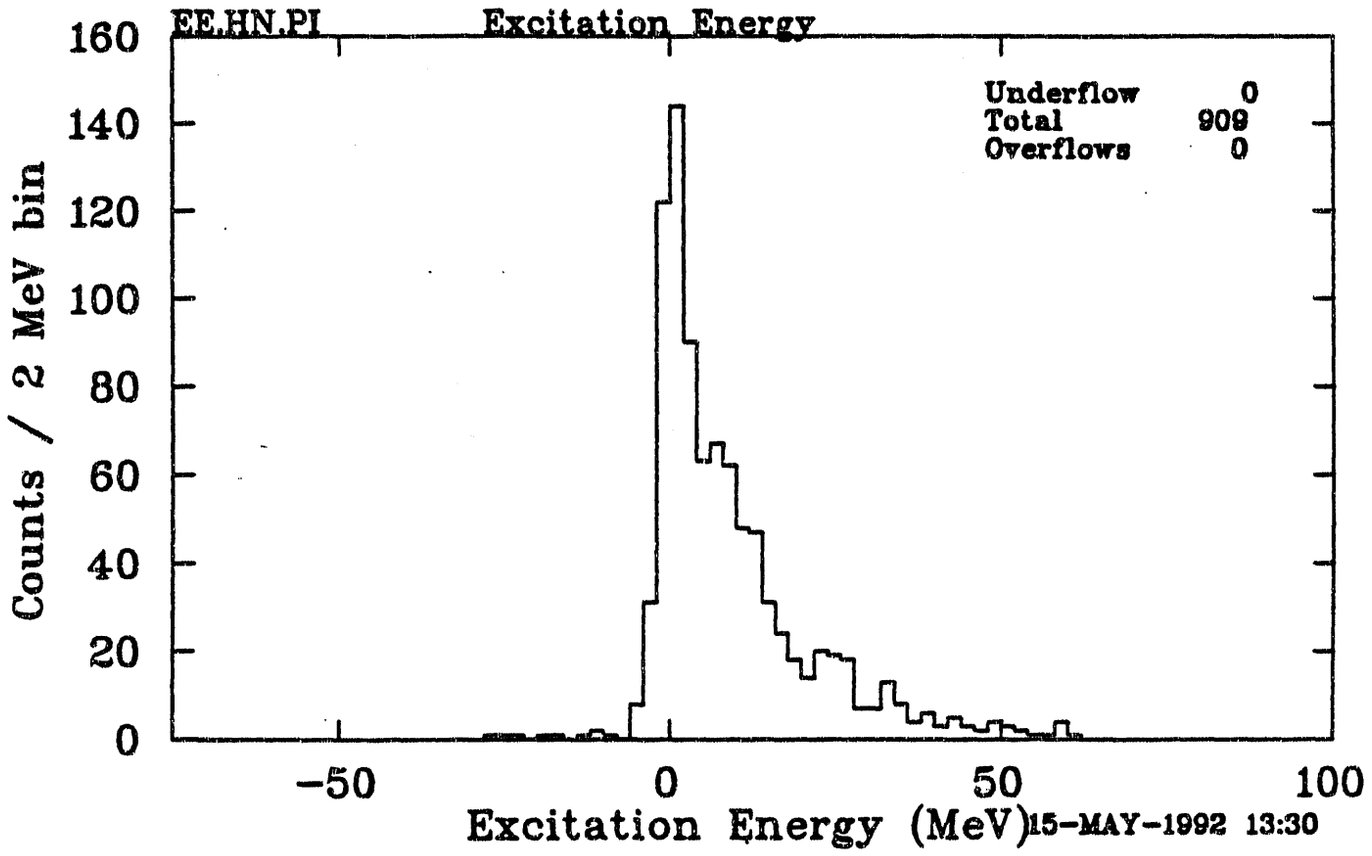

Fig. IV.D.2 The excitation energy spectrum for identified protons. The minimum cuts included in the generation of this histogram include (1) requiring a (K^-, π^-) formation reaction, (2) removal of the background reaction $K^- \rightarrow \pi^- + \pi^o$, and (3) requirement of a pion in the out of beam detector array.

5) D. P. Heddle and L. S. Kisslinger. Hybrid quark-hadron model of Λ nonmesonic decay: Finite nuclei. *Phys. Rev.*, **C33**, 335, 1986.

6) J. Cohen. Decays of Λ-Hypernuclei. *Progress in Particle and Nuclear Physics*, **25**, 1990.

7) J. J. Szymanski and et.al. Nonleptonic weak decay of ${}^{5}_{\Lambda}$He and ${}^{12}_{\Lambda}$C. *Phys. Rev.*, **C43**, 849, 1991.

8) M. M. Block and et. al. The decay modes of the ${}^{4}\mathrm{He}_{\Lambda}$. *Nuovo Cimento*, **28**, 290, 1963.

9) R.D. Grace. *Weak Decay of P Shell Lambda Hypernuclei.* PhD thesis, Carnegie Mellon University, 1986.

10) C.B. Dover. Few Body Hypernuclear Systems: Weak Decays. *Few-Body Systems*, . 77, 1989.

11) John Szymanski. *The Weak Decay of Lambda Hypernuclei.* PhD thesis, Carnegie Mellon University, 1987.

IV.E. Test of the ΔI=1/2 Rule.

The weak decays of strange mesons and free hyperons strongly favor ΔI=1/2 amplitudes over ΔI=3/2 amplitudes. It is not known to what extent this rule applies to the non-mesonic interactions of the type $\Lambda p \rightarrow np$ and $\Lambda n \rightarrow nn$. A recent paper[1] examined existing data on non-mesonic decays of light hypernuclei in order to obtain a quantitative estimate of the relative strength of the two isospin channels. The data show that a pure ΔI=1/2 decay amplitude may well be ruled out at the 1.6σ level, and favor a solution where either: 1) both isospin channels contribute about equally, or 2) the ΔI=3/2 channel dominates by an order of magnitude. A possible future direction, then, at the 2.0 GeV/c beam line is the continued study of weak decays of light hypernuclei.

An unresolved question which has endured for many years is why strangeness changing weak interactions prefer the ΔI = 1/2 channel over the *a priori* comparably strong ΔI = 3/2 channel. This effect can be large in K decay amplitudes and in the mesonic decays of hyperons. However, little experimental information exists to test the ΔI=1/2 rule in the strangeness changing weak interaction between two baryons, such as a Λ and a nucleon. The only practical way to study the strangeness changing YN interaction is to examine the non-mesonic decays of hyperons embedded in nuclei. In the mesonic decays, where the ΔI = 1/2 rule is known to work well, the typical center-of-mass momenta are 100 MeV/c, while in non-mesonic decays the typical momenta are about 400 MeV/c. Cohen[2] has pointed out that in one-pion exchange models the non-mesonic decays probe the parity conserving, higher momentum p-wave part of the weak interaction, which is masked by the strong interaction in non-strange NN interactions. All current models of non-mesonic decays make the assumption that the ΔI = 1/2 rule is valid, and have achieved moderate agreement with data on the total non-mesonic decay rates. However, no model has succeeded in reproducing the measured ratios of $\Lambda n \rightarrow nn$ and $\Lambda p \rightarrow np$ widths. It is interesting, therefore, to further test the validity of the isospin rule for the less well understood, high momentum, parity conserving part of the interaction. Our recent examination of the data for non-mesonic decays of He and H hypernuclei suggests a violation of the usual ΔI = 1/2 rule.

The non-mesonic decay rates for $\Lambda + p \rightarrow n + p$ and $\Lambda + n \rightarrow n + n$ are sensitive to the spin-isospin structure of the strangeness-changing weak interaction in nuclei. Figure IV.E.1 illustrates the paths by which a ΛN initial state can decay non-mesonically to an NN final state. Note that comparing information obtained from several light hypernuclei, such as ${}^{5}_{\Lambda}$He and ${}^{4}_{\Lambda}$He, can provide a way of extracting the strength of specific transitions. At a purely phenomenological level, one can estimate directly from the data whether the ΔI=1/2 rule is satisfied by the data for non-mesonic weak decay. The rule requires, for any reaction mechanism, that the neutron stimulated rate is twice the proton stimulated rate for I=1 final states. Defining R_{NS} as the rate for $\Lambda N \rightarrow NN$ from spin state S, it follows that $R_{n0} = 2R_{p0}$ and $R_{n1} \leq 2R_{p1}$. What is measured experimentally are combinations of these quantities. In an approach introduced by Block and Dalitz[3], and recently updated by Dover[4], one can define

$$\gamma_5 \equiv \frac{\Gamma_n}{\Gamma_p}({}^{5}_{\Lambda}\mathrm{He}) = \frac{3R_{n1}+R_{n0}}{3R_{p1}+R_{p0}} = \frac{0.20\pm0.11}{0.21\pm0.07} = 0.93 \pm 0.55,$$

$$\gamma_4 \equiv \frac{\Gamma_n}{\Gamma_p}(^4_\Lambda\mathrm{He}) = \frac{2R_{n0}}{3R_{p1}+R_{p0}} = 0.40 \pm 0.15, \text{ and}$$

$$\gamma \equiv \frac{\Gamma_{n.m.}(^4_\Lambda\mathrm{He})}{\Gamma_{n.m.}(^4_\Lambda\mathrm{H})} = \frac{3R_{p1}+R_{p0}+2R_{n0}}{3R_{n1}+R_{n0}+2R_{p0}} = 0.51 \pm 0.20.$$

The numerical values come primarily from Refs. 3 and 5, though several other data sets were examined in arriving at these "best" values[1]. Solving the three equations one obtains the ratio:

$$\frac{R_{n0}}{R_{p0}} = 0.23$$

This ratio tests the $\Delta I=1/2$ Rule, which predicts a value of 2; examination of the experimental errors leads to the conclusion that the pure $\Delta I=1/2$ hypothesis is excluded at about the 1.6 σ or 90% confidence level. Clearly, it would be useful to have more measurements of these quantities to check this result.

The weak link in the presently available data is the measurement of the non-mesonic decay rate of $^4_\Lambda$H. The old data result from a handful of emulsion hyperfragment events. We can, with mostly existing equipment, make this hypernucleus and measure its non-mesonic decays using the reaction ^{4}He$(K^-,\pi^0)^4_\Lambda$H. Examining the phase space for this reaction shows that an annular photon detector surrounding the beam line at about 10^0 will permit us to trigger on the photons from decay of the π^0. This detector would have to be constructed: possibly a BGO shower detector, segmented in angle in a manner similar to the Los Alamos BGO Ball. A liquid helium target with a good internal charged particle veto would be used to reduce background from pionic hyperon decays which lead to in-time background neutrons. The target used for E788 would be adequate. The "neutron detectors" used for the H-particle experiment would be used to detect both the proton and neutron stimulated decays of the hypernucleus. See Fig. IV.E.2.

The goal of this experiment would be measurement of the partial decay rates

$^4_\Lambda\mathrm{H} \rightarrow \mathrm{n} + \mathrm{p} + (\mathrm{nn})$ proton stimulated decay,

$^4_\Lambda\mathrm{H} \rightarrow \mathrm{n} + \mathrm{n} + (\mathrm{pn})$ neutron stimulated decay,

and the lifetime, τ, of the $^4_\Lambda$H nucleus. The data would be used in an analysis similar to the one outlined above to address the issue of the validity of the $\Delta I=1/2$ rule in strangeness-changing weak decays.

Chapter IV.E References

1) R. A. Schumacher, contributed talk at Conference on Hypernuclear and Strange Particle Physics, Shimoda, Japan, Dec., 1991, and to be published in Nucl. Phys.
2) Joseph Cohen, Progress in Particle and Nuclear Physics **25**, 139 (1990).
3) M.M. Block and R.H. Dalitz, Phys. Rev. Lett. **11**, 96 (1963).
4) Carl B. Dover, Few Body Systems, Suppl. **2**, 77 (1987).
5) J.J.Szymanski *et al.*, Phys. Rev. C **43**, 849 (1991).
6) John F. Dubach, Nuclear Physics **A450**, 71c (1986).

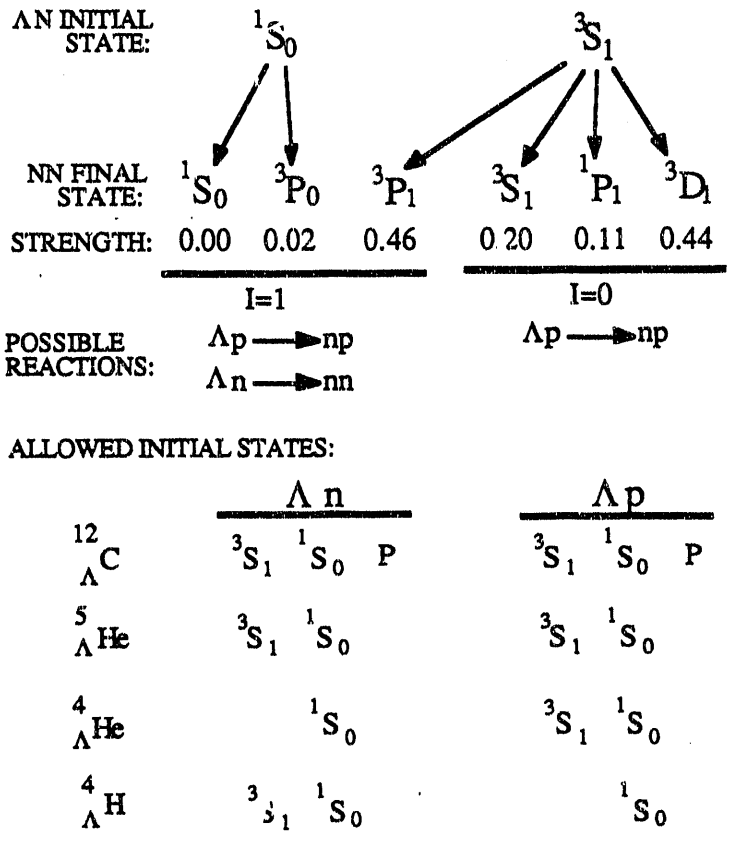

Fig. IV.E.1. Spin and isospin combinations for non-mesonic weak decay of light hypernuclei. The predicted strengths for the separate channels are from Ref 6.

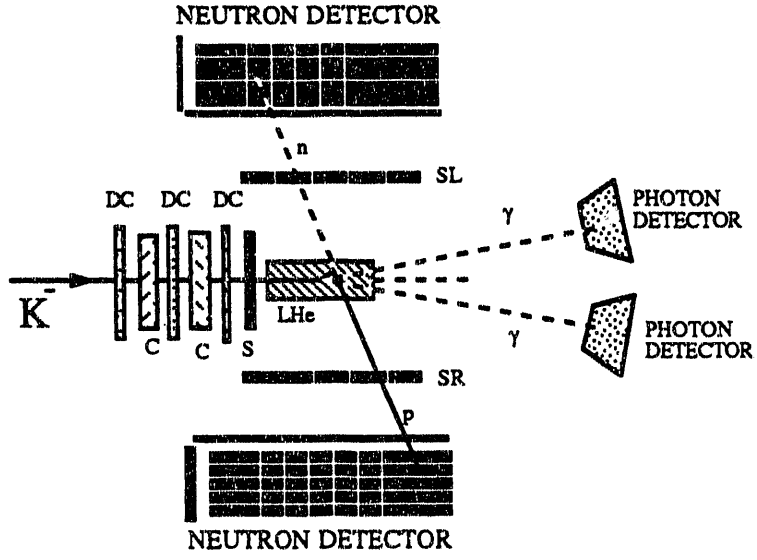

Fig. IV.E.2. Schematic layout of a possible new experiment to measure the non-mesonic weak decay rates of the hypernucleus $^4_{\Lambda}H$. The hypernucleus is formed in the reaction $^4He(K^-,\pi^o)^4_{\Lambda}H$, where π^o decay photons are detected in coincidence in new detectors (e.g. BGO). Most of the apparatus would come from existing detectors used for E788 and E813.

V. Search for Strangelets Using the 2 GeV/c Beam Line (AGS E886)

V.A. Introduction

Strange quark matter, which consists of u, d and s quarks in one bag, was suggested by E. Witten as a dark matter candidate produced during the phase transition from the quark-gluon phase to the hadron phase in the early universe.[1] The possibility of light strange quark matter, "strangelets," has also been suggested based on the bag model.[2,3] The stability of strange quark matter may be qualitatively understood as being due to the fact that for a system composed of many u and d-quarks, the addition of an s-quark may be more energetically favorable than an additional u or d-quark because of the Pauli principle. Quantitatively we have to solve a multi-quark problem based on QCD. The existence of a stable or meta-stable strangelet is, therefore, an important subject concerning the confinement aspect of QCD.

Experimental efforts to search for such strange matter have been made, especially in cosmic rays and terrestrial materials. Searches for heavy strange quark matter ($M > 10^9$ GeV/c^2) traveling in our galaxy have been conducted using various detectors, such as large scintillators, a gravitational wave detector, and in ancient mica.[4] For masses up to 10^{26} GeV/c^2, the upper limit obtained for the flux is already below the limit given by assuming strange quark matter as a dark matter candidate. Lighter strange quark matter (strangelets), in the form of super-heavy isotopes between H and Na, has been searched for in terrestrial materials using a mass spectrometer, sometimes accelerated by a tandem Van de Graaf.[4] Strangelets of mass range up to 10^4 GeV/c^2 are almost ruled out as a dark matter candidate. However, the existence of strangelets is not ruled out in general; if the lifetime of a strangelet is shorter than the life of the universe, strangelets produced in the early universe would have decayed away.

One possible way to produce strangelets may be through relativistic nucleus-nucleus collisions, perhaps as a result of the formation of a quark-gluon plasma. The formation of quark-gluon plasma in nucleus-nucleus collisions is still an open problem as is the existence of stable or meta-stable strangelets. The primary goal of relativistic nucleus-nucleus collisions is the observation of a phase transition from nuclear matter to a quark-gluon plasma. If the phase transition occurs and the strangelet is stable or metastable, the strangelet may be observed. The detection of a strangelet can provide evidence for the formation of a quark-gluon phase in nucleus-nucleus collisions.[5] Therefore, the search for strangelets is related to the study of quark-gluon plasma in addition having relevance to our understanding of non-perturbative QCD and astrophysics.

Since the mass of the s-quark is heavier than the u and d-quarks, the number of u and d-quarks is expected to be larger than that of s-quarks. The strangelet is, therefore, expected to be positively charged but have smaller value of Z/A than stable nuclei. Several experiments to search

for such particles in nucleus-nucleus collisions have been carried out and no evidence has been found.[6] Furthermore since there is no reliable theoretical calculation of the production cross section of strangelets, it is important to search with as high a sensitivity as possible.

Following a suggestion by Ken Imai, a collaboration of physicists from Kyoto, Kyoto Sangyo, Birmingham, BNL, Carnegie Mellon, Vassar, Yale, LAMPF, University of New Mexico, and Freiburg submitted a proposal to use the existing 2 GeV/c K-beam line as a mass spectrometer to search for particles which have anomalously large M/Z value. Ken Imai, Kyoto University, and Phil Pile, BNL, are cospokespersons for the collaboration. The February BNL PAC granted approval for an initial test run during the heavy ion running period which began in April of 1992.

V.B. Experimental Technique

In this experiment the two electrostatic separators which are usually used to select K-mesons are tuned to select particles of large M/Z value and reject background particles, such as π^+, K^+, proton, deuteron and other light nuclei. The detectors which are placed downstream of the mass slits do not have to handle high multiplicity or high particle intensities. We can, therefore, carry out a very clean (background free) experiment which utilizes a primary beam of maximum intensity. As a result, we expect high sensitivity for the detection of new exotic particles in spite of a rather modest acceptance of the spectrometer.

In this experiment, production cross sections of some isotopes such as ^{8}He and ^{11}Li, can also be measured. The production cross sections of various isotopes in nucleus-nucleus collisions have been measured at low energies (~100 MeV/N), and compared with a coalescence model.[7] There is no such measurement at high energy. Therefore, this experiment can provide new data and new information about the reaction mechanism of relativistic nucleus-nucleus collisions.

The D6 medium energy K-beam line was built to provide up to 2 GeV/c kaons for our H-search experiments (E813/836). The parameters of the beam line spectrometer are listed in Table V.B.1, and the spectrometer is schematically shown in Fig. V.B.1. Using magnetic and electrostatic fields, particles of same M/Z are focused at two mass slits (MS1 and MS2). The mass slits (heavy metal collimators) are adjusted to select particles in a particular range of M/Z. For a fixed value of central momentum (p/Z), the electrostatic separators select the velocity, β, or M/Z of particles. For p/Z=2.0 GeV/c, the bending angle, θ is obtained from $\theta=0.23 \times E/\beta$(mrad), where E is the electric field (kV/cm). The vertical deflection of the particles depends linearly on E/β. The accepted range of M/Z is determined by the electric field and the mass slit opening.

The detectors used for this experiment are shown schematically in Fig. V.B.2. We measure time-of-flight (TOF) between hodoscopes (H1) after the first mass slit and a timing scintillation counter (T1) at the final focus, and also between T1 and the TOF wall (T2). The dE/dx detector which consists of 4 thin scintillation counters, is placed at the final focus to measure the charge (Z) of particles. Several chambers (DC1-5) are used for the tracking. A lucite Cherenkov counter is placed at the final focus as a triggering aid. The E813/836 spectrometer can be used for a second, independent, momentum and velocity determination.

The distance between H1 and T1 is about 15m and that between T1 and T2 is 7 m. The TOF resolution is 0.5 nsec (rms) for the first TOF measurement and 0.25 nsec (rms) for the second TOF measurement. There are good enough to obtain the value of M/Z. The mass resolution is mainly determined by the momentum resolution which is expected to be 1%. We expect to obtain a mass resolution of $\delta(M/Z)=38$ MeV/c^2 for M/Z=3 GeV/c^2 and $\delta(M/Z)=100$ MeV/c^2 for M/Z=10 GeV/c^2, at p/Z=2.0 GeV/c.

The energy loss, dE/dx, in a scintillator is measured to determine the charge, Z, of particles. For particles with large M/Z the difference of dE/dx is quite large for different charge states. As the dE/dx detector, we used 4 thin (1-2 mm) plastic scintillators. The use of 4 detectors allowed a truncated mean of the energy loss to be used. The truncated mean, $\langle dE/dx \rangle_{tr}$ is the average energy loss of the smallest two pulse heights out of four scintillators. This technique provides better dE/dx resolution than a simple average.

The kinematic dependence of the spectrometer acceptance as a function of rapidity, $y = \tanh^{-1}(P_L/E)$, and transverse momentum, P_T, has been estimated by a Monte Carlo calculation using the parameters of the beam line spectrometer listed in Table 1. The kinematic acceptance of the spectrometer is limited to relatively low rapidities (i.e. $y < 0.6$) depending on Z/A. Moreover the rapidity acceptance is very narrow (< 0.05 units). Depending on the A of the strangelet, the spectrometer has non-zero acceptance over a range of P_T from 0.1 to 0.9 GeV/c. Typical acceptance values vary from 1 to 5% over this range in P_T.

Based on the calculated spectrometer acceptance, the sensitivity is estimated in the follow-

TABLE V.B.1.

Production angle	5 degrees
Beam length	31.1 m
Horizontal acceptance	±50 mr
Vertical acceptance	±8 mr
Momentum acceptance	±3%
Acceptance	8.6 msr%

ing way. The number of strangelets, dN_S, detected at (y,P_T) in the range $dydP_T$ is given by the product,

$$dN_S = n_B \Delta t \lambda \varepsilon dR, \quad dR = (d^2R(y,P_T)/dydP_T)\, dydP_T$$

where

n_B = beam rate,

Δt = length of run in seconds,

λ = interaction length of platinum (Pt) target,

$\varepsilon(y,P_T)$ = detection efficiency at y and P_T,

$d^2R/dydP_T$ = differential strangelet production rate/collision.

Taking $n_B = 10^9$ ions/sec, λ=0.3, $\Delta t = 2 \times 10^5$ sec (=200 hours with a 25% duty cycle), ε=0.05, and $dN_S < 2.3$ (90% C.L.), a null result will set an upper limit for the strangelet production rate, $dR(y,P_T)$, within the acceptance of the spectrometer in the neighborhood of

$$dR(y,P_T) < 1 \times 10^{-12} \text{ per collision (90\% C.L.).}$$

To convert this to a production cross section limit, one multiplies dR by the total nucleus-nucleus interaction cross section under consideration (e.g. 6 barns for Au-Pt and 3.5 barns for Si-Pt.)

If we assume a Si ion as 28 nucleons and a Au ion as 197 nucleons, we can expect 3×10^6 protons/spill for 10^9 Si/spill and 2.0×10^7 protons/spill for 10^9 Au/spill in the beam line (scaled from the beam yield of the KEK-K2 beam line where the primary proton momentum is 13 GeV/c). In 200 hours of running with a beam of 10^9 Au/spill, the sensitivity is expected to be 6×10^{-13} (90% C.L.) relative to the proton yield. No more than about 10^8 Si ions/spill are expected so the relative sensitivity for silicon running will be less.

V.C. 1992 Run

With the exception of the simple dE/dx counters, all the detectors were already installed for E813/836. In addition, E813 had a very successful engineering run in 1991. The installation of the dE/dx counters and modifications of the trigger electronics and gates were begun immediately after receiving approval for the test run from the PAC. Some detectors were removed to minimize dE/dx losses. We were ready for the test measurement with the Si and Au beams by April.

Figure V.C.1 shows the first results from the run with the separators off to allow protons through the mass slits. The time time-of-flight spectra obtained during the run show clear separations of particles species. These spectra were used to produce the ratios shown in Fig. V.C.2. A

complete off line analysis utilizing the dE/dx counters and tracking through the spectrometer is underway. We hope to produce additional results in the near future.

Chapter V. References

1) E. Witten, Phys. Rev. **D30** , 272 (1984).
2) S.A. Chin and A.K. Kerman, Phys. Rev. Lett. **43** , 1292 (1979).
3) E. Farhi and R.L. Jaffe, Phys. Rev. **D30** , 2379 (1984).
4) K. Imai, Nucl. Phys. **A527** (1991) 181c, and references therein.
5) H.C. Liu and G.L. Shaw, Phys. Rev. **D30** , 1137 (1984).
6) BNL/AGS Experiments E814 and E858.
7) L.D. Csernai and J.I. Kapusta, Phys. Rep. **131** , 223 (1986).

BNL-AGS 2.0 GeV/c K BEAM LINE

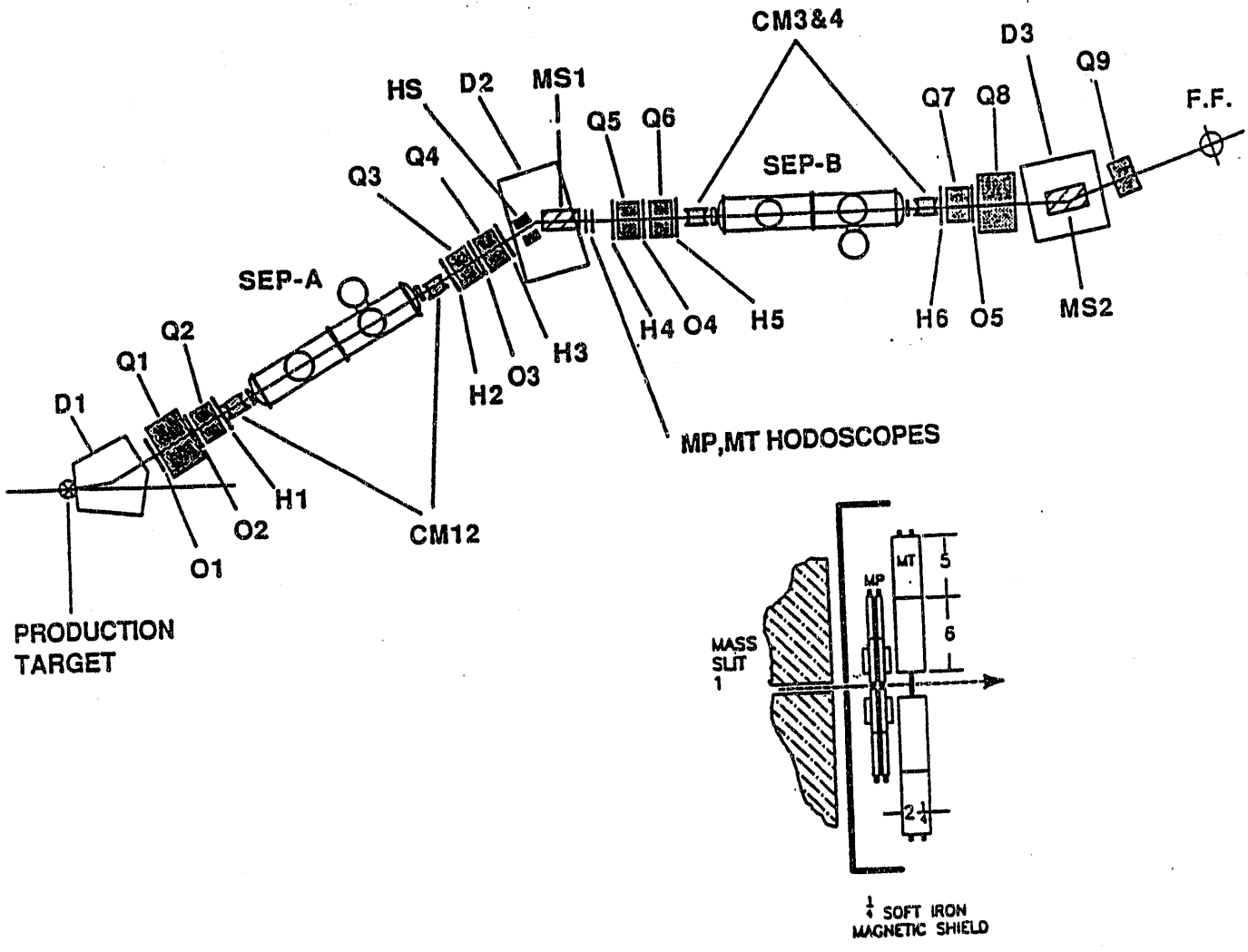

Fig. V.B.1. The BNL/AGS 2.0 GeV/c K-beam line which is used as a mass spectrometer.

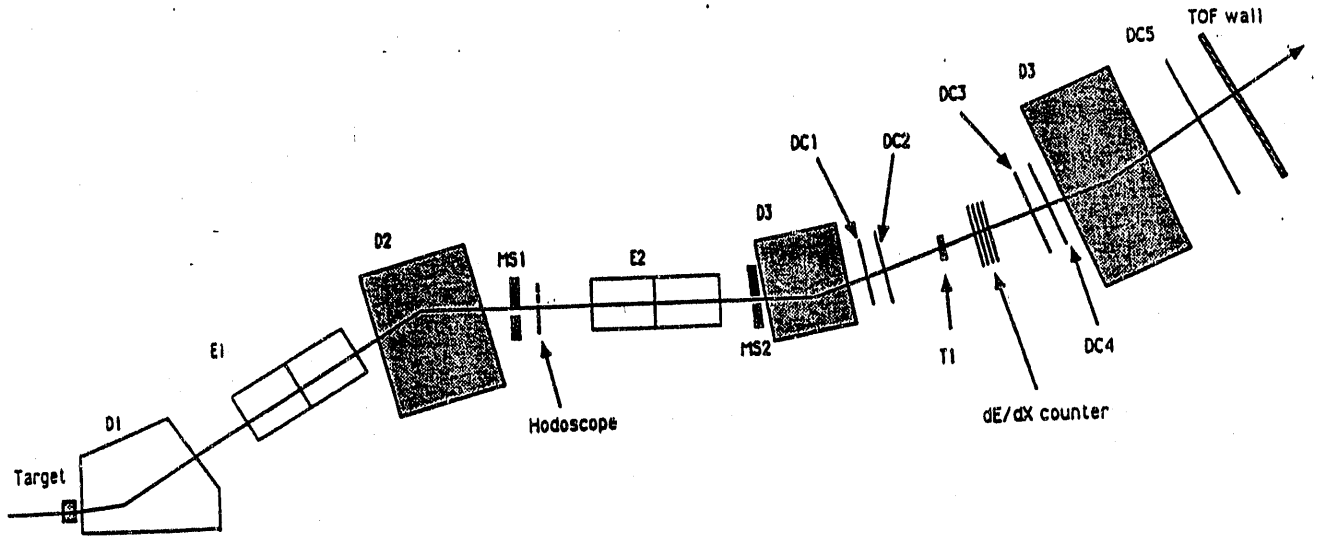

Fig. V.B.2. Experimental setup. Details about the detectors are in the text.

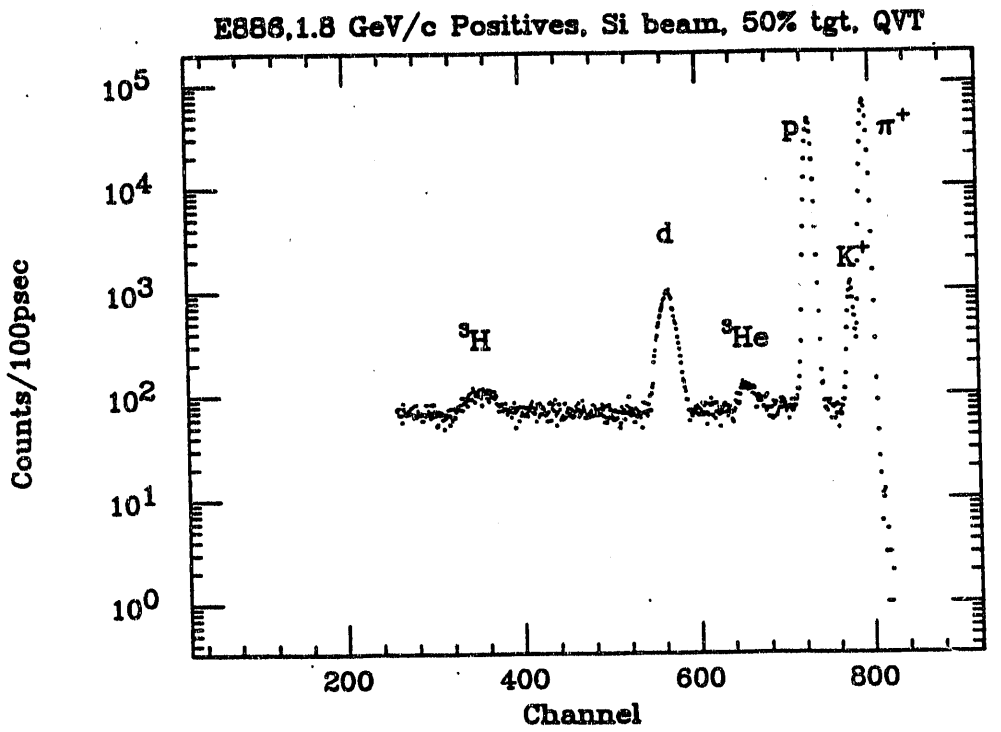

Fig. V.C.1. On-line time-of-flight spectrum with separators off showing particle species.

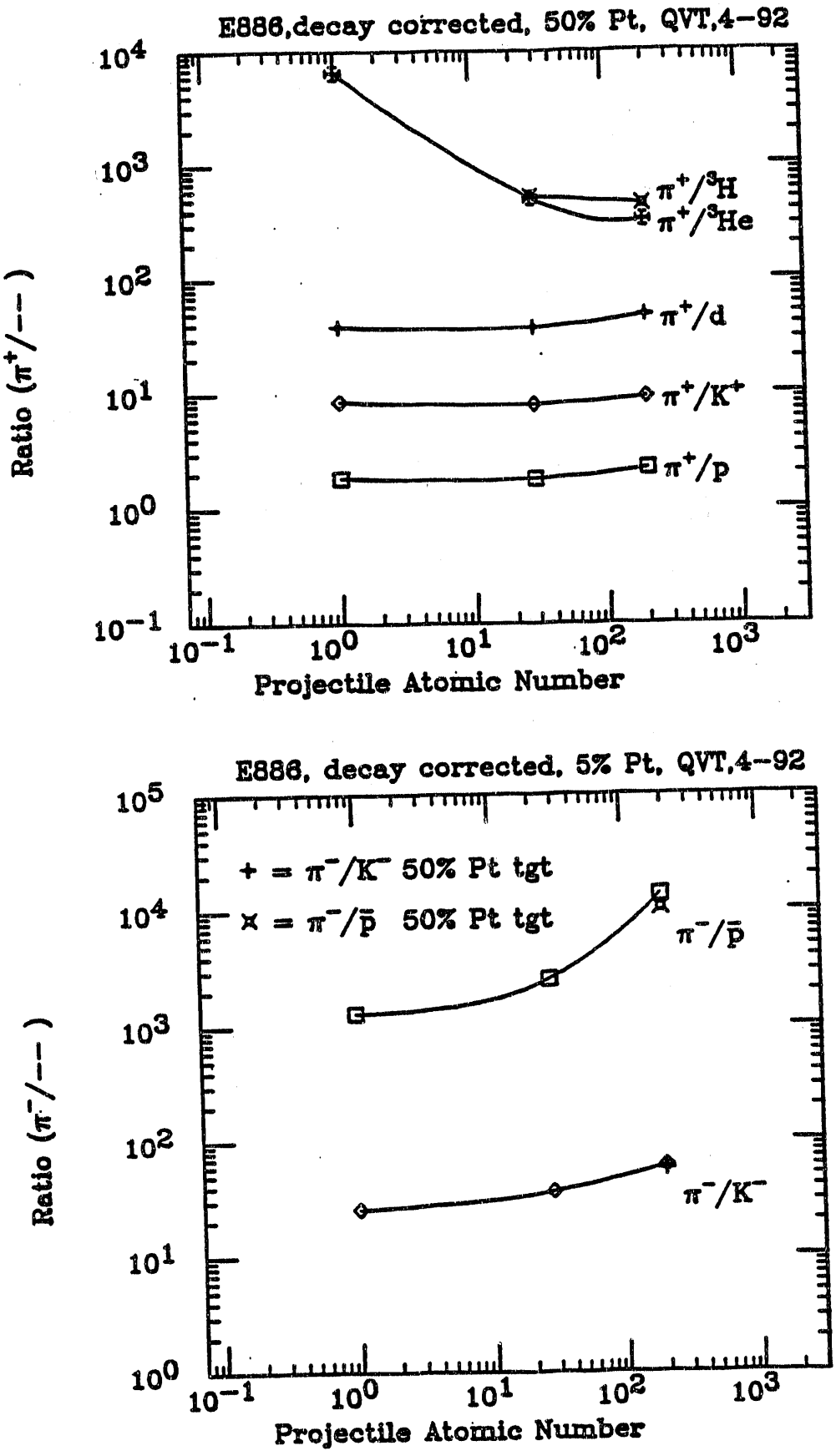

Fig. V.C.2. Ratios of particles for p, Si, and Au beams from test run. Positively charged particle ratios are shown at the top, negative particles at the bottom.

VI. Experiment to Detect Double Lambda Hypernuclei

VI.A. Double Lambda Hypernuclei

Measurements of the ΛΛ residual binding energy in double lambda hypernuclei can provide important insight into two-baryon forces, while studies of the decay modes of double lambda hypernuclei can provide indirect evidence concerning the existence of the H-dibaryon. To date, the emulsion-based experiments searching for double lambda hypernuclei have been unable to obtain more than a single candidate event for any one hypernuclear species. In addition, the two events reported in the 1960's[1,2] and the recent KEK event[3] appear to give inconsistent ΛΛ binding energies. A high statistics counter experiment is needed.

It is possible to create double hypernuclei through the reaction $K^- + Z \rightarrow K^+ + {}_{\Lambda\Lambda}(Z-2)$. Calculations of cross sections for reactions of this type have been performed by Baltz, Dover and Millener[4]. Unfortunately, the reaction involves a two-step process with large momentum transfer and the cross-sections are correspondingly small. As an alternative approach, M. May of BNL has suggested stopping Ξ^- hyperons in lithium[5]. In this case, the double lambda hypernuclei would be formed from the reaction:

$$(\Xi^-, {}^6\mathrm{Li})_{\mathrm{atom}} \rightarrow {}^{6}_{\Lambda\Lambda}\mathrm{He} + \mathrm{n}.$$

Observation of the monoenergetic neutron, T~31 MeV, in coincidence with a stopping Ξ^-'s identifies the formation of ${}^{6}_{\Lambda\Lambda}$He, and the neutron energy is used to determine the ${}^{6}_{\Lambda\Lambda}$He mass. This hypernucleus consists of 2 neutrons, 2 protons and 2 lambda particles, all in s-states. Like the alpha particle, ${}^{6}_{\Lambda\Lambda}$He is expected to be particularly stable. The branching ratio for this process has recently been calculated and is expected to be in the neighborhood of 4%[6].

We have calculated that the ${}^{6}_{\Lambda\Lambda}$He mass can be measured to 0.5 MeV using this method. Data accumulated in the course of this experiment will be relevant to several additional questions: The K^- will also interact with the carbon nuclei in the CH_2 target. This can lead to ΛΛ hypernuclear final states through $K^- + {}^{12}C \rightarrow {}^{2}{}_{\Lambda\Lambda}Be + K^+$, or to quasifree production of the H particle through $K^- + {}^{12}C \rightarrow K^+ + H + \Xi^-$. Data on these processes will be recorded concurrently. Detection of decay products of the S=−2 system can distinguish ΛΛ hypernuclei from a near-threshold H particle. The experiment will utilize the 2 GeV/c K^- beam, spectrometer, and detectors developed for our H particle searches.

A proposal to perform this experiment was presented to the Brookhaven AGS Program Advisory Committee in February, 1992, by a collaboration consisting of most of the institutes involved in the E813 H dibaryon search: Brookhaven National Laboratory, Carnegie Mellon University, University of New Mexico, University of Manitoba, TRIUMF, Kyoto Sangyo University, and Vassar College. It was approved for 1000 hours of running. Morgan May (BNL)

and Gregg Franklin (CMU) are cospokespersons. The discussion found in the following sections is based on the proposal presented to the PAC by the collaboration.

The collaboration will meet to consider the relative priorities of this new double lambda experiment and the E836 ^{3}He dibaryon search after the 1992 E813 run.

VI.B. Experimental Technique

We have measured the flux at 1.7 GeV/c to be 0.8×10^6 K^-s per 10^{13} incident protons. It is expected to exceed 1.0×10^6 per 10^{13} incident protons at 1.8 GeV/c. The identification of the production of Ξ^-'s will use the apparatus from our H particle search. The pions are rejected at the trigger level using two aerogel Cerenkov detectors in veto mode. Off-line time-of-flight cuts will also be used to reject pion induced events.

Fig. VI.B.1 shows the E813 spectrometer instrumented to detect, identify and momentum analyze the K^+ mesons. The aerogel Cerenkovs FC and BCA are used to veto pions. Chapter III contains a detailed discussion of our technique for producing tagged Ξ^-'s and the results from our E813 experiment clearly establish that the apparatus is working as designed.

The protons from elastic and inelastic K^-p scattering created a undesirably high trigger rate for E813, and we expect that the rate of these reactions will be even larger in the double lambda experiment due to the increased target mass. In E813, a critical angle Lucite Cerenkov, BCL, was used in the trigger during the 1991 E813 run to reduce the number of false triggers from elastic and inelastic K^-p scattering. However, this detector did not reject all the protons. Our University of New Mexico collaborators are working on the design of a liquid hydrogen Cerenkov counter, shown as FCH in Fig. VI.B.1, which could be placed downstream of the target. We are also testing a Cerenkov detector which uses aerogel produced with a recently developed process which has an index of refraction near 1.1. A second level time-of-flight trigger will further reduce the trigger rate.

A tungsten degrader slows the Ξ^-, which is brought to rest in a ^{6}Li hydride target. Ξ^-'s which are about to stop give a large pulse height in the silicon detector. The target design under consideration, shown in Fig. VI.B.2, would be similar to the E813 target in geometry but much simpler to construct since it would not require cryogenics.

The use of the silicon detector is combined with the in-beam detectors to produce a clean set of tagged Ξ^- events. The stopping efficiency is strongly dependent on the outgoing K^+ angle. A Monte Carlo simulation gives:

$$\varepsilon\Delta\Omega = \int \text{stopping probability} \cdot d\Omega = 1.1 \text{ msr}$$

Since most of the Ξ^- stops result from K^+ mesons entering the spectrometer within a 12 msr kinematic region, the K^+ mesons in this region of interest can be selected off-line. The fraction of these events which result in (Ξ^- , ^{6}Li)$_{atom}$ is thus 1.1msr/12msr or 9%. The simulations show that 27% of the selected (Ξ^- , ^{6}Li)$_{atom}$ events give a Ξ^- tag in the silicon detectors and 33% of these tags result in (Ξ^- , ^{6}Li)$_{atoms}$. This compares favorably to the E813 value of $\varepsilon\Delta\Omega$ =0.12 msr. The factor of 9 increase is due to the increased stopping power of the Li-hydride target compared to the liquid deuterium target.

The signal-to-noise ratio can be greatly improved by tagging events with coincident energetic protons in the out-of-beam detector array. We note that in a hypernucleus, in addition to the usual free decay modes of the lambda:

$$\Lambda \rightarrow p\,\pi^-$$
$$\Lambda \rightarrow n\,\pi^o$$

new weak processes can occur:

$$\Lambda p \rightarrow np$$
$$\Lambda n \rightarrow nn.$$

Detection of the fast proton from the nonmesonic decay clearly identifies a lambda bound to a nucleus. Two fast protons indicate either a $\Lambda\Lambda$ hypernucleus or two Λ hypernuclei. The Q value of these nonmesonic decays is approximately 180 MeV so that the final state nucleon typically has 90 MeV kinetic energy as opposed to 5 MeV for the nucleon in free Λ decay. In hypernuclei with A>10, the nonmesonic decays are more than 5 times more numerous than the decays accompanied by pions. Our hypernuclear decay experiment, E788, has shown that 25% of the $^5_\Lambda$He decays give a proton with kinetic energy $\geq$ 30 Mev[7].

Decay protons and pions will be detected in the neutron counters. These neutron counters are arranged in five layers and cover one third of the solid angle in the configuration of experiment 813. We plan to arrange the counters so that 50% of the solid angle is covered by the counters in two layers. The same neutron efficiency results. We plan to add a layer of thin (1/4") scintillation counters in front of the neutron counters in addition to the existing veto layer to aid in distinguishing protons from pions. The time-of-flight of the decay particles from out-of-beam scintillators on each side of the target to the neutron detector arrays is used to determine the velocity of the decay products. Particle identification is done with a combination of β, range, and dE/dx measurements.

Wire chambers surrounding the target will trace the trajectory of the pions so a path length correction can be made for timing. It should be noted that successful identification of hypernuclear decay products was achieved with these neutron detectors in experiment 788. With 50% of the solid angle covered and a 25% probability of energetic proton emission on each of the two weak decays, the probability of detecting at least one energetic proton becomes $1-(1-.50\times.25)^2 = 0.23$.

Thus the signal is reduced by a factor of four when coincident protons are required but the signal-to-noise ratio will improve.

VI.C. Branching Ratio

When a Ξ^- stops in ^{6}Li, it is captured in an atomic orbit with a large principle quantum number. The orbit from which the Ξ^- is eventually captured depends on the details of the electromagnetic cascade and on the strength of the Ξ^- nucleon inelastic interaction. It is anticipated that the Ξ^- is captured 20% of the time from a *p* state and 80% of the time from a *d* state. It should be noted that only Ξ^- capture from the *p* state results in ${}^{\;\;6}_{\Lambda\Lambda}$He, a system in which both lambda particles are in *s* orbits. This selection rule results from angular momentum conservation.

When the Ξ^- interacts with a proton in the ^{6}Li target, the final state consists of two lambda particles, an alpha particle and a neutron. If both lambdas are bound to the alpha, ${}^{\;\;6}_{\Lambda\Lambda}$He and a monoenergetic neutron result. It is also possible that neither, or only one lambda is bound to the alpha:

$$(\Xi^-, {}^6\mathrm{Li})_{\mathrm{atom}} \rightarrow \Lambda + \Lambda + \alpha + n$$
$$(\Xi^-, {}^6\mathrm{Li})_{\mathrm{atom}} \rightarrow \Lambda + {}^{\;\;5}_{\Lambda}\mathrm{He} + n$$

The neutron spectra from these two reactions are shown in Fig. VI.B.3, along with the peak resulting from ${}^{\;\;6}_{\Lambda\Lambda}$He formation which is clearly separated from these other processes. This figure is a result of a detailed calculation which predicts the spectrum shape and the branching ratio for ${}^{\;\;6}_{\Lambda\Lambda}$He formation to be 3.4%. Reactions which break up the alpha particle have a much lower Q value and are suppressed by phase space. For example,

$$(\Xi^-, {}^6\mathrm{Li})_{\mathrm{atom}} \rightarrow {}^{\;\;3}_{\Lambda}\mathrm{H} + {}^{\;\;3}_{\Lambda}\mathrm{H} + n$$

has a maximum neutron kinetic energy of only 1 MeV.

We plan to stop the Ξ^-'s in ^{6}LiH, since it has a higher density than metallic ^{6}Li. If a $(\Xi^-,p)_{\mathrm{atom}}$ is formed, transfer usually occurs to the Li. This transfer favors capture from lower l values in the $(\Xi^-, {}^6\mathrm{Li})_{\mathrm{atom}}$ which in turn increases the rate of ${}^{\;\;6}_{\Lambda\Lambda}$He formation due to the *p* capture selection rule.

If ${}^{\;\;6}_{\Lambda\Lambda}$He is formed in the $s_\Lambda p_\Lambda$ configuration, the p_Λ is unbound by 2-3 MeV. The width of this state may be smaller than the 3 MeV resolution of the experiment. Since this state can be formed by the more prevalent *d* capture, it may appear at a higher rate than the ground state.

Calculations are in progress concerning targets other than ^{6}Li. In particular, we are studying ^{9}Be. If a more favorable case is found we have reserved the option to use it.

VI.D. Rate and Background Calculations for ${}^{\;\;6}_{\Lambda\Lambda}$He Production

Assume 10^{12} K^-'s on a 30 cm long CH_2 target of design as shown. This flux corresponds to 800 hours of beam at 10^6 K^-'s/spill. This results in 30,000 stopping Ξ^-'s in the ^{6}Li. The

efficiency × solid angle for detecting the 30 MeV neutron is 10%. A branching ratio for the ${}^{6}_{\Lambda\Lambda}$He formation of 3.4% results in 100 events in the time-of-flight peak.

The main source of neutron background is π^- capture where the π^-'s come from lambda decay. Each stopping π^- in ^{6}Li gives .02 neutrons per MeV near 30 MeV neutron kinetic energy (if the pion stops in the tungsten degrader, the number may be 25% lower). Since the neutron energy resolution is 3 MeV, we have a background under the signal of .06 neutrons/π^- stop. Each Ξ^- stop produces 2 Λs ; each Λ produces 2/3 π^-; we assume that half of the π^- stop. Therefore we have .04 neutrons/Ξ^- stop. Thus a 4% branching ratio will give 1:1 signal to background from this source. We expect one Ξ^- stopping in the ^{6}Li for every three Ξ^- tagged by the silicon detector array. Thus we increase the estimated background by a factor of 3.

Accidental counts: For a branching ratio of .04 and a neutron detection efficiency of .1 we have 750 tags per good event. The 3 MeV energy resolution corresponds to .5ns timing resolution. A counting rate of 1.5×10^6 in the neutron counters gives an accidental rate which is 60% of the signal. This assumed counting rate is somewhat lower than observed in experiment 813 and assumes improvement due to improved performance of the electrostatic separator.

Thus the signal to background will be 1:3.6. A signal of 100 counts would constitute a 5.3σ measurement. With 3 MeV resolution in the neutron detectors, the centroid of the peak would be measured to a statistical uncertainty of approximately 0.5 MeV rms.

VI.E. Direct Production of $\Lambda\Lambda$ Hypernuclei and the H particle

As described above, a CH_2 target is used to produce the Ξ^-'s. $\Lambda\Lambda$ hypernuclei will also be produced directly

$$K^- + {}^{12}C \rightarrow {}^{12}_{\Lambda\Lambda}Be + K^+.$$

In the two body reaction, missing mass gives the spectrum of hypernuclear states. A search can be made for $\Lambda\Lambda$ hypernuclei produced in this manner concurrently with the ${}^{6}_{\Lambda\Lambda}$He experiment although the target is thicker than one would like for good resolution. The energy loss of the K^- and K^+ traversing the full thickness of the target is 50 MeV. The full width of the energy loss distribution is approximately 20% or 10 MeV.

Because of the large momentum transfer, this reaction in most cases leads to continuum states. Calculations of the cross section for the reaction to individual bound states have been made for 1.1 GeV/c K^-. Cross sections should be higher for 1.8 GeV/c K^- for a variety of reasons; 1.1 GeV/c is below threshold for Ξ^- production, 1.8 GeV/c is at the peak of the two body Ξ^- production cross section. Up to an order of magnitude increase might be obtained by small admixtures of hypernuclear states. Here, however, we assume the 1.1 GeV/c cross sections which we regard as a lower limit.

We assume 10^{12} K^- on a 30 gm/cm^2 CH_2 target; a solid angle of the K^+ spectrometer of 65 msr; a factor of .45 for K^+ decay and of .75 for efficiencies. This gives a sensitivity of 33 events per nb/sr. The calculated cross section to hypernuclei with both lambdas bound is 12 nb/sr. Thus we expect 400 double hypernuclei below the lambda escape threshold.

Approximately 15 MeV are required to remove a lambda from $^{12}_{\Lambda\Lambda}$Be; thus even the modest resolution of this spectrometer is sufficient to pick out the $\Lambda\Lambda$ hypernuclear region. Also, 24 MeV is required for $^{12}_{\Lambda\Lambda}$Be to fission into 2 single hypernuclei (somewhat more if the Coulomb barrier is taken into account). Thus we have a 24 MeV region where detection of two decays signals a $\Lambda\Lambda$ hypernucleus.

If the H particle exists, it could be observed in the reaction

$$K^- + {}^{12}C \rightarrow K^+ + H + X$$

As discussed by Aerts and Dover[8], this quasifree H production will result in a peak in the (K^-,K^+) missing mass spectrum. This approach has been applied in an experiment at KEK[9]. The spectra we obtain in the course of our search for $\Lambda\Lambda$ hypernuclei will improve these limits by orders of magnitude.

VI.F. Auxiliary Measurements

The out-of-beam detector instrumentation is configured similar to the hypernuclear lifetime experiment 788. This will permit measurements of the lifetime and branching ratios. In a $\Lambda\Lambda$ hypernucleus new weak decay modes are possible. We may observe the weak interaction between two lambda particles

$$\Lambda\Lambda \rightarrow \Lambda n$$
$$\Lambda\Lambda \rightarrow \Sigma^- p$$
$$\Lambda\Lambda \rightarrow \Sigma^0 n$$

The branching fraction for these channels has been estimated to be in the 3-6% range[10]. A scintillating fiber array designed to detect the energetic Λ's which would be ejected from the target with a characteristic decay length of 3 cm is being studied. This would result in a few detected $\Lambda\Lambda \rightarrow \Lambda n$ events from $^{12}_{\Lambda\Lambda}$Be decays if the lower estimate of 400 bound $^{12}_{\Lambda\Lambda}$Be events is used, but could be much larger if the effect of Ξ^- admixtures is significant, the $\Lambda\Lambda$ system is closely correlated in the nucleus, or the H particle is formed.

VI.G. Responsibilities

Carnegie Mellon will be responsible for much of the overall organization of the collaboration in addition to specific roles in the neutron detector, data acquisition and analysis, drift chamber FD3, and electronics. We are also working on Monte Carlo simulations and plan to develop the scintillating fiber array device along with our KEK and Kyoto Sangyo colleagues.

BNL will develop the out-of-beam detector package that will augment our existing neutron detector package. Additional collaboration responsibilities will be discussed this summer.

Chapter VI References

1) M. Danysz *et al.*, Phys. Rev. Lett. **11**, 29 (1963).
2) D. Prowse, Phys. Rev. Lett. **17**, 782 (1963).
3) S. Aoki *et al.*, Phys. Rev. Lett. **65**, 1729 (1990).
4) A.J. Baltz, C.B.Dover, and D.J. Millener, Phys. Lett. **123B**, 9 (1982).
5) M. May, Nuovo Cimento **102**, 401 (1989).
6) D. Zhu, C. B. Dover, A. Gal, and M. May, Phys. Rev. Lett. **67**, 2268 (1991).
7) J.J. Szymanski, *et. al.*, Phys. Rev. C **43**, 849 (1991).
8) A.T.M. Aerts and C. B. Dover, Phys. Rev. Lett. **49**, 1752 (1982); Phys. Rev. **D28**, 450 (1983).
9) S. Aoki *et al.*, Phys. Rev. Lett. **65**, 1729 (1990).
10) M. May, C. B. Dover in preparation.

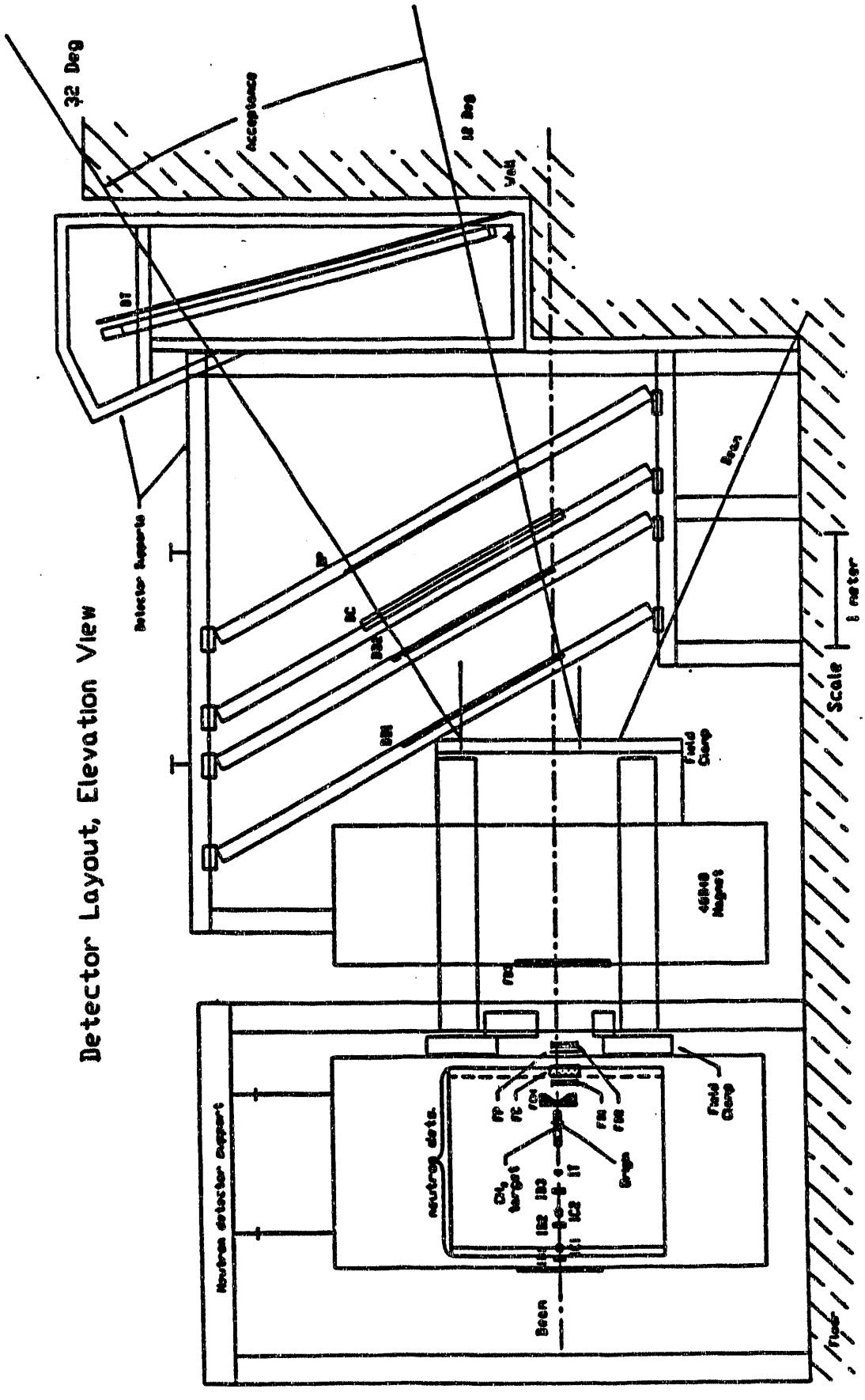

Fig. VI.B.1 Detector configuration for ΛΛ experiment. Drift chambers ID1, ID2, and ID3 determine incoming K^- trajectory and are combined with upstream hodoscope data to determine K^- momentum. Drift chambers FD1, FD2, FD3, BD1 and BD2 determine K^+ momentum. Scintillators IT and BT determine K^+ time-of-flight. Hodoscopes FP and BP determine spectrometer acceptance. Aerogel Cerenkovs IC1, IC2, FC, and BC reject pions. Hydrogen Cerenkov FCH rejects protons.

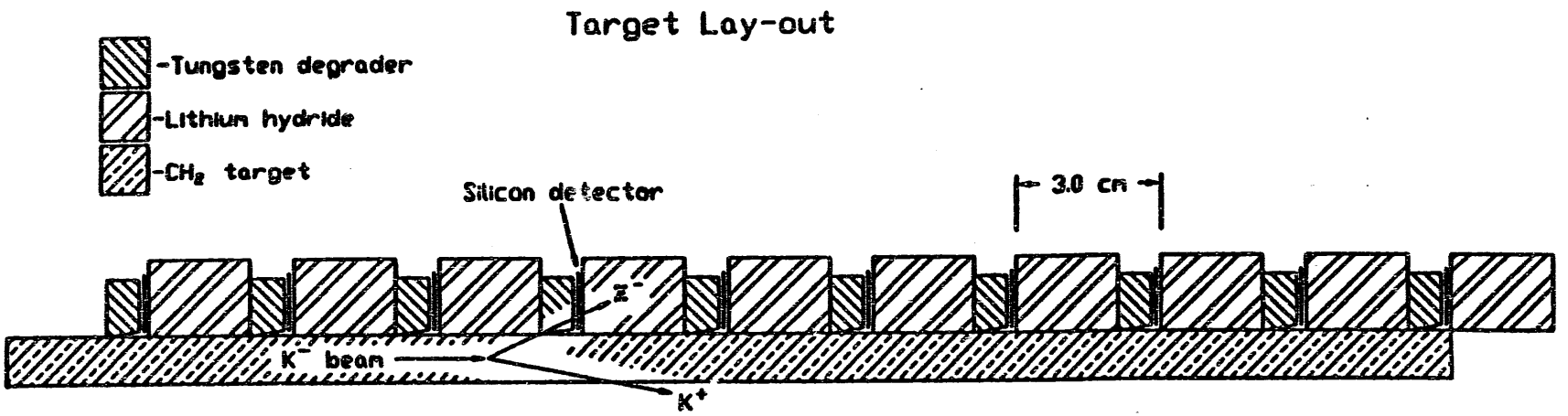

Fig. VI.B.2 Schematic diagram of target. Ξ^- hyperons are created in the CH_2, slowed in the tungsten, tagged by the silicon detectors, and stopped in the Lithium-Hydride.

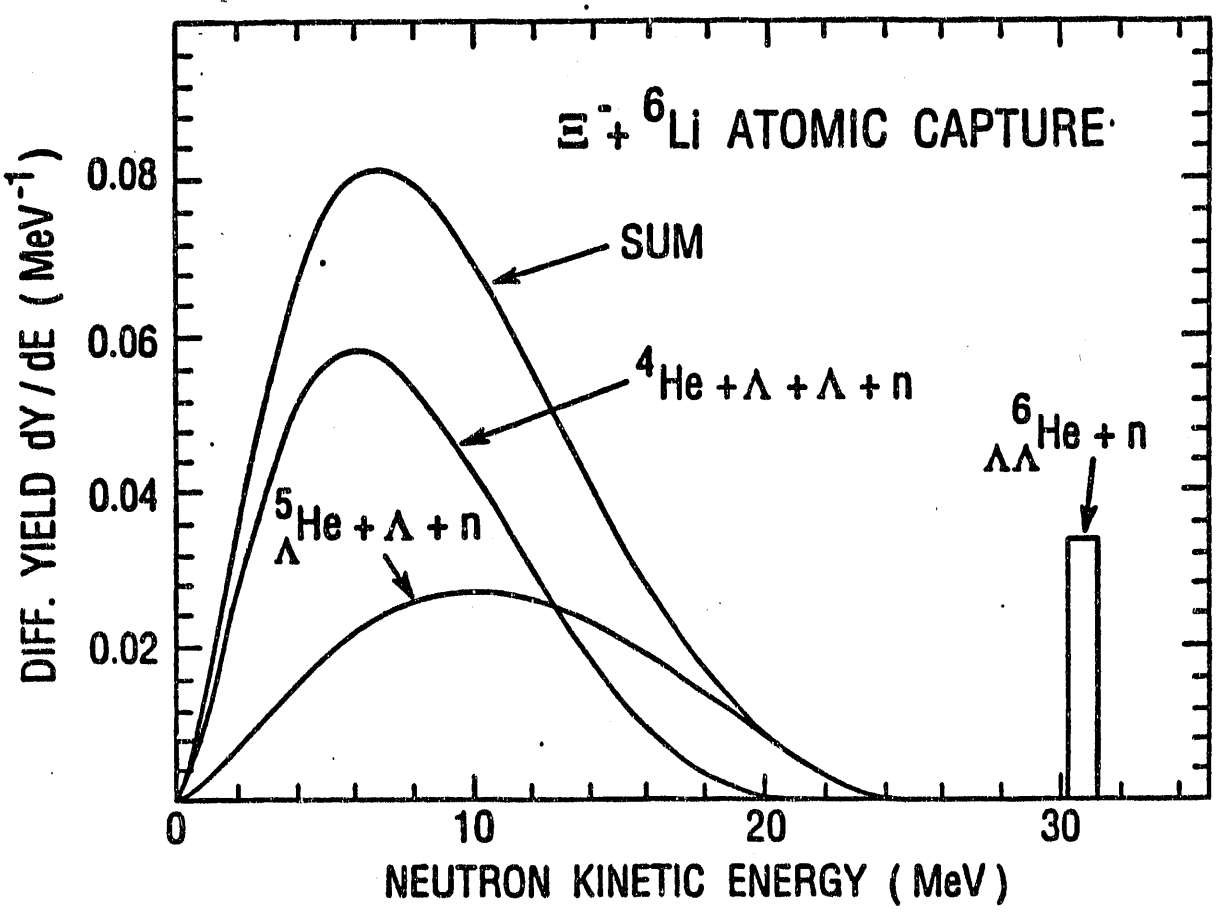

Fig. VI.B.3 Calculated differential yield $d\,Y/d\,E$ as a function of the outgoing neutron kinetic energy, for $\Xi + {}^{6}Li$ capture at rest. The contributions of other reaction branches, as well as their sum, are indicated, assuming 20% p capture and 80% d capture. Assuming 1 MeV energy resolution for the neutron, the contribution of the $n + {}^{6}_{\Lambda\Lambda}He$ channel is shown as a rectangle centered at 30.7 MeV; the integrated yield for this branch is about 3.4% per stopped Ξ^{-}.

VII. Hyperon Photoproduction at CEBAF

VII.A. Introduction

The Continuous Electron Beam Accelerator Facility (CEBAF) in Newport News, Virginia, is a 4 GeV electron accelerator laboratory which will provide medium energy physicists with an unmatched tool for probing the structure of nuclei and elementary hadrons. Among the features which make this laboratory special are its 100% duty factor electron and photon beams, and experimental apparatus which will detect several final state particles simultaneously. Coincidence experiments with continuous beams will help us probe much deeper than before into the dynamics of nuclear reactions and the structure of baryons. This accelerator is presently under construction and is scheduled to begin operations with electron and photon beams in 1994.

In the fall of 1989 we submitted a proposal to CEBAF entitled "Electromagnetic Production of Hyperons". Section VII.B. provides an overview of the physics motivation of this experiment. The experiment was approved by the CEBAF Program Advisory Committee in March, 1990, and granted 700 hours of beam time. The group of people involved in this effort include the CMU faculty in the Medium Energy Group, as well as physicists from CEBAF, Los Alamos National Laboratory, Catholic University of America, the University of Washington, and Virginia Polytechnic Institute. This experiment will use the CLAS spectrometer in Hall B, which is a large-acceptance, toroidal-field magnetic spectrometer; its design is optimized for detecting several particles resulting from the decay of an excited baryon, hyperon, or nucleus.

CEBAF needs and expects significant University participation in the development of experimental facilities. At Carnegie Mellon we have focussed on the Region 1 drift chamber package as an area in which we will participate. This detector package sits in the center of the CLAS, close to the target but outside a "mini-toroid" which shields the detector from low energy electrons. An overview of this detector is given in Chapter VIII. There we also discuss the specific role which Carnegie Mellon is playing in the design and construction of this detector.

VII.B. Strangeness Photoproduction Physics

The following is a brief overview of the physics motivation and experimental requirements for the study of the electromagnetic production of strange particles. Studies of systems with one or more strange-quarks add to our understanding of fundamental two particle interactions by providing an opportunity to extend models developed for N-N, π–N, and γ-N (i.e. non-strange) interactions. Our first experiments will focus on the elementary photoproduction of the Λ, Σ^0, and Σ^+ using real photons.

The electromagnetic creation of $\bar{s}s$ quark pairs adds degrees of freedom to baryon spectroscopy which have not been adequately explored. The goals of our proposed measurements

are an improved knowledge of the strangeness production mechanism and of the nucleon-hyperon coupling constants. The proposed first-round measurements which will be done with the CEBAF Large Acceptance Spectrometer (CLAS) are the three possible elementary strangeness-producing reactions on the proton: 1) the elementary photoproduction of Λ hyperons, measuring the polarization of the Λ as well as the differential cross section from threshold to about 1.8 GeV; 2) the production of Σ^0 hyperons under the same kinematic conditions as the Λ's; and 3) the production of Σ^+ hyperons. Experimentally, we detect the kaons and the decay products of the hyperons in the reactions:

$$\gamma + p \rightarrow K^+ + \Lambda \qquad (1)$$
$$\rightarrow \pi^- + p$$

$$\gamma + p \rightarrow K^+ + \Sigma^o \qquad (2)$$
$$\rightarrow \gamma + \Lambda$$
$$\rightarrow \pi^- + p$$

$$\gamma + p \rightarrow K^o + \Sigma^+ \qquad (3)$$
$$\rightarrow p + \pi^o$$
$$\rightarrow \pi^- + \pi^+$$

The differential cross section for reaction (1) is moderately well established, but the proposed addition of polarization data will permit significant progress in the understanding of the strangeness photoproduction elementary amplitudes. Reaction (2) has rarely been measured due to the lack of appropriate tagged photon beams and detectors. Additional data should further constrain the spin-isospin structure of photoproduction models. Reaction (3) has never been measured and data are needed to round out our knowledge of these reactions.

The associated production of strange particles (reactions in which an S= +1 particle is produced along with an associated S= −1 particle) has been studied with reactions such as $\pi^- + p \rightarrow K^o + \Lambda$ [1], $p + \bar{p} \rightarrow \Lambda + \bar{\Lambda}$ [2], and $p + p \rightarrow \Lambda + X$ [3]. Figure VII.B.1 shows the quark flow diagrams for some of these reactions. The final state hyperons formed through these reactions have been found to be strongly polarized. The cause of this polarization may be partially due to elementary $s\bar{s}$ quark-pair production and partially due to initial and final state interactions. The photoproduction of Λ–K and Σ–K pairs are reactions well suited to the study of polarization effects, since initial state interactions are absent.

Significant new information can be obtained by performing production experiments with either real or virtual photons. Virtual photoproduction (i.e. electron scattering) allows exploration of much of the (Q^2,ν) response structure of the reaction[4]. But an advantage of studying real photoproduction over electroproduction is that only four complex amplitudes need to be considered. Experimentally, real photoproduction may be simpler also, because one less particle needs to be detected in the multi-particle detector. Also, background problems should be less severe using a real photon beam. We will discuss only real photo-production.

The reaction $\gamma + p \rightarrow \Lambda + K^+$ has been studied since the late fifties[5], and received considerable experimental and theoretical attention in the 60's and early 70's. The differential cross section is moderately well established from threshold (at 911 MeV) up to 1.4 GeV, while the polarization of the Λ has been measured at only a few angles and energies, typically with large error bars. Figs. VII.B.2 and VII.B.3 give overviews of some of the existing differential cross section data and polarization data[6,7]. Note that the polarization data shown in Fig. VII.B.3a, which are for a kaon c.m. angle of $90^\circ \pm 5^\circ$, represent well over half of the data points ever measured. The others are scattered in angle and energy.

Presently, there are no calculations of strangeness photoproduction inspired directly by the quark model, though one might expect such models to be constructible, as they have been for the reaction $p\bar{p} \rightarrow \Lambda\bar{\Lambda}$, for example[8]. Instead, traditional calculations have been undertaken using tree-level Feynman diagrams. In addition to the graphs involving the exchange of ground state baryons and mesons, one must generally include graphs with low-lying N* (s-channel), Y* (u-channel), and K* (t-channel) intermediate states. Partly due to a lack of sufficient good data, the proper formulation of the interaction has remained uncertain, particularly regarding which graphs should be included. One consequence of this is a long-standing uncertainty in the basic coupling constants $g_{KN\Lambda}$ and $g_{KN\Sigma}$. Analyses of photoproduction data have produced values for $g_{KN\Lambda}$ roughly a factor of two smaller than those obtained from hadronic data. Recent authors have attempted to understand the source of this difference. Adelseck and Wright [9] found that including $K_1(1280)$ (formerly Q(1280)) exchange in the t-channel increased $g_{\Lambda KN}$ to the hadronic value. Tanabe, Kohno, and Bennhold [10] (TKB), on the other hand, pointed out the necessity of including $K^+\Lambda$ final state correlations, which are absorptive in the low partial waves, and can also affect the values for the coupling constants obtained. By including a partial wave dependent absorptive factor in addition to the usual Born and resonance terms, TKB fit the total cross section data at higher energies (above 1.5 GeV) and claim to get the hadronic-reaction value for $g_{\Lambda KN}$. Cohen [11], on the other hand, has concluded that the couplings derived from photoproduction experiments actually produce *better* agreement with low energy KN scattering data than the standard hadronic values in an effective Lagrangan model. Hence the theoretical situation is not at all settled.

Various authors [6,7,10,11] have pointed out that progress could be made in this field if better Λ polarization data were available. For example, it is clear from Fig. VII.B.3 that improved polarization data would discriminate among various values of the coupling constants. Figure VII.B.3a shows the older analysis of Renard[7] which clearly indicates the sensitivity of the models to Λ polarization data. Fig. VII.B.3b is from the newer analysis of Adelseck and Wright[9] (same data with opposite sign convention), showing again the poor quality of the present data. Apart from better differential cross section data, Λ polarization measurements would be the principal contribution of new experiments at CEBAF, which would be designed to look for the self-analyzing decay of the Λ into π^- p in coincidence with the kaon which tags production of the Λ.

This will be possible with a large acceptance device capable of detecting the Λ decay products as well as the kaons.

In the future, CEBAF will be able to provide polarized hydrogen targets and polarized photon beams. Thus, experiments measuring a wide range of spin correlations in the Λ production reaction are possible. The benefits of such measurements have not yet been explored.

We now turn to the elementary photoproduction of the Σ^o hyperon. There exists little data[7,12] on the photoproduction of the Σ^o hyperon (threshold at 1046 MeV). This is because single bremsstrahlung beam experiments normally separate the production of the Σ^o from the Λ by the difficult method of bremsstrahlung endpoint fitting. The bremsstrahlung difference method has also been used, but it is slow and cumbersome. The tagged photon method is an attractive way to measure both Λ and Σ production simultaneously since it offers adequate missing-mass resolution to resolve the Σ^o, and can cover a wide range of photon energies simultaneously.

The Λ and Σ^o hyperons are in the same spin-parity octet, and are related at the quark level by spin flips of two quarks. The production ratio of these two hyperons is predicted by spin-flavor SU(6) to be $\sigma(\gamma p \rightarrow K^+\Sigma^o) / \sigma(\gamma p \rightarrow K^+\Lambda) = 1 / 3$, while experiment yields about unity[13]. Since the Σ^o has isospin 1, rather than isospin 0 like the Λ, the isospin 3/2 Δ resonances can play a role in the production process. The fact that additional terms are needed to describe Σ^o photoproduction point out the desirability for more and better data on this reaction. Furthermore, no polarization information exists at all for Σ^o production. Because the Σ^o decays 100% via an M1 transition to the Λ, any measurement of the decay Λ polarization also measures the polarization of the Σ^o.

The third elementary hyperon photoproduction reaction possible on the proton is $\gamma+p \rightarrow K^o+\Sigma^+$. The study of this reaction is interesting to compare with the previous reaction since many of the same diagrams contribute. This reaction has no t-channel exchange. The decay asymmetry for the Σ^+ is very large (α=–0.98), so its decay into $p\pi^o$ reveals information about the Σ^+polarization. To our knowledge, this reaction has never been measured.

VII.C. Experimental Requirements

CEBAF offers several distinct advantages over previous facilities for the experimental study of hyperon photoproduction. These advantages are: the CW nature of the CEBAF beam which makes multi-particle final states easier to measure, the possibility of using a tagged photon beam to establish the kinematics of the initial state, and the expected availability of a detector with large solid angle and large momentum acceptance. Combined with up-to-date electronic readout and triggering, this facility will allow a large quantity of new, kinematically complete data on photoproduction to be obtained in an efficient manner.

We have studied the phase space of the reaction $\gamma + p \rightarrow K^+ + \Lambda$. Assuming isotropic production of kaons in the γp center-of-mass frame near the reaction threshold, Monte Carlo calculations show that the heavier particles in the (K,p,π) final state are strongly forward peaked (below about 60^o) and that the pions have only a slight tail to large angles. This underlines the importance of good forward angle coverage in the CLAS detector.

To get an idea of the CLAS acceptance for the final states needed to detect Λ polarization, calculations were made with FASTMC, a Monte Carlo program written at CEBAF for modeling the behavior of the CLAS detector. The acceptance for detecting the kaon in the lambda production reaction is shown in Fig. VII.C.1. For example, we found that better acceptance will be obtained by reducing the field of the CLAS to less than half of its nominal value, because this increases the acceptance of particles at the low momentum end of the phase space. Fig. VII.C.2 shows a GEANT simulation of a typical event which may be seen in the detector, one in which all three final state particles reach the trigger counters.

The common experimental feature of the reactions discussed above is the need to filter out the copious non-strange events by identifying strangeness production. The total production cross section for Λ photoproduction is close to 1μb in the energy range E_γ between 1 and 2 GeV. For a 1.0 gram/cm^2 liquid hydrogen target (14 cm in length) and a total photon tagging rate (over all energies) of 10MHz, one obtains a raw production rate of 6 Λ's per second. The ratio of the production rate of hyperon events which decay into three charged particles to all events with three charged particles is about 1:200. One can exploit the fact that the production and decay in the above reactions are all two-body interactions, so that one-to-one mapping between kinematic variables exists (for example between kaon angle and kaon momentum). These measurements could, in fact, be made with a non-magnetic imaging detector which only provided tracks of all charged final state particles. An example of this approach is the PS185 experiment at LEAR [2]. The momentum information is obtained by a magnetic detector at the added cost of reconstructing curved tracks and some loss of dynamic range since low momentum particles will be swept out of the detector. The benefit of a magnetic detector is the contribution of redundancy checks from the momentum information in analyzing the data.

Another useful kinematic feature in these measurements is the fact that neutral strange hyperons have a decay length of several centimeters. This allows the possibility of using the

neutral "V" to signal the production of strange particles. The vertex defined by the $\Lambda \rightarrow \pi^- + p$ decay will be spatially separated by distances on the order of centimeters from the track of the K^+. A cut on the minimum distance between the kaon track and the Λ vertex can be used to select events with strange particles. The off-line analysis will use this technique to select the "good" events. Note that with increasing momentum, the kaon time-of-flight identification will become more difficult while the Λ will have an increasing decay length, making the latter method more useful in identifying strangeness production.

The total hadronic background rate is not very energy dependent. The total cross section for γp going to one nucleon plus at least two charged pions is about 130μb. The expected raw trigger rate might be about 1000 Hz if we trigger on at least three charged particles. One source of background is expected to be the reaction $\gamma + p \rightarrow \Delta^o + \pi^+$ followed by $\Delta^o \rightarrow \pi^- + p$. The positive pions produced in this reaction are kinematically almost indistinguishable from the kaons, with the added complication that the Δ^o is a resonance which is broad enough to significantly overlap the Λ and Σ mass region. Thus, K/π particle separation is very important.

In summary, we believe that useful and interesting new physics can be learned through the experimental study of elementary strangeness photoproduction at CEBAF. The photon tagging facility and a large-acceptance detector system make new measurements possible which will improve our knowledge of the reactions we have discussed above: 1) the elementary photoproduction of Λ hyperons, measuring the polarization of the Λ as well as the differential cross section; 2) the elementary photoproduction of Σ^o hyperons under kinematic conditions similar to the Λ's; and 3) the Σ^+ production reaction which has not been measured and which is complementary to the others.

Chapter VII References

1) See for example: R. Schwarz *et al.*, AIP Conf. Proc. **95** "High Energy Spin Physics," G. Bunce, Ed., (1982) 114.
2) P.D.Barnes *et al.* Phys Lett. B **189** (1987) 249.
3) K. Heller, AIP Conf. Proc. **95** "High Energy Spin Physics," G. Bunce, Ed., (1982) 320, and references therein.
4) See for example: C.J.Bebek *et al*, Phys Rev Lett. **74** (1974) 21.
5) Earliest published measurements: P.L.Donoho and R.L.Walker, Phys. Rev. **107** (1957) 1198; A. Silverman, R.R.Wilson, and W. M. Woodward, Phys. Rev 108 (1957) 501; P.L.Donoho and R.L.Walker, Phys. Rev **112** (1958) 981; B. D. McDaniel, A. Silverman, R.R.Wilson, and G. Cortellessa, Phys. Rev. **115** (1959) 1039. Earliest Λ polarization measurements: H. Thom, E. Gabathuler, D. Jones, B.D.McDaniel, and W.M.Woodward, Phys Rev. Lett. **11** (1963) 433.
6) Available data are summarized in R.A.Adelseck, C. Bennhold, and L.E.Wright, Phys. Rev **C32** (1985) 1681.
7) Y.Renard Nucl. Phys. **B40** (1972) 499.
8) M. Kohno and W. Weise, Phys Lett. B **179** (1986) 15.
9) R.A.Adelseck and L.E.Wright, to be published 1988; Ralf Anton Adelseck, PhD thesis, Ohio University (1988).
10) H. Tanabe, M. Kohno, and C. Bennhold, Contribution to 1988 CEBAF Summer Workshop; and Mainz Preprint, 1988.
11) Joseph Cohen, Phys. Lett. B **192** (1987) 291; Joseph Cohen, Phys. Rev. C **37** (1988) 187.
12) P. Feller, D. Menze, U. Opara, W. Schulz, and W.J.Schwille, Nucl. Phys. **B39** (1972) 413.
13) Harry J. Lipkin, Phys. Rep. **8C** (1973) 175.

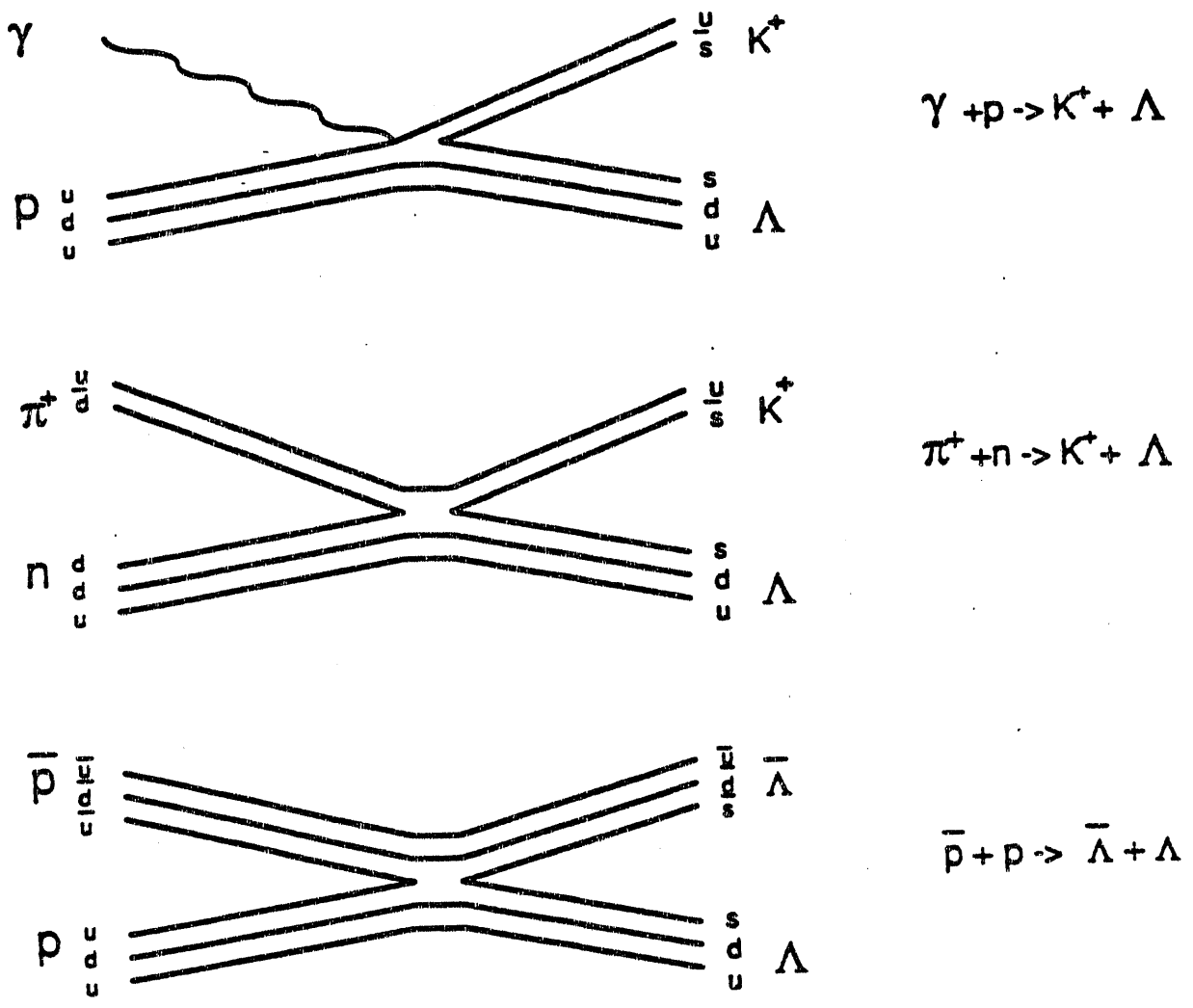

Fig. VII.B.1 Quark flow diagrams for strangeness production in three different reactions. Real and/or virtual strangeness photoproduction can be studied at CEBAF.

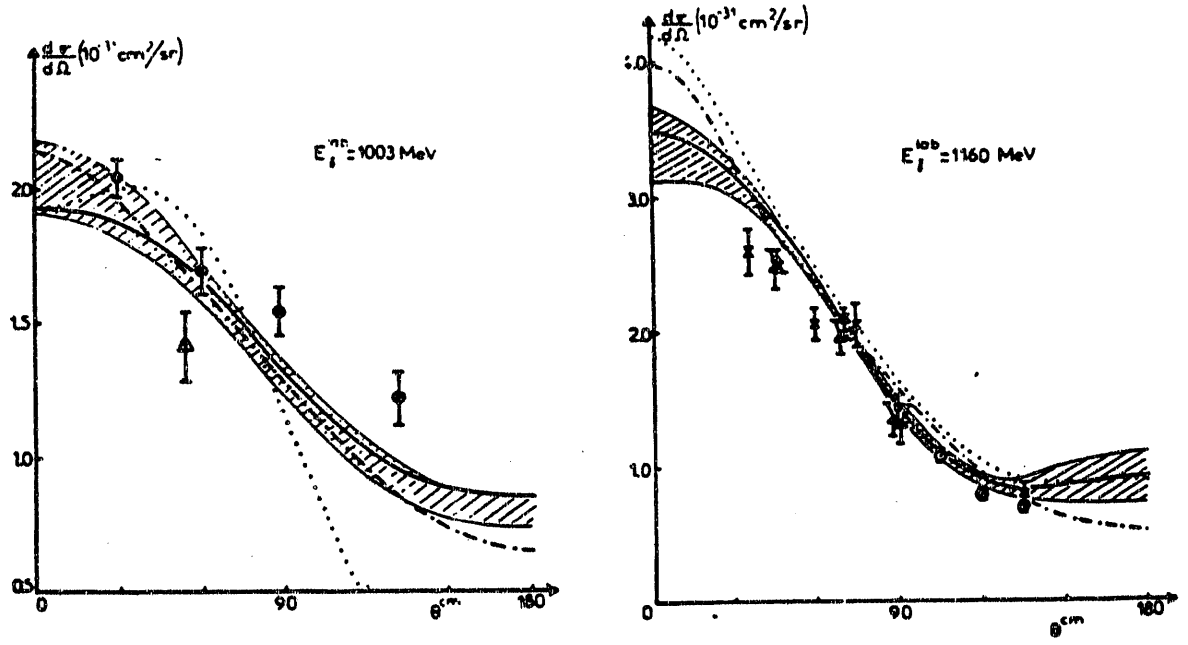

Fig. VII.B.2 Sample of the existing strangeness photoproduction differential cross sections for $p(\gamma,K^+)\Lambda$ from Renard (Ref 7). Differential cross sections for K^+ production are plotted as a function of kaon c.m. angle. The shaded region corresponds to $g_{\Lambda KN} / (4\pi)^{1/2}$ varying from 1.1 to 2.8.

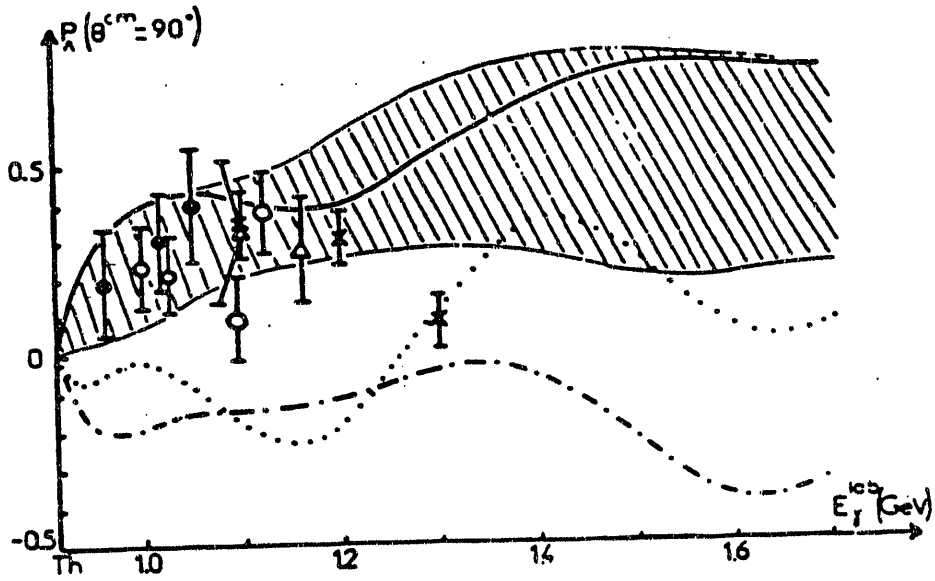

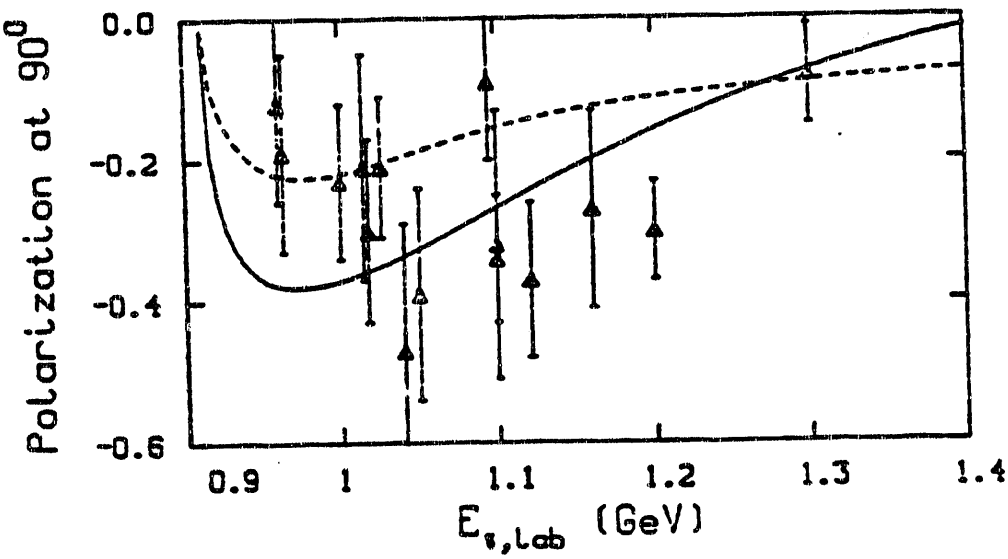

Fig. VII.B.3 Overview of the Λ polarization data for $p(\gamma,K^+)\Lambda$ for a kaon c.m. angle of $90^\circ \pm 5^\circ$. (a) From Renard (Ref. 7), with curves corresponding to those in Fig. VII.B.2. Note the sensitivity of this model to the polarization data. (b) From a newer compilation and calculation by Adelseck (Ref. 9).

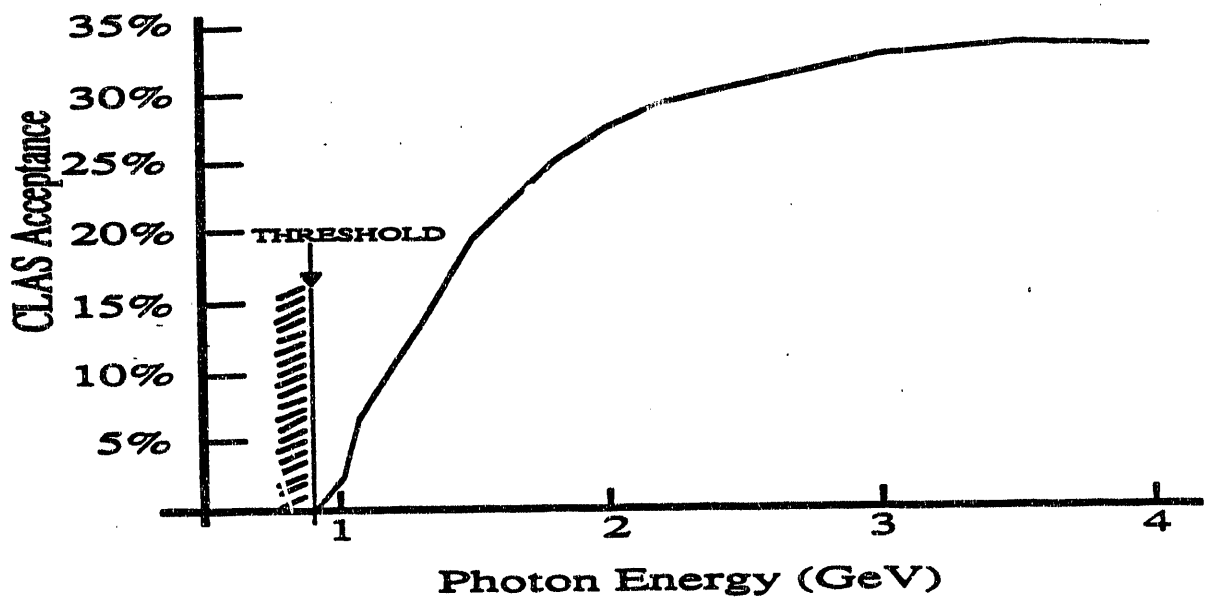

Fig. VII.C.1 Acceptance of the CLAS for the reaction $\gamma + p \rightarrow K+ \pi^- + p$, triggering on the K^+ only, using FASTMC (a CEBAF Monte Carlo program) with one fifth of the nominal field strength and positive particles bending outward.

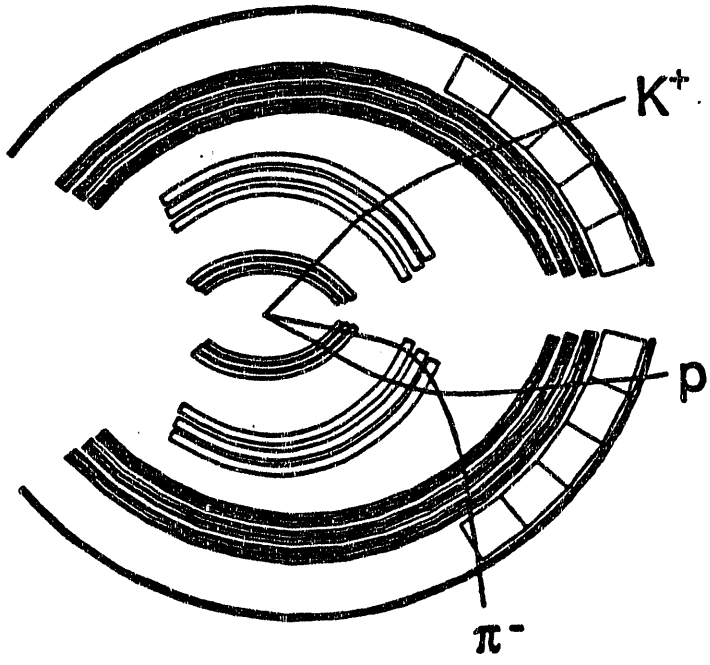

Fig. VII.C.2 GEANT simulation of $\gamma + p \rightarrow K+ \pi^- + p$ at 1.8 GeV, showing an event where all three final state particles reach the trigger scintillators. The Region 1 drift chamber package is represented by the innermost set of arcs, and is actually about 2m long.

VIII. The Region 1 Drift Chambers for the CLAS Spectrometer

VIII.A. Introduction

The CEBAF CLAS collaboration is one of the first in which physicists from predominantly nuclear and medium energy physics backgrounds have undertaken to design and construct an experimental detector facility of a size which a few years ago would have been found only in high energy physics projects. Approximately 30 Universities are involved in this task, and the contribution of manpower and equipment from these schools is vital. In October of 1991, our group at Carnegie Mellon signed a Memorandum of Understanding with CEBAF to engage in the design, prototyping, construction supervision, commissioning, and initial operation of the CLAS Region 1 Drift Chamber package, to be utilized in CEBAF's Hall B CLAS spectrometer. This chapter will describe the work which has been done at Carnegie Mellon in the past year towards this commitment. Two other schools are collaborating with us on this project. The University of Pittsburgh medium energy group is working side by side with us on the mechanical design and prototyping of this detector. The University of Massachusetts at Amherst group is doing the design and fabrication of the rather complex electrical layout for the readout circuitry. We view Carnegie Mellon as central to the whole effort, since we are the only one of the three institutions to have both the design capability (AUTOCAD, large plotters, etc.) and the in-house technical capability (tools, space, and skilled technician) to rapidly create and test methods for constructing this rather novel form of detector.

By the early part of 1992 we had completed the design of the so-called endplates (see descriptions below) of the detector. We decided, with CEBAF management, that CMU and Pitt would undertake the procurement of these structures from an outside machine shop. The endplates are 8 foot long structures with thousands of precision holes, which only a shop with specialized machine tools and expertise could make. The bidding procedure is now complete and we are ready to award a contract. After review of our procedures by CEBAF management, CMU has been awarded a contract which will allow us to make this large purchase; the grant also allows for upcoming smaller purchases of equipment which we will need to continue this work.

VIII.B. Design Considerations

Tracking charged particles through the CLAS spectrometer calls for a series of high accuracy position measurements at many points along the trajectory of each track. It is crucial that good measurements be made close to the target, before the particles enter the high field region of the toroidal magnetic field. These measurements anchor the track curvature determination at one end, and add crucial information to the vertex location measurement, which is used for rejecting

background and for identifying certain decay topologies. The present design of the Region 1 detector package calls for a total of 1248 independent drift cells in each of the six identical sectors, arranged in two "superlayers," one axial to the magnetic field direction, the other tilted at a small angle to provide stereo information.

Two main considerations have driven the design of the Region 1 drift chamber. Our most important goal is to build a detector which tracks particles accurately, for the full acceptance of the CLAS experiment, with the smallest possible amount of material within the acceptance. We have arranged the endplates responsible for mechanical support within the "shadow region" defined by the edge of the cryostat tanks. Furthermore, as a practical matter, the shapes of the main magnet and of the minitoroid limit the amount of space available for the chamber with its electronics and require that we pursue all aspects of the design with details of assembly, installation, and operation in mind. Fig. VIII.B.1 shows the Region 1 drift chamber in its relationship to these magnets. The main magnet imposes a strict limitation at the upstream end of the chamber, where all chamber hardware must pass through a relatively narrow aperture. The requirement that the minitoroid magnet be removable independently of the Region 1 drift chamber affects both the inner profile of the chamber and the design of the forward support.

VIII.B.1 Wire Layout

For the majority of particles passing through the Region 1 drift chamber, between 8.0 degrees and 118 degrees, there will be ten separate measurements of the particle track, grouped in two "superlayers." Fig. VIII.B.2 shows equipotential contours for a small section of axial wire superlayers as calculated by the Garfield program. Each hexagonal drift cell will feature a 20 micron gold-plated tungsten sense wire surrounded by 140 micron gold-plate aluminum field wires at 8 mm. To help resolve ambiguities associated with tracks which run along the lines of a drift cell, we will offset sense wires in rows by 300 micron alternately upstream and downstream along a layer.

The outer superlayer will have layers of drift cells tilted at a small angle to resolve the coordinate along the axial wires. To keep this angle effectively constant for tracks coming at all polar angles, we have come up with a modified stereo scheme for the upstream section of the chamber. In the extreme upstream section, where the chamber passes through the throat of the magnet cryostats, the two superlayers will have just three layers each to give acceptable tracking for the moderate particle flux which will pass through.

In all, the Region 1 drift chamber will have nearly thirty thousand wires in a complex wire pattern. We have written a program in Turbo Pascal to compute the positions of the wires and to translate these positions into a CAD file specifying the wire feedthrough positions at the endplates.

We plan to place the sense and field wires in the neighborhood of +1300V and -1300V respectively; a row of guard wires near ground potential will shape the electric field at the edges of the superlayer. The high voltage will distributed in a way that will allow us to control small sections of the chamber independently in order to deal with varying charged particle occupancies.

VIII.B.2 Endplates

Six pairs of endplates will support most of the mechanical loads of the Region 1 drift chamber, bearing both the wire tensions and the weight of all the hardware. and transmitting these forces to the two main supports at the two ends. See Fig. VIII.B.3. When we string and test the individual sectors, metal compression posts will span the active region of the chamber, keeping the two endplates in the correct relative positions Afterwards, when the sectors have been integrated into a single chamber, the endplates of neighboring sectors will be parallel to one another, both to maximize the volume available for electronics and cables in the forward section, and to simplify design of the interconnecting struts.

After extensive research into the advantages and disadvantages of a variety of materials, both electrically conducting and insulating, we have selected aluminum as the best choice. Its combination of machinability and rigidity will allow us to maintain the mechanical tolerances we require both during fabrication and operation without sacrificing economy. With the proper surface treatment, there should be very little likelihood of electrochemical damage or distortion of the drift field near the ends of the wires.

Our collaborators at the University of Massachusetts at Amherst are designing circuit boards to service the wires, one of them distributing high voltages to the chamber segments, the other amplifying the AC coupled signals by means of custom single in-line packages (SIPs) mounted at the periphery of the endplates. See Fig. VIII.B.4. To maximize the space available for the circuit boards between the endplates, we plan to run manifolds for chamber gas on the active volume side of the endplates.

VIII.B.3 Internal Supports

The final Region 1 chamber structure is held together as a whole under tension. Essential in this scheme are the internal interconnections between sectors which must provide the reaction forces needed to keep the wires from changing from their lengths as strung. Even though we require these struts to have good dimensional stability, during assembly struts must also be adjustable so that tension may be transferred from the temporary compression posts to the struts. We plan to do this by making each strut in two pieces of non-magnetic stainless steel which are rigidly mounted to the endplates before stringing. When we need to perform the "tension transfer

maneuver" joining the sectors, we will rejoin the two halves with special double-headed screws, at the same time monitoring the wire tensions.

VIII.B.4 Forward Supports

There are three elements to the forward support structure for the Region 1 drift chamber: the individual sector plates which close off the front of each sector, a six-sided pipe which joins the sectors together, and a cylinder which is fixed to the cryostat structure surrounding the beampipe. See Fig. VIII.B.5. The primary job of the supports is to bear the gravitational load of the chamber and the wire tensions in a way that is independent of the location of the minitoroid. A second important function is to provide a reliable means of docking the drift chamber into place during installation. Finally, it should provide some shielding of the detectors against low energy particles which are not absorbed in the minitoroid shielding. None of these functions will be allowed to conflict with the forward acceptance requirements of the CLAS detector. The sector plates must provide mechanical rigidity to the sector, making it a gas-tight volume. The outer piece will be attached rigidly to the six-sided pipe during tension transfer. This portion of the detector is the current focus of our design and prototyping work.

Because of the restriction imposed on the drift chamber by the throat of the cryostats, it must both translate and rotate during installation. The six-sided pipe will have ball bearings on the inner surface of the chamber pipe to ride on the smooth, hardened outside surface of the fixed cylindrical support during installation. To fix the final position of the chamber, a pair of receptacles on the cryostats will mate with steel pins projecting from the six-sided pipe, lifting it off of its bearings. In this way, the mechanical load of the minitoroid and of its massive lead shielding should not be coupled to the support of the Region 1 drift chamber.

VIII.B.5 Upstream Supports

The upstream support of the drift chamber will be subjected to large moments due to the weight of the chamber and the bundles of cables attached to it. Each sector will have an aluminum plate, with stiffeners, to span the region between endplates and maintain their relative alignment. These individual plates would be fastened to a large annulus to integrate the six sectors into a single structure. This has the advantages of stiffening the structure against bending moments and of providing a surface to which the gas windows can be attached. During installation, a rail-mounted upstream carriage with a rotisserie hub will attach to the annulus to support the chamber while still allowing both translation and rotation. Afterwards, the annulus will be anchored to the aft ring of the cryostat support structure.

VIII.B.6 Feedthroughs

Experience with the Region 3 drift chamber prototype at CEBAF suggests that the material used to make the wire feedthroughs may strongly affect the aging of the chamber very close to the feedthroughs. Our design for the Region 1 feedthroughs is guided by the needs of protecting the wires from chemical attack or mechanical abrasion. We have chosen Noryl plastic for the body of the feedthrough. To avoid the possibility that polarization in the dielectric can potentially cause high electric fields, hazardous to the wires, we will insert a flared metal tube molded directly into the tip of the plastic. For a solid electrical and mechanical contact, a gold-plated copper pin will be pneumatically crimped onto the wire and will taper to fit into the metal tube. Epoxy will be used as gas seal around and inside the feedthrough. The CMU group has worked closely with the University of Pittsburgh group to design and develop these feedthroughs; it has been agreed that Pitt will handle the procurement of feedthroughs.

VIII.C. Prototyping and Current Status

VIII.C.1. Two Plate Test

To verify the deflection estimate from the ANSYS finite element simulation of the endplates, we assembled a two plate mechanical mockup of neighboring endplates connected by struts. We have checked both the accuracy of the approximations in the simulation as well as the boundary conditions applied at the endplate support nodes. The two mockup endplates were made of carbon steel, 1/4" thick. Steel struts and support plates were positioned in approximately their final locations. No feedthrough holes were drilled. To simulate the rigid mounting points of the endplates which were assumed in the computer model, we constructed a massive steel L-frame by welding a steel pipe to a steel box beam. We measured gravitational deflections before and after lowering the frame to an angle 60 degrees from the vertical by means of mechanical plunger dial gauges.

Simple loading tests of the frame, repetition of individual measurements, and spread in the experimental deflection measurements, all indicate to us that we can trust our data to a level of about ± 0.1 mm. The test results compared quite well with the finite element computer calculations, with systematic discrepancies suggesting a minute amount of twisting of the L-frame. These results increased our confidence in the computer simulation for the more complex system of our complete drift chamber structure.

VIII.C.2 Wire Stringing Support Structure

The most labor intensive part of constructing the Region 1 detector will be the stringing of thousands of individual wires on each sector. To hold each sector while this procedure is in progress, and to permit accurate positioning of the sector in the process, we have constructed a

special support structure, shown in Fig. VIII.C.1. Made of heavy steel, it is designed to be as rigid as necessary to prevent highly undesirable twists or asymmetric sags in the sector frame. It is based on a revolvable shaft on which the sector sits, counterweighted, which allows us to arbitrarily position and work on the single sector.

VIII.C.3 Six Sector Mechanical Mockup

Our design work on this very complex mechanical system convinced us of the need of building a realistic prototype in which all of interactions between sectors would be present and which will test our ability to meet the mechanical tolerances we have set. We are in the process of ordering aluminum endplates for this six sector mockup which will be assembled later this year. It will feature six endplate pairs (without feedthrough holes) to be connected together with struts, forward, and upstream supports, and a set of taut steel wires near the midline of the two endplates in a sector to simulate the chamber wire tensions. We will also place a number of pairs of wires at various locations around the chamber, which we will excite electrically to read out their resonant frequencies and infer their tensions during tension transfer and installation.

VIII.C.4 Single Sector Prototype

Certain crucial elements of the Region 1 drift chamber design can be tested only with an actual full-size drift chamber prototype. These include the development of procedures for machining the endplates and other hardware to meet the necessary tolerances, design of a wire stringing setup, measurement of the chamber efficiency, crosstalk, drift speed, pulse height, and spatial resolution for different parts of the sector.

We are ordering two aluminum endplates, fully drilled for feedthroughs, to be outfitted with feedthroughs, translator boards, sense and field wires, gas windows, and cables in late 1992, at Pitt. The single sector stringing structure has already been constructed at CMU and will be tested with the prototype drift chamber. The assembly and installation structures will also be checked with the single sector prototype for mechanical compatibility. To check for signs of wire aging, we will operate it on a long-term basis as we begin work on the final detector.

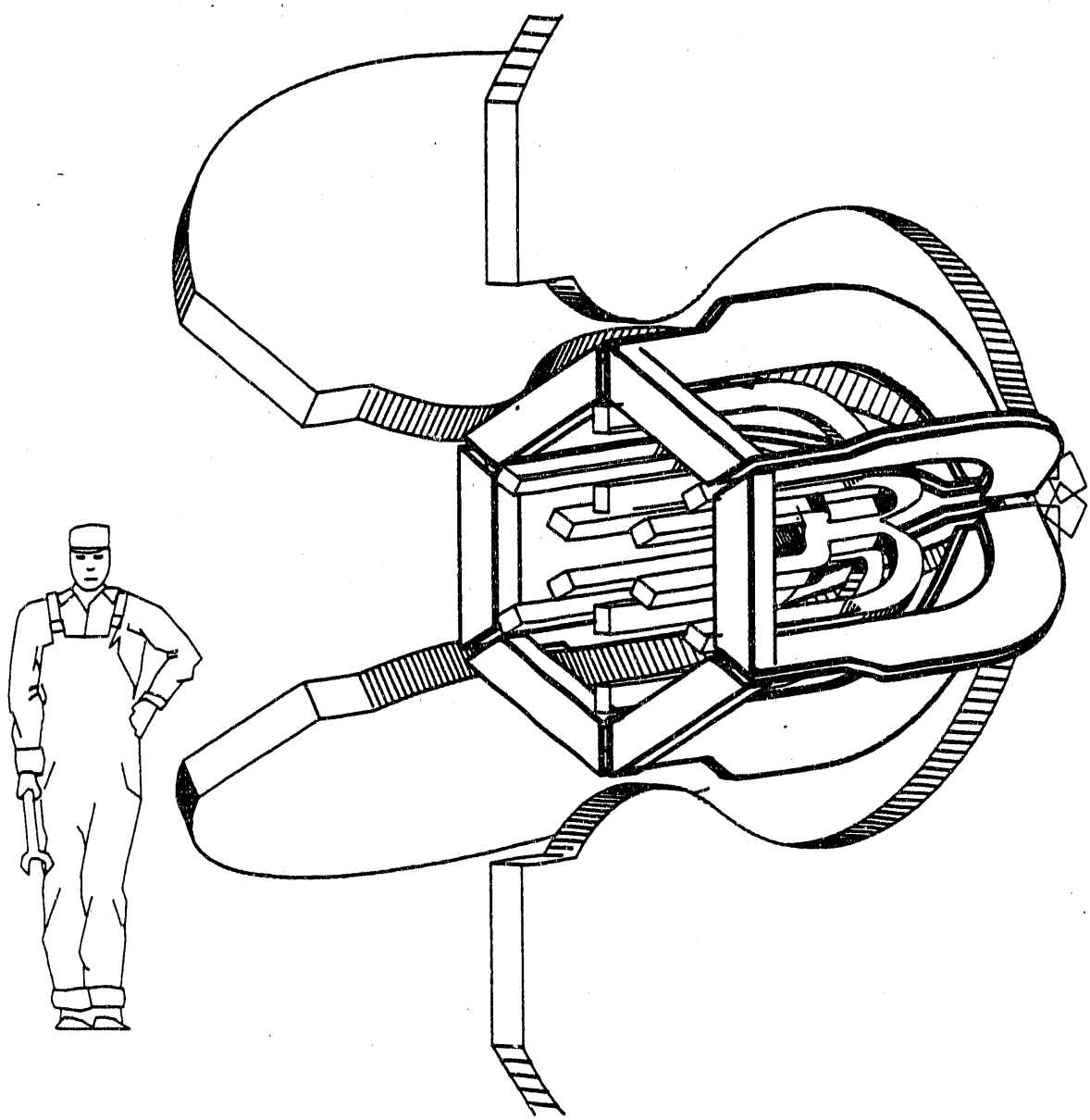

Fig. VIII.B.1 Perspective view of the Region 1 drift chamber within the main CLAS toroid structure and outside the minitoroid structure. The beam would be incident from the left.

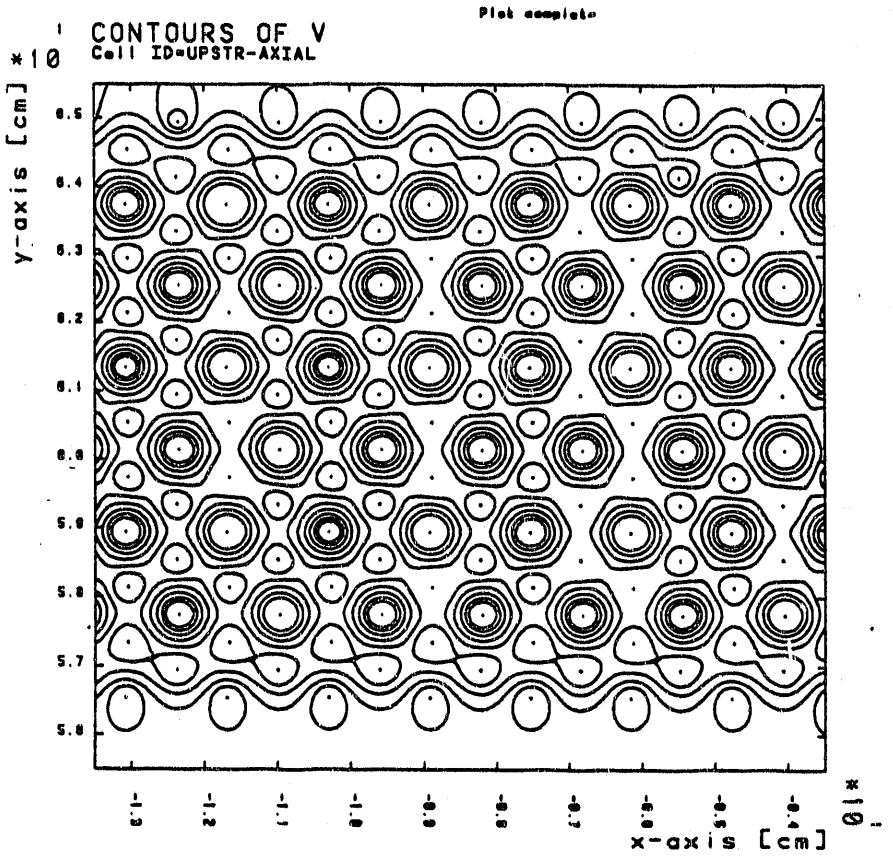

Fig. VIII.B.2 Plot of equipotential lines in a small section of the axial wires of the Region 1 detector. There are six layers of sense wires in a hexagonal pattern. Plot was generated using the program Garfield.

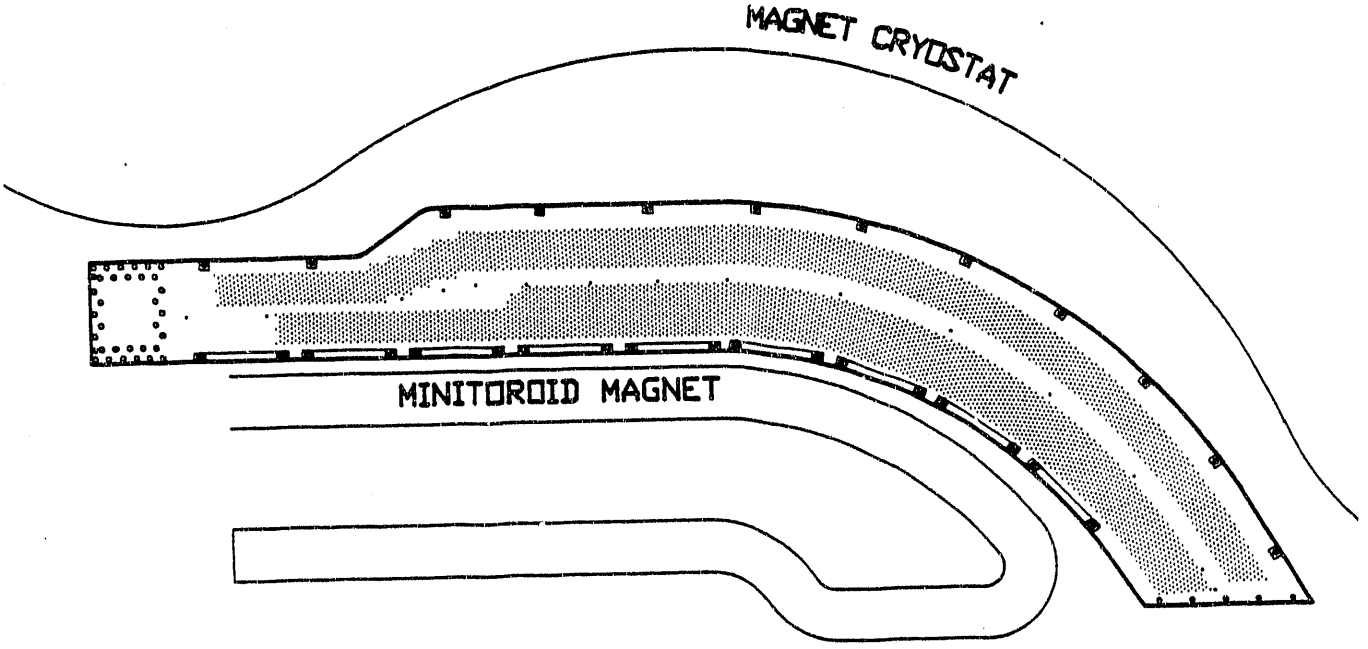

Fig. VIII.B.3 View of one endplate of the Region 1 detector, showing its relationship to the main magnet and minitoroid magnet. Shown also are the hole positions of the sense wires and the mechanical support holes.

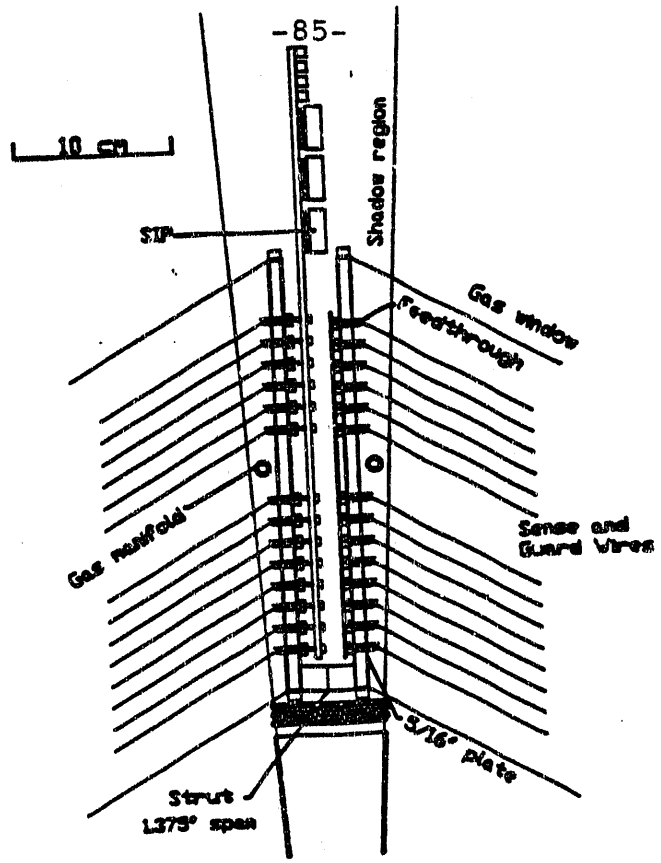

Fig. VIII.B.4 Cross sectional view of the Region 1 detector showing the relative positions of wires, feedthroughs, circuit boards, electronics and some of the cabling.

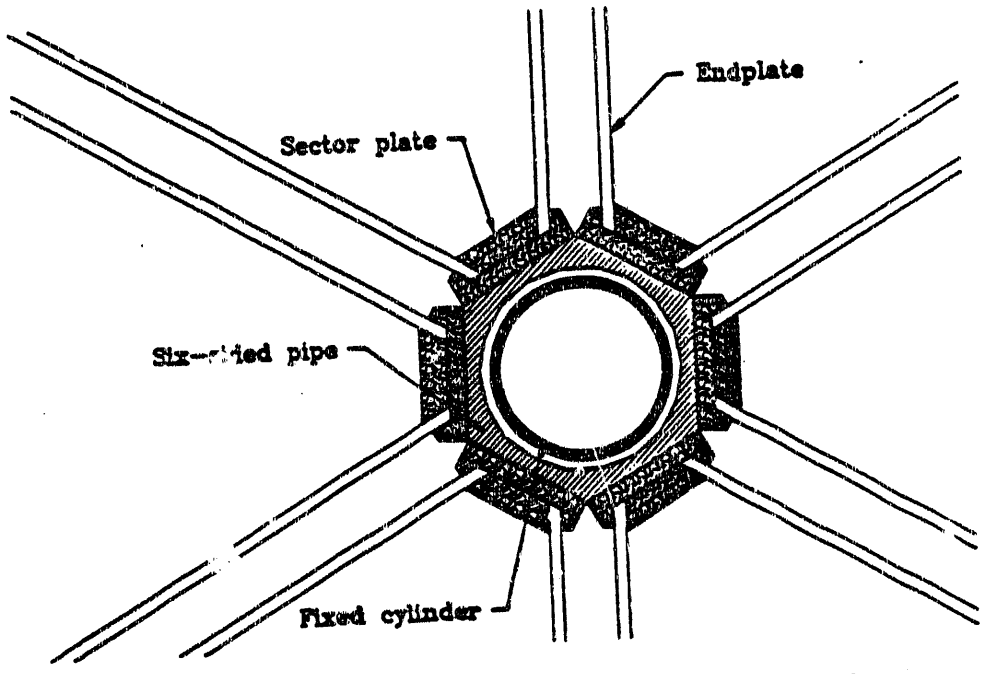

Fig. VIII.B.5 Cross section of the forward (downstream) part of the detector where the six sectors, each held together by a sector plate, are connected to a hexagonal pipe, which in turn rides on a fixed cylindrical pipe that runs the length of the spectrometer during the assembly step.

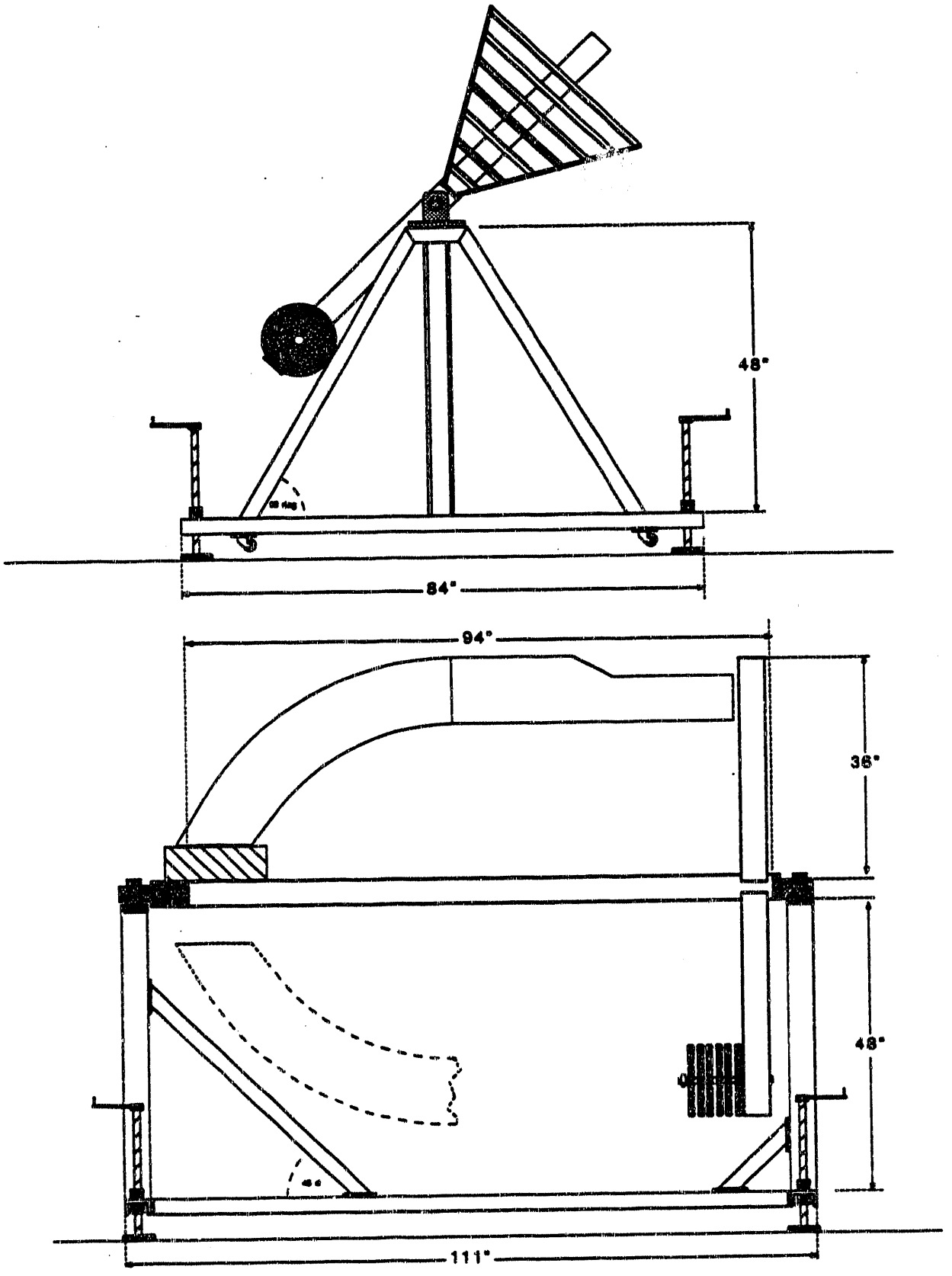

Fig. VIII.C.1 Single sector stringing support structure for holding a single sector assembly during the wire stringing process.

IX. Parity Violating Electron Scattering from the Proton: the G^0 Experiment at CEBAF

IX.A. Introduction

The Medium Energy Group is part of a collaboration which has recently proposed an experiment at CEBAF to measure parity violating electron scattering from the proton. The experiment is presently considered 'conditionally approved' by the CEBAF management. It will be reviewed this summer along with other proposed parity experiments, by a panel of experts on the subject of parity measurements.

The distributions of electric charge and current within the proton have been well measured by elastic electron scattering. This information alone, however, is not enough to determine the distributions of the quarks which make up the proton. Measurement of the form-factors associated with parity violating electron scattering could provide important additional constraints on the quark distributions. The form factors themselves are of direct, fundamental interest as a probe of baryon structure which is still largely unknown. Additionally, combination of the parity violating form factors with the ordinary form factors permits determination of flavor-singlet combinations of QCD current-quark distributions, $G_E^0(q^2)$ and $G_M^0(q^2)$. It is important to note that this extraction is model-independent, within the framework of QCD, and that the distributions extracted are those of the massless current quarks, rather than some effective constituent quarks. The distributions are themselves well defined and, in principle, calculable within QCD. These distributions may be of particular interest in view of recent evidence which suggests that strange quarks play a significant role in the structure of the proton[1]. Combining neutron electromagnetic form factors with the proton data also allows direct determination of the strange quark distribution within the nucleon. But it should be noted that this latter analysis is not model-independent in that it is based upon isospin symmetry.

The form factor of the distribution of a particular quark flavor within the proton may be expressed as matrix elements of the total quark and anti-quark current of that flavor. Because anti-quarks have opposite charge to quarks of the same flavor, these currents are sensitive to the difference of the distributions of quarks and corresponding anti-quarks. This has the advantage of canceling divergences in the distributions at high q and of making the normalization of the these form factors relate simply to the number of constituent quarks of a given flavor.

The total charge (E) or current (M) form factors of the nucleon for electromagnetic (γ) or weak (Z) interactions are simply related to these current-quark distributions as a sum over all relevant flavors, weighted by the appropriate quark charge:

$$G_{E(M)}^{\gamma(Z),p} = \sum_{j = \text{quark flavors}} Q_j^{\gamma(Z)} \, G_{E(M)}^{j,p}$$

where Q_j^γ are the ordinary electric charges of the quarks of flavor j and Q_j^Z are the weak charges. It should be noted that the current quark distribution functions which enter are identical for weak and electromagnetic proton form factors. This makes it possible to combine measurements of these distinct form factors to determine properties of the quark distributions.

In particular, the flavor-singlet form factors of the proton:

$$G_{E(M)}^{0,p} = \frac{1}{3}\left(G_{E(M)}^{u,p} + G_{E(M)}^{d,p} + G_{E(M)}^{s,p}\right)$$

can be extracted as a simple linear combination:

$$G_{E(M)}^{0,p} = (2 - 4\sin^2\theta_W)\, G_{E(M)}^{\gamma,p} - 4\, G_{E(M)}^{Z,p}$$

if the weak form factors, $G_{E(M)}^{Z,p}$, can be determined.

Parity violating electron scattering is very sensitive to weak neutral currents because the electromagnetic interaction, by itself, does not violate parity. One measurable quantity which is sensitive to parity violation is the asymmetry, A, of the electron scattering cross section with change in electron beam helicity:

$$A = \frac{\sigma_+ - \sigma_-}{\sigma_+ + \sigma_-}$$

where $\sigma_{+(-)}$ are the cross sections for scattering of electrons incident with +(–) helicity. The asymmetry is a relatively sensitive probe of the weak structure functions because of the interference between the weak and electromagnetic interactions. This asymmetry can be written as[2]:

$$A = -\frac{G_F Q^2}{\pi\alpha\sqrt{2}} \frac{\left(\varepsilon\, G_E^{\gamma,p} G_E^{Z,p} + \tau\, G_M^{\gamma,p} G_M^{Z,p} - \kappa\, G_M^{\gamma,p} G_A^{Z,p}\right)}{\varepsilon\,(G_E^{\gamma,p})^2 + \tau\,(G_M^{\gamma,p})^2}$$

where ε, τ and κ are simple kinematic factors, $G_{E(M)}^{\gamma(Z),p}$ are the form factors which have been introduced earlier, and $G_A^{Z,p}$ is the axial-vector form factor. The latter term is largely suppressed at forward angles because κ is small. Even at larger angles the contribution of $G_A^{Z,p}$ (complete with radiative corrections) can be determined and subtracted off by also measuring quasi-elastic electron scattering from deuterium.

It is possible to separate the electric and magnetic parts of the weak interaction, by a technique analogous to Rosenbluth separation, if A is measured at two or more angles for a given momentum transfer. This separation is possible because ε is a calculable function of scattering angle while τ is independent of scattering angle at fixed momentum transfer.

The expected magnitude of the asymmetry can be predicted[3] within the context of existing vector meson dominance model fits to the proton form factor[4]. Even with the enhancement resulting from interference, the asymmetry is expected to be only a few parts per million in the momentum transfer (q) range of $0.1\ (GeV/c)^2 < q^2 < 0.3\ (GeV/c)^2$. Because this fit includes a term resulting from coupling to the ϕ-meson, a small $s\bar{s}$ component of the proton appears naturally. It is interesting to note that a significant (30%) change occurs in the predicted value of the asymmetry if the $s\bar{s}$ component is simply 'turned off' by ascribing the strength near the ϕ mass to unidentified non-strange vector meson coupling.

Measurement of the asymmetry can be expected to provide useful new information about the structure of the proton if the errors on the measurements are smaller than $\sim 10^{-6}$. The G^0 collaboration has been formed to make a set of measurements of A with an uncertainty of approximately 2×10^{-7} at a series of q^2 points in the range of $0.1\ (GeV/c)^2$ to $\sim 0.5\ (GeV/c)^2$. These measurements will allow separation of electric and magnetic weak form factors by combining forward and backward angle measurements at a given momentum transfer. This will be accomplished partly by combining the data with back-angle measurements from the SAMPLE experiment at Bates.

IX.B. Apparatus

Accurate measurements of such a small asymmetry require very high statistics ($\sim 10^{14}$ counts). Both high luminosity and large acceptance are needed to allow measurements to be made in a reasonable amount of time. This must be achieved without compromising the control of systematic errors in the measurement. Small-angle electron scattering presents the potential hazard of extreme sensitivity to beam position and direction. In particular, any correlation of these parameters with beam helicity would introduce a bias in the measurements which could easily swamp the actual signal. Such a correlation may be expected to occur because of differences in the beam-loading of the accelerator due to minute differences in the source intensity with change in polarization.

The experiment has been designed to minimize these systematic errors. Rather than detecting forward-scattered electrons at small angles, the apparatus will detect the recoiling protons from the elastic scattering. These protons will scatter at much larger angles ($\sim 67°$–$77°$), reducing the sensitivity to beam position and angle. Back-angle measurements, on the other hand, will be made by observing the scattered electrons. Use of a toroid spectrometer will provide large solid angular acceptance and, more importantly, allow careful control of systematic variations of beam parameters with helicity change.

The layout of the apparatus is shown schematically in Fig. IX.B.1 (with the detector package configured for detection of the protons from small angle electron scattering) while Fig.

IX.B.2 shows the design of the coils which provide the toroidal field. The spectrometer is iron-free to eliminate systematic errors which might arise from helicity dependence of pole face scattering from the aligned electrons in magnetized iron. Normal (not superconducting) conductors are used, and the coils are shaped to provide a field which eliminates first order dependence of the final coördinate at the focal plane on the point of interaction within the target.

The momentum of the scattered particle is a function of the scattering angle for elastic scattering. Because of this, measurement of the position at which a trajectory intersects the focal plane alone is sufficient information to allow unique determination of the momentum transfer for elastic scattering events. Such a momentum determination does not require track reconstruction based on read-out of multiple hit positions for each track. Event-by-event readout, which would be necessary for full track reconstruction, is precluded by the need for a very high data rate (~50 MHz) to accumulate the required statistics.

The detector array consists simply of sets of scintillators along the focal planes of each of the toroid octants. Simultaneous measurements at several momentum transfers are made possible by subdividing each focal plane into ten sections. The scintillator elements for each section will be curved to match the azimuthal distributions of particles corresponding to a given momentum transfer. In contrast to many previous parity-violation experiments, it is expected that it will be possible to count individual particles crossing the focal plane. Doing so, rather than integrating the total signal from the PMT's, greatly reduces sensitivity to gain shifts, linearity, and background.

A pulsed beam will be used (with one pulse every 32 nS) allowing the protons from elastic scattering to be identified by time of flight. The electronics which will count particles hitting the detector elements and bin them by time of flight is described in the following sections.

In principle, the asymmetry can be measured by simply comparing the counts per unit incident charge at a given momentum transfer for positive and negative beam helicity. In fact many precautions must be taken to minimize systematic errors. The anticipated tolerances on beam parameters and detector asymmetry are given in Table IX.B.1. Measurements will be divided into 'macropulses' of one thirtieth of a second (a subharmonic of line frequency, to minimize noise). Helicity will be reversed such that sets of four consecutive macropulses are taken with a pattern of either + – – + or – + + –. After each such set of four macropulses, the choice of which of these two patterns to use for the next set of four will be made randomly. This ensures that there is no long term periodicity to the measurement, but provides an order to the measurements which would be lost if each helicity reversal was made randomly after each macropulse. Each set of four such consecutive macropulses provides an independent measurement of A (albeit with very low statistics) for which the + and – helicity measurements are symmetrically made, so that any linear drifts over the four-macropulse interval will exactly

cancel. The final measurement of A (for each momentum transfer) will actually be made as a weighted average of these independent measurements.

Table IX.B.1 Tolerances on determination of beam and spectrometer parameters.

Incident energy	1×10^{-5}
Incident charge	4×10^{-5}
Beam position at target	800 μm
Beam direction at target	14 μr
Detector asymmetry	5×10^{-3}

IX.C. Readout Electronics

IX.C.1. Overview

The CMU group has undertaken to provide all the electronics for the readout of the focal-plane detectors. This includes the specialized electronics which will subdivide the counts in each scintillator according to time of flight relative to the incident beam burst. In addition, we intend to provide the data acquisition hardware and software which will record these counts, read them out, transfer the totals to tape every thirtieth of a second, provide on-line monitoring and transfer some fraction of the data to more powerful computers for additional on-line analysis. It is envisioned that the data acquisition system will be similar to that presently used for the H-particle experiments– a VME-based system using FIC microprocessors to read out the data, write it to exabyte tape drives and transfer some of it to a dual-ported memory shared by an on-line analysis computer.

As indicated above, the experiment will use a toroidal spectrometer with 8 sectors, each of which acts independently as a detector for the recoiling protons or electrons from elastic scattering. As shown in Fig. IX.B.1, each of the 8 detector segments views the 20 cm. long target in the same way. The magnetic element bends the particles toward the focal plane and, independent of the position of the scattering along the target, gives a separation of particles along the focal plane according to momentum transfer. Sufficient position resolution will be provided by subdividing the focal plane into 10 scintillator elements per spectrometer segment (80 in all). The scintillators will be curved so each follows the locus of constant momentum transfer.

Measurement of time of flight will allow identification of inelastic background and of prompt particles such as photons and electrons. A typical trajectory for a scattered particle has a length of about 2 meters. Thus particles with $\beta \approx 1$ (mostly electrons and positrons) require no

more than 7 ns to reach the focal plane. The 'gamma flash' will be absorbed by shielding the detectors from line-of-sight view of the target. Elastic protons with q^2 between 0.1 and 0.3 $(GeV/c)^2$ (corresponding to $\beta = 0.32$ and 0.50) require about 20 nS . Inelastic protons of higher momentum (and smaller scattering angles) will arrive at earlier times while those of lower momentum will arrive later. These backgrounds can be identified by their flight times.

Each of the 80 curved scintillator elements which make up the detector will be viewed by two PMT's, one at each end. Because of the length and shape of these scintillator bars, pulse heights may be expected to have a large dynamic range. Good timing must be achieved without off-line walk corrections because the desired data rate (50 MHz) precludes event-by-event data recording. Constant-fraction discriminators will be used to eliminate walk while meantimers will compensate for propagation time through the scintillators. The constant fraction discriminators are commercially available (and we have had satisfactory experience with them in the past, having used several hundred channels in the H particle experiment described in Chapter III). Although the preferred meantimers are no longer commercially available, the manufacturer (LeCroy) has agreed to resume production to provide the modules required for this experiment.

The 32 ns beam micropulses will be grouped artificially into 'macropulses' roughly $\frac{1}{30}$s long, separated by a few microseconds during which the accumulated data must be read out, the beam helicity reversed, and the relevant accelerator parameters recorded. For each micropulse, the electronics must separately record the time of flight for each scintillator element which is hit. These 80 time-of-flight spectra must be accumulated for the duration of a macropulse, then read out with minimal dead time. This kind of performance is not commercially available in off-the-shelf electronics, but a fairly simple technique has been devised by this group, to allow the spectra to be accumulated in ordinary high speed scalers. This method is described in the following section.

IX.C.2. The Readout Electronics

A specialized circuit board, outlined in Fig. IX.C.1, will be used to bin each of the 80 signals into 2 ns time bins for the time-of-flight region of interest. Wider time bins will be used in the background region. The output from these boards will go to a set of scalers. These scaler channels will essentially store a time-of-flight spectrum for each scintillator.

The time sorting of the events is achieved by sending each of the 80 meantimed signals into the serial input of a 16 bit shift register. (This is formed by connecting in series two 8-bit, 700 MHz shift registers, such as SY100E141. Each signal will be latched at the input to ensure that at most one hit is detected from any scintillator element after a beam pulse. This will simplify the dead-time corrections and render them insensitive to the discriminator widths.

The shift registers and latches will be cleared before the expected arrival time of fast particles (photons and electrons). The registers will then receive a train of 12 clock pulses (covering the duration of the time of interest). This will shift a copy of the input along the series of data bits. At the end of the clock train, the depth of the bits which have been set, if any, will indicate the arrival time of the signal. (Because of the latch, the string of bits set will always extend back to the first bit.) The earlier a signal arrives, the more bits it will set before clocking stops. If no signal arrives no bits will be set.

High speed storage of this information can be effected by sending the signals from the shift register bits to individual scaler channels. If a particular bit is set during the clocking, the corresponding scaler channel will increment exactly once. A set of strobed D registers will act as an interface between the shift registers and scalers. They will be strobed after the clocking of the shift registers has ended. While the shift registers are cleared for the next beam pulse, the D registers will serve to stretch the signal to the scalers out to 10 ns and to drive the ECL lines. They will also eliminate the random time structure of the input to the scalers, keeping the instantaneous rate below 30 MHz. As described below, not all shift register bits need be sent to scalers. Jumpers between the shift registers and the D registers will select which bits go to scalers.

After a series of beam pulses (one macropulse) the difference between two adjacent scaler channels will then equal the number of events for which the shifted input bit reached exactly as far as the first of the two scaled bits. That is, the difference of adjacent scaler channels will be the number of pulses which arrived within a specific time bin. If these scalers monitor adjacent bits, then the width of the time bin will be one clock 'tick' (2 ns). Background can be easily monitored in coarser time bins (with a corresponding savings in scaler channels per scintillator) by connecting only a subset of the corresponding bits to scaler channels.

The clock signal will be derived from the CEBAF master oscillator signal. The 1500 MHz signal will be divided down to give a 500 MHz clock. Good timing resolution will require that the phase of the clock signal be adjusted to reflect any drift (or abrupt change with helicity reversal) in the arrival time of the beam pulses at the target relative to the oscillator. This will be accomplished by using a beam pickup to measure average phase difference over many beam pulses. This signal will provide feedback to a phase-shifter, which will change the clock phase to null the difference.

It is anticipated that the 2 ns time resolution will be sufficient, even in the time interval corresponding to protons of interest. Should future developments show that an improved resolution in time digitization is merited, a 1 ns binning can be achieved. This would be accomplished by sending each mean-timed signal to the input of two parallel series of shift

registers which shift 180° out of phase. Differences in scalers on these interleaved registers would then give the number of hits within a time bin of half the clock period.

Latching scalers, such as LeCroy 4434 CAMAC scalers, will be used for storage of these time-of-flight spectra. These require only a very short interruption of data-collection at the end of each $\frac{1}{30}$second macropulse. Front-panel signals can be used to load the present scaler readings into latches and clear the scalers. Data taking can then resume in less than 0.4 μs, while the readout of the latched values from the previous macropulse occurs over the CAMAC backplane. Since $\frac{1}{30}$second would be available for readout and writing to tape, the demands on the data-acquisition system are very modest.

As described in the previous chapter, we expect to use VME-based CPU's to read out the scalers at the end of each macropulse. A simple VME branch-driver can then provide the link to CAMAC.

Although the required performance appears challenging (to read out time-of-flight spectra for a data rate of 50 MHz) the design of this readout system is reasonably conservative. Much of the data acquisition hardware is based upon equipment which we either already own, or have had experience working with. The next step in the development will be the fabrication of a working prototype of the time-binning board. The high speeds required eliminate the possibility of fabricating a simple 'bread-board' model. The prototype will be a multi-layer printed circuit layout. If all goes well, the prototype should be the actual final design for the board.

Chapter IX References

1) J. Ashman *et al.*, Nucl. Phys. **B328**, 1 (1989).
2) R.N. Cahn and F.J. Gilman, Phys. Rev. **D17**, 1313 (1978).
3) R.L. Jaffe, Phys. Lett. **229B**, 275 (1989).
4) G. Höhler, Nucl. Phys. **B114**, 505 (1976).

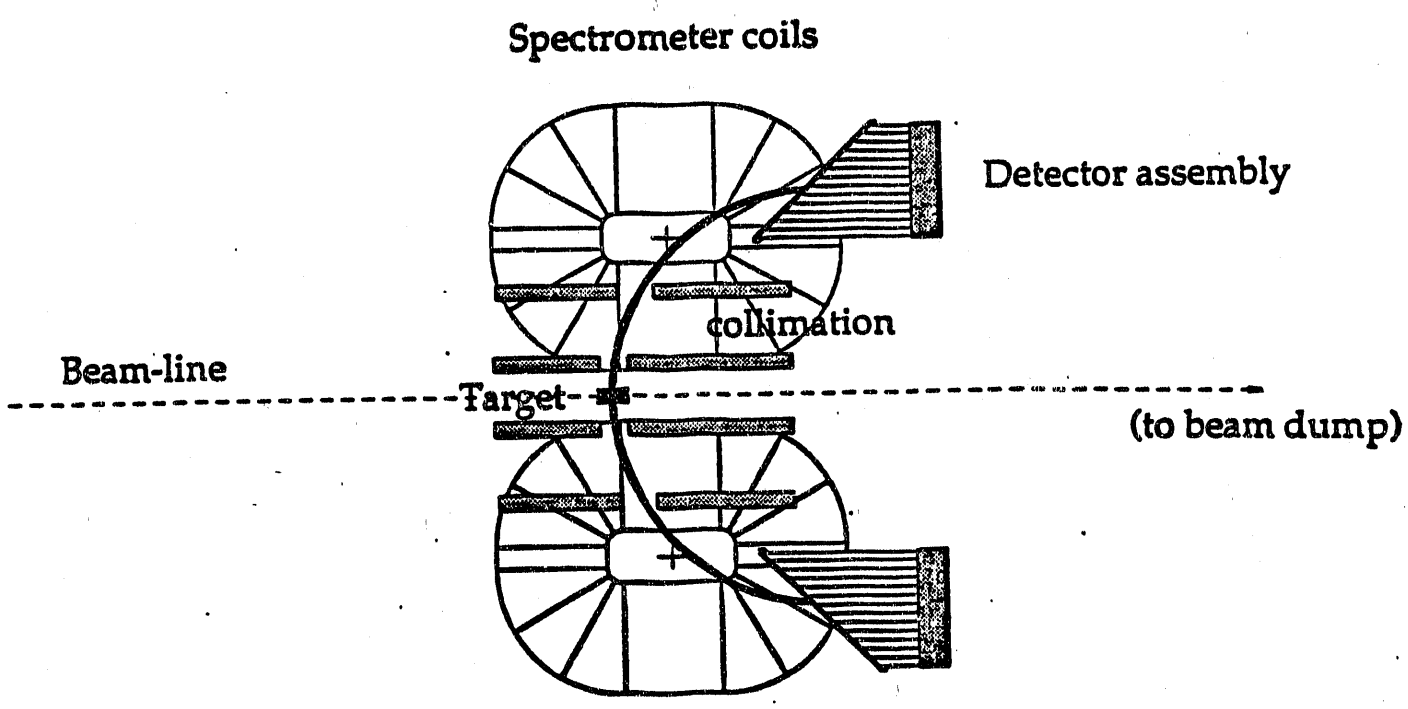

Fig. IX.B.1 The layout of the G^0 experiment, as configured for proton detection. The beam line is the axis of the toroidal spectrometer. The 20 cm thick liquid H_2 target is upstream of the center of the toroid. Scattered protons are focused onto the detector assembly which is on the downstream side of the toroid. For back-angle electron measurements the entire spectrometer would be rotated 180° about its center.

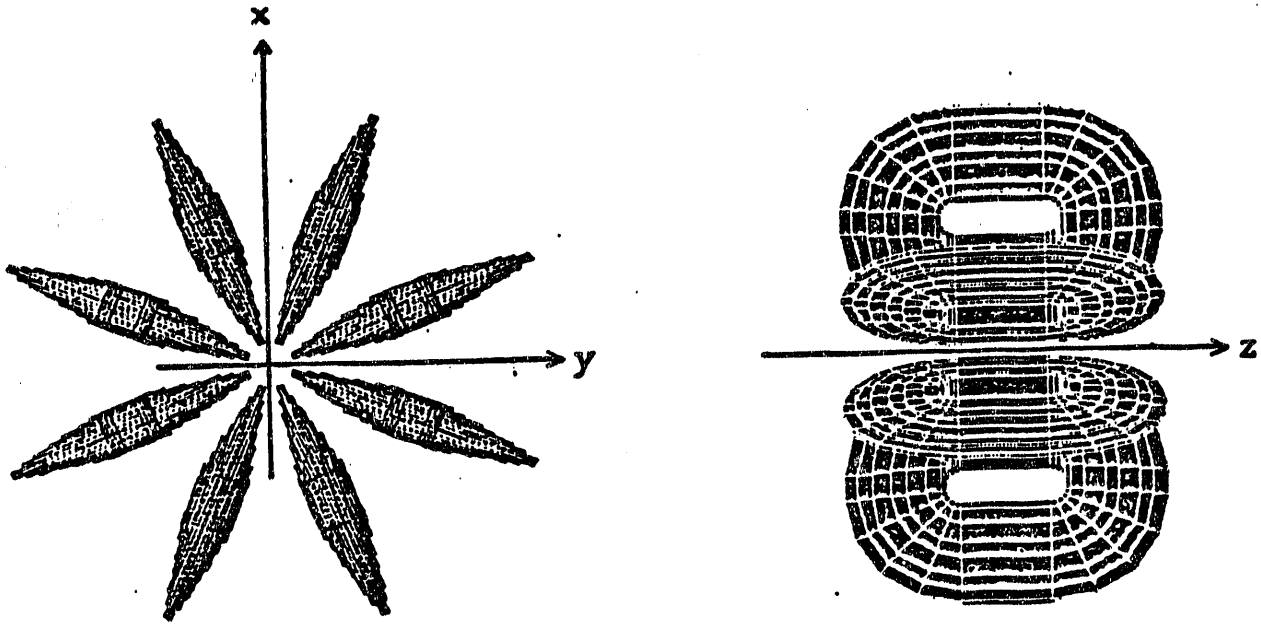

Fig. IX.B.2 The shape of the conductors which make up the toroidal spectrometer. The eight coils are normal conductor and are shaped to give the field the desired focusing properties.

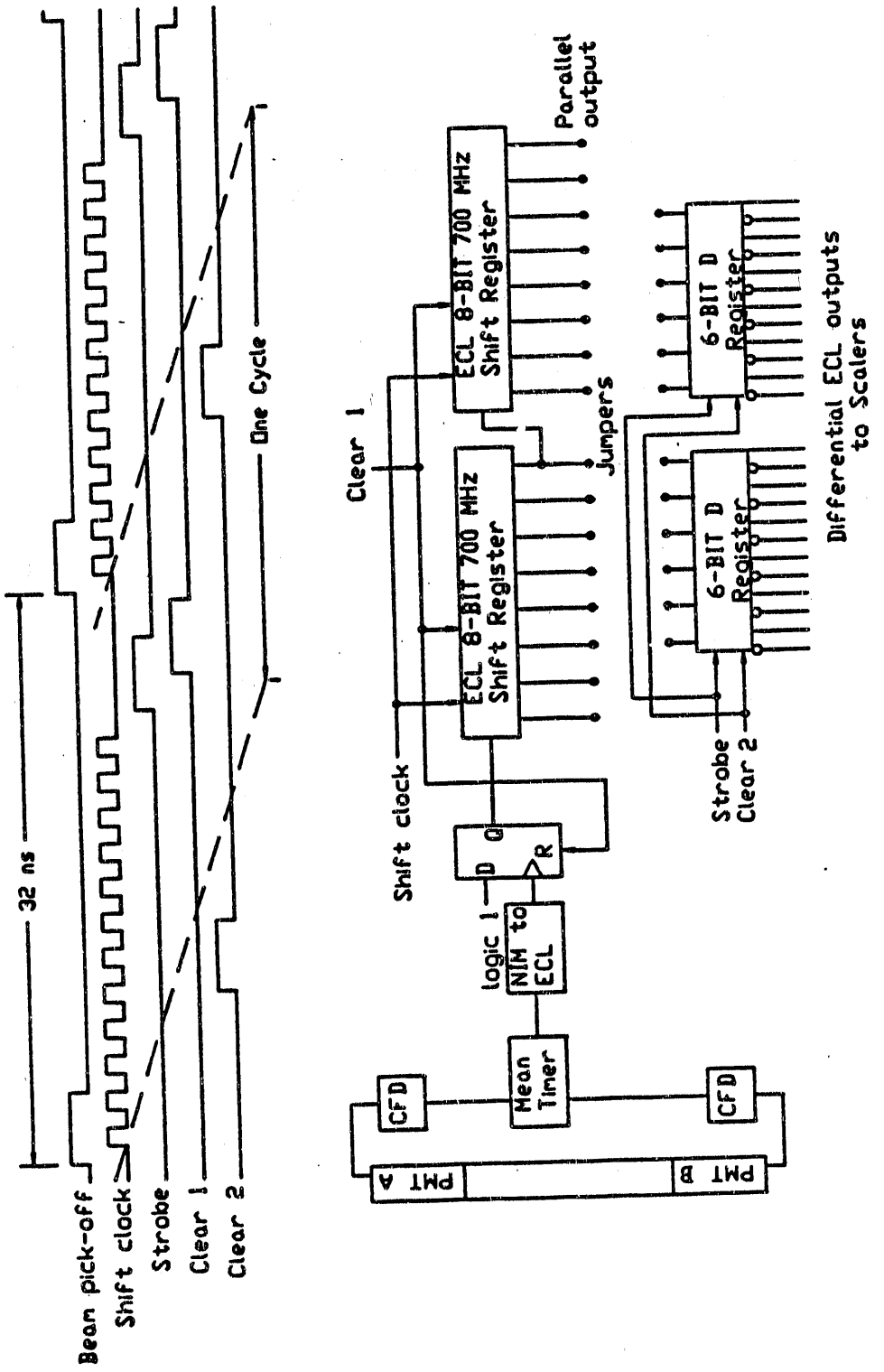

Figure IX.C.1 Timing diagram and schematic of the signal processing from detector to scaler. the logic pulses between the dashed lines in the timing diagram indicate signals associated with a given beam pulse.

X. Relativistic Heavy Ion-Nucleus Collisions at the SPS (NA36)

X.1. Introduction

Lattice QCD calculations have predicted a fundamental change in the behavior of hadronic matter at high density and temperature. The new form of matter is given the name quark-gluon plasma (QGP). In theoretical models of QGP, individual quarks can move about freely within the plasma rather than being confined within colorless baryons and mesons as in ordinary hadronic matter. Further, the strength of the quark-quark interactions is reduced because the quarks experience a "continual" state of asymptotic freedom due to the close proximity of other quarks; the high density of quarks and gluons effectively screens the color of any individual particle. The properties of the QGP and of the phase boundary between it and ordinary hadronic matter may provide new insight into non-perturbative QCD and unexplored bulk properties of quark matter.

Relativistic heavy ion collisions are the experiments which are most likely to form QGP and study its properties. Indeed, the study of QGP is the chief justification for the construction of the Relativistic Heavy Ion Collider (RHIC) at BNL. Meanwhile, fixed target programs have permitted the first relativistic heavy ion experiments at BNL's AGS (at 14 GeV per nucleon) and CERN's SPS (at 200 GeV per nucleon).

Production of strange particles has been suggested[1] as an channel in which experimental evidence of QGP formation be manifested. Either the abundance of strange particles or their kinematic distributions might differ significantly from predictions of cascade calculations if QGP is produced in these collisions. If such a discrepancy results from QGP production, it might be expected to be stronger for heavier targets and to be correlated with more central collisions.

X.2. Experiment NA36

CERN experiment NA36 was designed to study strange particle production at SPS energy, using a Time Projection Chamber (TPC) to image the neutral V's characteristic of Λ and K^0_S decay. Use of this three-dimensional imaging detector was central to the success of the experiment because of the huge number of charged particles tracks which may result from these collisions, and which must be disentangled from the V's of interest.

During the first heavy ion running period of the SPS in 1986, technical problems with the TPC and its readout system prohibited the study of strange particle production. Useful physics data was taken by NA36 during two subsequent heavy ion running periods. The 1987 run studied collisions of ^{32}S (at 200 GeV per nucleon) with three different targets: copper, silver and lead. The performance of the TPC during this early running period was marginal. Because of stability problems, the high voltage could not be brought up to the operating point, so the single-

hit efficiency of the chamber was only about 40%. The 1990 running used the same beam and largely the same experimental apparatus. The later running had a somewhat different kinematic acceptance, but the most significant differences were that only a single target (lead) was studied and that the efficiency of the TPC was much better, approaching 100%.

The analysis of the 1987 data was greatly complicated by the inefficiency of the TPC during that running period. While efforts to improve the operation of the detector continued and were successful in time for the 1990 running, analysis of the 1987 data was also undertaken. The analysis of Λ production on the three targets studied in the 1987 run was the subject of the Ph.D. thesis of CMU graduate student Guy Diebold. Despite the complexities introduced by the TPC inefficiency, this analysis was successfully completed last year. A paper based upon Guy's results was written over the past year and has been accepted for publication[2].

Some of the results are shown in Fig. X.2.1 and X.2.2. These results are unique in that they represent the only systematic study of target mass dependence carried on for ^{32}S beam at SPS energies. The statistics were quite low for this measurement because of the low efficiency and there were large combinatorial backgrounds, which were present for the same reason, which had to be determined and subtracted. These corrections were carefully checked however, and are believed to have an accuracy better than the statistics of the measurement. Fig. X.2.1 shows that significantly more Λ's were produced per unit rapidity, within our acceptance, than were predicted by the VENUS 4.02 event generator. The enhancement factor appears to be largely independent of target mass, in contrast to what might be expected if it were due to a QGP phase transition. Figure X.2.2 shows the observed distributions of Λ's (for central events) as a function of 'transverse kinetic energy', $T_T = \sqrt{p_t^2 + M_\Lambda^2} - M_\Lambda$ (where p_t is the component of the Λ's momentum transverse to the beam direction). The slopes of these distributions differ markedly from the predictions of VENUS for all targets. The effective 'temperatures' extracted from fits to these distributions are found to be approximately 0.22 GeV, essentially independent of target mass.

A paper presenting the Λ and $\bar{\Lambda}$ distribution results of the 1990 run is in preparation. Significant discrepancies are found between the observed rapidity distributions and predicted values. These high quality data promise to inspire a great deal of theoretical activity in the field.

Chapter X References

1) P. Koch, B. Mueller and J. Rafelski, Phys. Rep. 142, 167 (1986).
2) E. Andersen *et al*, to be published in Phys. Rev. C

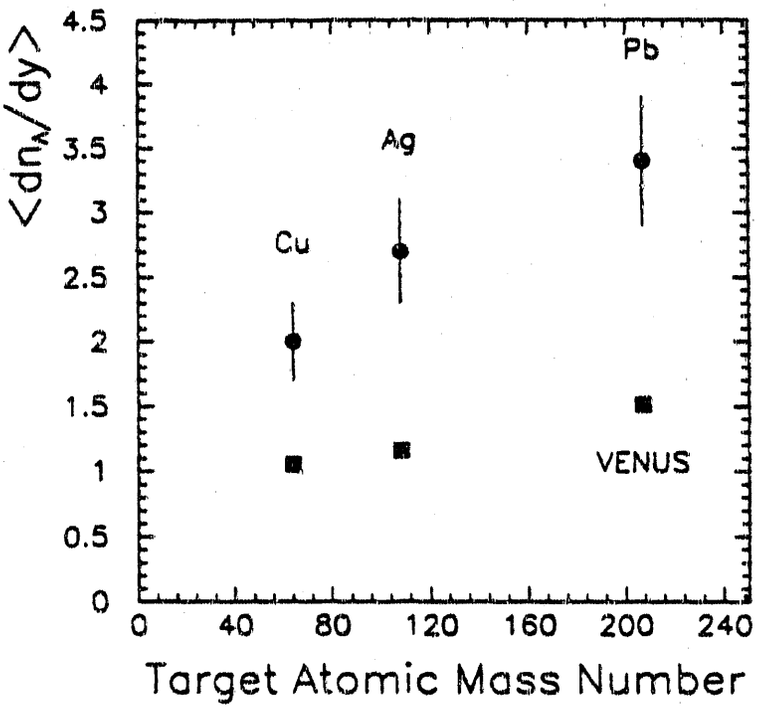

Figure X.2.1 The average Λ multiplicity (within the acceptance of the experiment) per unit rapidity, for central triggers, as a function of target mass. The kinematic acceptance of the experiment is from 2.0 to 4.0 units in rapidity, y, and above 0.5 GeV/c in transverse momentum, p_T. These cuts, as well as the central trigger requirement have also been imposed for the VENUS 4.02 predictions which are shown as squares.

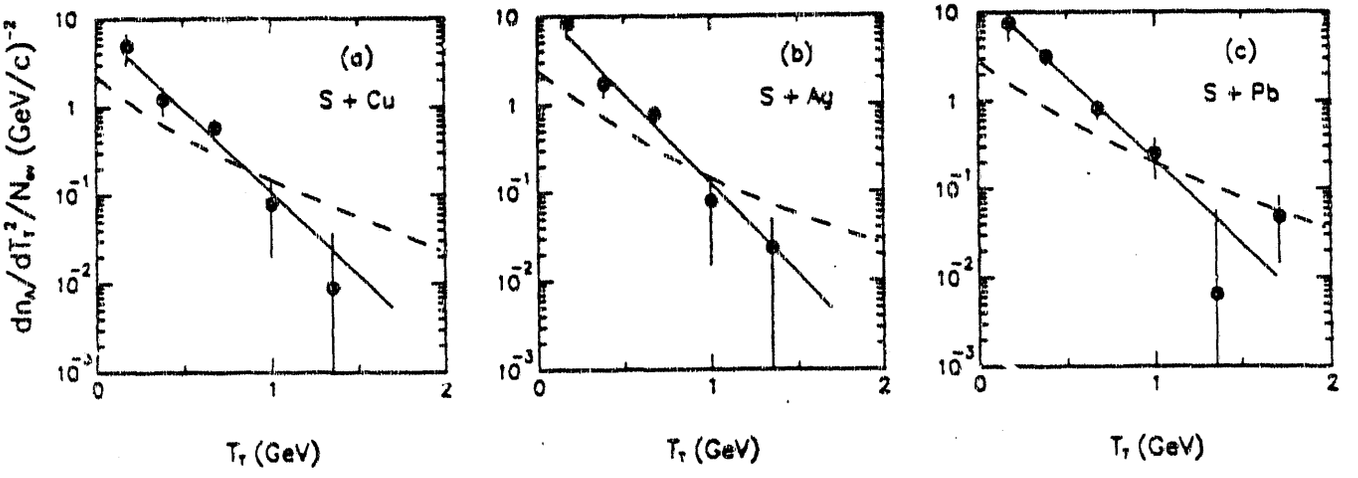

Figure X.2.2 Λ yields, per central trigger event, as a function of transverse kinetic energy, T_T (see text), within the acceptance of the experiment. Sections a), b), and c) show the distributions for copper, silver, and lead targets respectively. The dashed curves are the VENUS 4.02 predictions. The solid curves are best fits of the form: $\frac{dn}{dT_T^2} = A\, e^{-T_T/B}$. The best fit values for B are 0.232± .047 GeV for copper, 0.213± .037 GeV for silver, and 0.235± .034 GeV for lead.

XI. Professional Activities

XI.A. Committee Memberships

Professor Franklin has been active on the following committees:

- Member, Mellon College of Science (MCS) Committee for Untenured Faculty Promotions and Special Faculty Promotions, CMU
- Member, BNL Program Advisory Committee, Brookhaven National Lab.

Professor Schumacher has been active on the following committees:

- Member, University Committee for Non-Tenure Appointments, CMU
- Member, MCS Task Force on Undergraduate Advising
- Member, MCS Undergraduate Curriculum Committee

Professor Quinn has been active on the following committee:

- Member, MCS Committee on Special Faculty Positions

XI.B. Meetings Attended

XI.B.1. Physics Conferences

1. CEBAF Summer Workshop, Newport News, VA, June 6-14, 1991, R.A. Schumacher.

2. "Hadron 91" International Conference on Hadron Spectroscopy, College Park, MD, August 12-16, 1991, R.A. Schumacher.

3. SuperLEAR Workshop, Zurich, Switzerland, October 8-11, 1991, V.J. Zeps.

4. 1991 Annual Meeting of the Division of Nuclear Physics, East Lansing, MI, October 23-27, 1991, M.J. Athanas.

5. Workshop on Hyperon Physics with Proton Beams, Bloomington, IN, November 8-11, 1991, G.B. Franklin, V.J. Zeps.

6. CEBAF Program Advisory Committee, Newport News, VA, November 20-21, 1991, G.B. Franklin.

7. 20th INS International Symposium on Hypernuclear and Strange Particle Physics, Shimoda, Japan, December 9-12, 1991, R.A. Schumacher.

8. BNL Physics Review, Brookhaven National Lab., January 25, 1992, G.B. Franklin.

9. VIth Wire Chamber Conference, Vienna, Austria, February 15-22, 1992, R. Magahiz.

10. BNL Program Advisory Committee Meeting, Brookhaven National Lab., February 26-28, 1992, G.B. Franklin.

11. Ninth International Workshop on Photon-Photon Collisions, La Jolla, California, March 22-26, 1992, M.J. Athanas.

12. 1992 Joint April Meeting of the APS and AAPT, Washington, D.C., April 20-24, 1992, V.J. Zeps, M.J. Athanas, B. Quinn, F. Merrill.

XI.B.2. Collaboration Meetings/Working Groups

1. NA36 Collaboration Meeting, Geneva, Switzerland, July 8-16, 1991, B. Quinn.

2. G0 Collaboration Meeting, Urbana, IL, September 6-7, 1991, G.B. Franklin, R.A. Schumacher, B. Quinn, V.J. Zeps.

3. CEBAF CLAS Collaboration Meeting, Newport News, VA, September 11-14, 1991, R.A. Schumacher, R. Magahiz.

4. CEBAF CLAS Technical Advisory Committee, Newport News, VA, October 3-4, 1991, R. Magahiz.

5. PS185 Collaboration Meeting, Geneva, Switzerland, October 6-7, 1991, V.J. Zeps.

6. H Particle Collaboration Meeting, Brookhaven National Lab., November 15-17, 1991, G.B. Franklin, M.J. Athanas, R.A. Schumacher, R. Sukaton, B. Quinn, V. Zeps, F. Merrill, R. Magahiz.

7. CEBAF CLAS Technical Advisory Committee, Newport News, VA, December 4-6, 1991, R. Magahiz.

8. G0 Collaboration Meeting, Urbana, IL, December 17, 1991, V.J. Zeps, B. Quinn.

9. CEBAF CLAS Collaboration Meeting, Newport News, VA, January 8-11, 1992, R.A. Schumacher, R. Magahiz.

10. CEBAF CLAS Technical Advisory Committee, Newport News, VA, February 6-7, 1992, R. Magahiz.

11. CEBAF CLAS Meeting, Newport News, VA, February 23-25, 1992, R.A. Schumacher.

12. H Particle Collaboration Meeting, Brookhaven National Lab., March 27-29, 1992, G.B. Franklin, R.A. Schumacher, R. Sukaton, B. Quinn, V. Zeps, F. Merrill, R. Magahiz.

13. CEBAF CLAS Meeting, Newport News, VA, May 18, 1992, R.A. Schumacher.

XI.B.3. Committee Meetings

AGS User's Executive Committee Meeting, Brookhaven National Lab., October 11, 1991, G.B. Franklin, Member.

XII. Publications, Reports, Talks, Etc.

XII.A. Publications

XII.A.1. Journals

1. E. Andersen, P.D. Barnes, R. Blaes, H. Braun, J.M. Brom, B. Castano, M. Cherney, M. Cohler, B. de la Cruz, G.E. Diebold, C. Fernandez, G.B. Franklin, C. Garabatos, J.A. Garzon, W.M. Geist, D. Greiner, C. Gruhn, M. Hafidouni, J. Hrubec, D. Huss, J.L. Jacquot, P.G. Jones, J.P.M. Kuipers, M. Ladrem, P. Ladron de Guevara, D. Liko, S. Lopez-Ponte, G. Lovhoiden, J. MacNaughton, C.J. Maher, A. Michalon, M.E. Michalon-Mentzer, J. Mosquera, Z. Natkaniec, J.M. Nelson, G. Nuehofer, C. Perez de los Heros, M. Plo, P. Porth, B. Powell, B. Quinn, A. Ramil, J.L. Riester, H. Rohringer, G. Sakrejda, I. Sakrejda, T. Thorsteinsen, J. Traxler, C. Voltolini, A. Yanez, P. Yepes, R. Zybert,
"Target Dependence of Central Rapidity Λ Production in Sulfur - Nucleus Collisions at 200 GeV/c per Nucleon"
(to be published in Phys. Rev. C).

2. D.J. Mack, P.G. Roos, H. Breuer, N.S. Chant, S. D. Hyman, F. Khazaie, B.G. Ritchie, J.D. Silk, G.S. Kyle, P.A. Amaudruz, Th.S. Bauer, C.H.Q. Ingram, D. Renker, R. A. Schumacher, U. Sennhauser, W.J. Burger,
"Dominance of the Two-Nucleon Mechanism in $^{16}O(\pi^+,pp)$ at 115 MeV"
Physical Review C **45**, 1767 (1992).

3. A. Rahav, J. Alster, D. Ashery, J. Lichtenstadt, I. Navon, E. Piasetsky, P. Amaudruz, M. Botje, W. Burger, C.H.Q. Ingram, R. A. Schumacher, U. Sennhauser, S.A. Wood,
"Measurement of the $^{12}C(\pi,2\pi)$ Reactions and Possible Evidence of a Double-Δ Excitation"
Phys. Rev. Lett. **66**, 1279 (1991).

4. M. D. Mestayer, C. L. Tam, K. Wang, H. Baghaei, S. Christo, S. A. Dytman, G.P.Gilfoyle, J. D. Hewitt, F. W. Hersman, R. S. Hicks, R. A. Miskimen, R. Schumacher, and M.F. Vineyard,
"Effects of Non-Parallel Magnetic Fields on Hexagonal Cell Drift Chambers"
(submitted to I.E.E.E. Transactions).

5. The New Muon Collaboration (NMC):
P. Amaudruz, M.Arneodo, A. Arvidson, B. Badelek, G. Baum, J. Beaufays, I.G. Bird, M. Botje, C. Broggini, W. Brueckner, A. Bruell, W.J. Burger, J. Ciborowski, R. van Dantzig, H. Doebbeling, J. Domingo, J. Drinkard, H. Engelien, M.I. Ferrero, L. Fluri, P. Grafstrom, D. von Harrach, M. van der Heijden, C. Heusch, Q. Ingram, K. Janson, M. de Jong, E.M. Kabuss, R. Kaiser, T. Ketel, F. Klein, B. Korzen, U. Kruener, S. Kullander, U. Landgraf, F. Lettenstrom, T. Lundqvist, G.K. Mallot, C. Mariotti, G. van Middelkoop, Y.

Mizuno, J. Nassalski, D. Nowotny, N. Pavel, C. Peroni, H. Peschel, B. Povh, R. Rieger, K. Rith, K. Roehrich, E. Rondio, L. Ropelewski, A. Sandacz, C. Scholz, R. Schumacher, U. Sennhauser, F. Sever, T.A. Shibata, M. Siebler, A. Simon, A. Staiano, G. Taylor, M. Treichel, J.L. Vuilleumier, T. Walcher, R. Windmolders, F. Zetsche,
"Transverse Momentum Distributions for Exclusive ρ^0 Muoproduction"
(to be published in Zeitschrift fur Physik).

6. The New Muon Collaboration (NMC):
P. Amaudruz, M.Arneodo, A. Arvidson, B. Badelek, G. Baum, J. Beaufays, I.G. Bird, M. Botje, C. Broggini, W. Brueckner, A. Bruell, W.J. Burger, J. Ciborowski, R. van Dantzig, H. Doebbeling, J. Domingo, J. Drinkard, H. Engelien, M.I. Ferrero, L. Fluri, P. Grafstrom, D. von Harrach, M. van der Heijden, C. Heusch, Q. Ingram, K. Janson, M. de Jong, E.M. Kabuss, R. Kaiser, T. Ketel, F. Klein, B. Korzen, U. Kruener, S. Kullander, U. Landgraf, F. Lettenstrom, T. Lundqvist, G.K. Mallot, C. Mariotti, G. van Middelkoop, Y. Mizuno, J. Nassalski, D. Nowotny, N. Pavel, C. Peroni, H. Peschel, B. Povh, R. Rieger, K. Rith, K. Roehrich, E. Rondio, L. Ropelewski, A. Sandacz, C. Scholz, R. Schumacher, U. Sennhauser, F. Sever, T.A. Shibata, M. Siebler, A. Simon, A. Staiano, G. Taylor, M. Treichel, J.L. Vuilleumier, T. Walcher, R. Windmolders, F. Zetsche,
"Precision Measurement of the Structure Function Ratios F_2^{He}/F_2^D, F_2^C/F_2^D and F_2^{Ca}/F_2^D"
Zeitschrift fur Physik C, Particles and Fields **51**, 387 (1991).

7. The L3 Collaboration:
R. Magahiz, *et. al.*,
"Search for Narrow High-Mass Resonances in Radiative Decays of the Z^0"
Phys. Lett. **B262**, 155 (1991).

8. The L3 Collaboration:
R. Magahiz, *et. al.*,
"A Test of QCD Based on 3-Jet Events from Z^0 Decays"
Phys. Lett. **B263**, 551 (1991)

9. The L3 Collaboration:
R. Magahiz, *et. al.*,
"Decay Properties of Tau Leptons Measured at the Z^0 Resonance",
Phys. Lett. **B265**, 451 (1991).

10. The L3 Collaboration:
R. Magahiz, *et. al.*,
"Search for Lepton Flavour Violation in Z^0 Decays",
Phys. Lett. **B271**, 453, (1991).

11. The L3 Collaboration:
R. Magahiz, *et. al.*,
"Measurement of the Strong Coupling Constant α_S for Bottom Quarks at the Z^0 Resonance",
Phys. Lett. **B271**, 461, (1991).

XII.A.2. Conference Proceedings

1. B. Quinn, "The Search for the H Dibaryon with the BNL 2.0 GeV/c Kaon Beam", 4th Conference on the Intersections Between Particle and Nuclear Physics, Tucson, AZ, May 24-29, 1991, AIP Conf. Proc. **243**, 579 (1992).

2. R.A. Schumacher, "Measurements of Non-Leptonic Weak Decays of Lambda Hypernuclei", 4th Conference on the Intersections Between Particle and Nuclear Physics, Tucson, AZ, May 24-29, 1991, AIP Conf. Proc. **243**, 594 (1992).

3. R.A. Schumacher, "Search for the H Dibaryon at the Brookhaven 2 GeV/c Kaon Beam Line", International Conference on Hadron Spectroscopy, College Park, MD, August 12-16, 1991, (to be published).

4. R.A. Schumacher, "Possible Violation of the $\Delta I=1/2$ Rule in Non-Mesonic Hypernuclear Weak Decay", 20th INS International Symposium on Hypernuclear and Strange Particle Physics, Shimoda, Japan, December 9-12, 1991, (to be published in Nuclear Physics).

XII.A.3. Bulletin of the American Physical Society

1. V.J. Zeps, G.B. Franklin, J.T. Watson, **"Silicon Detectors for use at Cryogenic Temperatures"**, B.A.P.S. **37**, 994 (1992).

2. M.J. Athanas, **"Measurements of Nonleptonic Weak Decays of Light Hypernuclei"**, B.A.P.S. **36**, 2155 (1991).

3. M.J. Athanas, P.D. Barnes, G.E. Diebold, G.B. Franklin, C. Maher, B. Quinn, F. Rozon, R.A. Schumacher, I. Sukaton, V.J. Zeps, S. Bart, R. Chrein, K. Johnson, P. Pile, R. Sutter, R. Sawafta, B. Bassalleck, J.J. Szymanski, R. Stearns, **"Measurement of the Nonleptonic Decays of $^{4}_{\Lambda}$He and $^{5}_{\Lambda}$He"**, B.A.P.S. **37**, 903 (1992).

XII.B. Theses, Reports, and Proposals

1. "Search for New Particles in Nucleus-Nucleus Collisions", AGS Research Proposal, G.B. Franklin, R.A. Schumacher, B. Quinn, *et. al.* (800 hrs. requested)

2. "Experiment to Detect $\Lambda\Lambda$ Hypernuclei", AGS Research Proposal, G.B. Franklin, R. Magahiz, F. Merrill, B. Quinn, R.A. Schumacher, V.J. Zeps, *et. al.* (1000 hrs. requested)

XII.C. Invited Talks, Seminars, Etc.

1. R.A. Schumacher, Invited Talk: "Hadron 91" International Conference on Hadron Spectroscopy, College Park, MD, August 12-16, 1991, "Search for the H Dibaryon at the BNL/AGS 2 GeV/c Kaon Beam".

2. M.J. Athanas, Contributed Talk: 1991 Annual Meeting of the Division of Nuclear Physics, East Lansing, MI, October 23-27, 1991, "Measurements of Nonleptonic Weak Decays of Light Hypernuclei".

3. R.A. Schumacher, Seminar: Society of Physics Students, CMU, October 24, 1991, "Physics with Strange Quarks".

4. B. Quinn, Seminar: CMU Medium Energy / Nuclear Physics Journal Club, October 25 1991, "Parity Violating Electron Scattering from the Proton".

5. R.A. Schumacher, Seminar: CMU Medium Energy / Nuclear Physics Journal Club, November 22, 1991, "$\Delta S = 1$ Decays of Kaon and Hyperons with Applications to the $\Delta I = 1/2$ Rule".

6. R.A. Schumacher, Contributed Talk: 20th INS International Symposium on Hypernuclear and Strange Particle Physics, Shimoda, Japan, December 9-12, 1991, "Possible Violation of the $\Delta I = 1/2$ Rule in Non-mesonic Hypernuclear Weak Decay".

7. G.B. Franklin, Contributed Talk: BNL Program Advisory Committee Meeting, Brookhaven National Lab., February 26-28, 1992, "Request for extension of AGS Experiment 813 - Search for a Strangeness -2 Dibaryon".

8. R.A. Schumacher, Seminar: TRIUMF, Vancouver, B.C., Canada, March 12, 1992, "Non-mesonic Hypernuclear Weak Decay and Possible Violation of the $\Delta I = 1/2$ Rule".

9. R.A. Schumacher, Seminar: University of Washington, Seattle, WA, March 13, 1992, "Non-mesonic Hypernuclear Weak Decay and Possible Violation of the $\Delta I = 1/2$ Rule".

10. V.J. Zeps, Seminar: Department of Physics, Indiana University, April 6, 1992, "Measuring the Properties of the Weak Baryon-Baryon Interaction".

11. M.J. Athanas, *et.al.*, Contributed Talk: 1992 Joint April Meeting of the APS and AAPT, Washington, D.C., April 20-24, 1992, "Measurements of Nonleptonic Weak Decays of Light Hypernuclei".

12. V.J. Zeps, Contributed Talk: 1992 Joint April Meeting of the APS and AAPT, Washington, D.C., April 20-24, 1992, "Silicon Detectors for use at Cryogenic Temperatures".

13. F. Merrill, Contributed Talk: 1992 Joint April Meeting of the APS and AAPT, Washington, D.C., April 20-24, 1992, "Longitudinal Measurements on the LAMPF Side-Coupled Linac".

END

DATE
FILMED
10/8/92